Spring 2016

Dual energy CT based approach to assessing early pulmonary vascular dysfunction in smoking-associated inflammatory lung disease

Krishna S. Iyer
University of Iowa

Recommended Citation

Iyer, Krishna S.. "Dual energy CT based approach to assessing early pulmonary vascular dysfunction in smoking-associated inflammatory lung disease." PhD (Doctor of Philosophy) thesis, University of Iowa, 2016.
http://ir.uiowa.edu/etd/3112.

DUAL ENERGY CT BASED APPROACH TO ASSESSING EARLY PULMONARY VASCULAR DYSFUNCTION IN SMOKING-ASSOCIATED INFLAMMATORY LUNG DISEASE

by

Krishna S. Iyer

A thesis submitted in partial fulfillment
of the requirements for the Doctor of
Philosophy degree in Biomedical Engineering
in the Graduate College of
The University of Iowa

May 2016

Thesis Supervisor: Professor Eric A. Hoffman

Graduate College
The University of Iowa
Iowa City, Iowa

CERTIFICATE OF APPROVAL

PH.D. THESIS

This is to certify that the Ph.D. thesis of

Krishna S. Iyer

has been approved by the Examining Committee
for the thesis requirement for the Doctor of Philosophy
degree in Biomedical Engineering at the May 2016 graduation.

Thesis Committee: ________________________________
Eric A. Hoffman, Thesis Supervisor

____
John D. Newell Jr.

____
Jessica C. Sieren

____
Sif Hansdottir

____
Mark T. Madsen

____
Joseph M. Reinhardt

To my parents, Shankar and Chhaya, who have sacrificed so much and who continue to support my dreams.

To my sister Kanchan, who has been a role model and source of emotional support

To my eleventh grade chemistry teacher, Mrs. Buckwalter, who sparked a passion for science and curiosity in me.

Finally, this thesis is also dedicated to my grandparents, especially my grandfather, who looks upon my achievements with everlasting pride.

“The important thing is not to stop questioning. Curiosity has its own reason for existing”

Albert Einstein, physicist and Nobel Laureate

"The most exciting phrase to hear in science, the one that heralds new discoveries, is not 'Eureka!' (I found it!), but 'That's funny....”

Isaac Asimov, science fiction writer'

“”In the realm of ideas everything depends on enthusiasm…in the real world rests on perseverance.”

Johann W. von Goethe, German writer and statesman

ACKNOWLEDGMENTS

I am grateful to my colleagues in the Advanced Pulmonary Physiomic Imaging Laboratory, including the graduate and undergraduate students, CT and veterinary technicians, faculty and staff for their support, personal guidance, and encouragement. There several people I would like to thank personally:

My lab colleagues, Samantha Dilger, Emily Hammond, Abhilash Puliyakote, and Dr. Jiwoong Choi for their help with studies, manuscript preparation, and their positive feedback during my comprehensive exam and in preparation of this thesis.

Former graduate students, specifically Dr. Matthew Fuld and Dr. Ahmed Halaweish, for their initial training and guidance during my first few years in the laboratory.

Members of the Quantitative Structural Image Analysis Laboratory: Dr. Junfeng Guo, for help with pulmonary analysis and troubleshooting; Dr. Punam K. Saha and Dakai Jin for their help with vascular measurements and valuable discussions

And finally I would like thank my thesis committee for their support and advice during my training, and lastly my mentor, Dr. Eric A. Hoffman, for his, encouragement, advice, and friendship during my doctoral training; Our discussions have helped shape my career goals and helped me become a more critical thinker and engaged scientist.

ABSTRACT

CT is a powerful method for noninvasive assessment of the lung. Advancements to CT hardware and imaging and visualization software have guided the high-resolution structural and functional assessment of normal and abnormal lung. This has helped make the transition from not only characterizing the structural severity of various lung diseases to phenotyping novel disease subtypes.

Chronic obstructive pulmonary disease (COPD) is a spectrum of inflammatory lung disease affecting lung parenchyma, airways, and the pulmonary and systemic vasculature. The majority of CT-based measures have focused on quantifying the extent of airway and parenchymal damage. Recently, functional lung measures, such as perfusion and ventilation imaging, have provided valuable information about early disease mechanisms. Perfusion CT method has demonstrated abnormal vascular blood flow in areas of inflamed lung, suggesting an early vascular etiology of smoking-associated centri-acinar emphysema (CAE), a subtype of the COPD spectrum. However, it is unknown if the alterations in the pulmonary vascular physiology in smokers with early CAE is a result of early parenchymal destruction or an intrinsic difference in the function of peripheral pulmonary vessels.

To address this question, we introduce dual energy CT-perfused blood volume (DECT-PBV) as a novel image-based biomarker to assess peripheral pulmonary vascular physiology. DECT-PBV is an easier to implement method of imaging pulmonary perfusion, compared to conventional perfusion CT, and in can be performed successively in human studies, such as before and after a drug intervention. We use this imaging method to test our hypothesis that smoking-associated pulmonary perfusion heterogeneity, a marker of abnormal blood flow, in the presence of smoking-associated lung inflammation, is due to peripheral vasoconstriction and is reversible process.

We validate our quantitative imaging approach in an animal model of hypoxic pulmonary vasoconstriction to establish useful quantitative regional PBV measures in physiological and disease-relevant model. In smokers with early signs of CAE, we show that PBV heterogeneity, a measure of the spatial distribution of PBV, is elevated due to peripheral pulmonary vasoconstriction and reversed with sildenafil, a potent pulmonary vasodilator used to treat pulmonary hypertension. We demonstrate this by 1) measuring changes in peripheral PBV heterogeneity using image-registered PBV datasets and 2) developing tools to quantify the change in central pulmonary artery dimensions before and after sildenafil. This data, in aggregate, supports the notion that vascular dysfunction in CAE-susceptible smokers is not a consequence of early stage parenchymal destruction but represents an intrinsic difference in the vascular response to smoking-associated lung inflammation which can be reversed.

The quantitative DECT-PBV imaging techniques developed here provide new functional and structural measures of the pulmonary vascular bed and central arteries. Our validated DECT approach and novel imaging findings in CAE-susceptible smokers extends our characterization of the vascular phenotype and provide a framework for future quantitative imaging studies to assess early targeted vascular interventions in hopes of reversing disease progression.

PUBLIC ABSTRACT

CT is a powerful method for noninvasive assessment of the lung. Advancements in the speed and spatial resolution has allowed for detailed assessment of small-scale changes in lung structure and function. This has helped transition CT from a tool purely for structural characterization of the lung in patients with lung disease to phenotyping novel sub populations with early disease based on differences in regional lung function.

In this thesis, we introduce dual energy CT-perfused blood volume (DECT-PBV) as a novel quantitative image-based biomarker to characterize early pulmonary vascular dysfunction in smoking-associated centri-acinar emphysema (CAE), a component of Chronic Obstructive Pulmonary Disease (COPD). We demonstrate that in smokers with early signs of CAE, there is an abnormal distribution of blood flow due to increase constriction of peripheral pulmonary vessels and the response to a conventional drug, used clinically to treat pulmonary hypertension, corrects this abnormal distribution by dilating peripheral vessels. We demonstrate this by measuring changes in central pulmonary arteries and changes in peripheral PBV in CAE-susceptible and non-susceptible smokers using sensitive CT methods.

This data supports the notion that vascular dysfunction in CAE-susceptible smokers is not a result of parenchymal (and peripheral pulmonary vasculature) damage but is rather associated with an early, intrinsically altered vascular response to smoking-associated parenchymal inflammation. DECT-PBV has a potential to differentiate early asymptomatic smokers with emphysema-dominant disease to determine if early intervention with drugs targeted to pulmonary vessels may aid in reversing lung

destruction, by restoring blood flow to areas of the lung that are inflamed and poorly perfused, to prevent further lung destruction.

TABLE OF CONTENTS

LIST OF TABLES

LIST OF FIGURES

CHAPTER 1: MOTIVATION AND AIMS

COPD is a chronic, debilitating inflammatory lung disease, with cigarette smoke as the largest single risk factor. No known cure for the disease exists and most treatments are symptom management. Centri-acinar emphysema (CAE) is a common subtype of emphysema largely attributed to smoking. In emphysema, there is an abnormal influx of inflammatory cells that respond to noxious stimuli, including smoke exposure, which sets off a series of pro-inflammatory events that increase the damage to lung tissue. Once initiated, this chronic inflammatory process is thought to be irreversible, leading to destruction of small airways, parenchyma. There is a crucial need for lung-specific biomarkers with prognostic value that help the exploration of disease etiology and the efficacy of targeted treatments to halt the progression and precipitous decline in lung function associated with this disease.

Computed-tomography (CT)-derived perfusion measures provide a novel functional imaging phenotype to assess vascular dysfunction in early CAE. It was recently shown by Alford et al, using dynamic, contrast-enhanced perfusion CT, that smokers with normal pulmonary function but early CT-evidence of emphysema had greater heterogeneity of pulmonary blood flow (PBF) compared to normal smokers without CT-evidence of emphysema (3). While vascular remodeling and loss of small vessels has been attributed to advanced disease, including COPD-associated pulmonary hypertension, the absence of overt parenchymal destruction (aside from minimal emphysema) in these subjects suggest alternate mechanisms.

Recent clinical and imaging studies support the link between hypoxia, endothelial dysfunction, and regional lung inflammation in the etiology of early COPD (10, 74, 143, 172). We extend the work of Alford et al. and hypothesize that increased perfusion heterogeneity observed in smokers susceptible to CAE is not attributed to pulmonary parenchymal destruction but rather an increase in pulmonary vascular tone, mediated by hypoxic pulmonary vasoconstriction (HPV) and therefore is reversible with a pharmaceutical intervention that blocks HPV.

The imaging protocol used in the human perfusion CT studies by Alford et al. (3) has many technical challenges, including a central catheter placement to inject contrast into the right atrium. This can be difficult for repeated imaging sessions, such as before and after the administration of a drug and is best suited for use in a research environment as opposed to a clinical CT setting. This is further complicated by measurement technique of first pass kinetics of the contrast bolus, which is sensitive to patient motion (including cardiogenic oscillations) during a long breath-hold. Such motion serves to shift the region of interest over time and complicates the assessment of time-intensity curves The method for assessing PBF is also limited to axial scanning because of the need to acquire temporally sequenced image data. Furthermore, because of the need for the acquisition of up to 10 to 15 time points, the radiation exposure for repeat studies is of some concern. Many of these challenges have been overcome by the introduction of dual energy CT (DECT) which provides the ability to assess perfused blood volume (PBV) with similar spatial resolution as conventional MDCT and without increased radiation exposure. The technique resolved issues with contrast placement (peripheral vein rather than central bolus) and the need for cardiac-gating. DECT-based PBV equivalence to PBF measures was performed by Fuld et al. in an animal model, using variations in airway inflation pressures and variably placed intra-pulmonary arterial balloon catheters to provide alterations in PBF distribution patterns. Under these conditions, PBF and PBV were shown to provide equivalent information (50).

Despite these advances in showing the feasibility of DECT, application of quantitative DECT PBV imaging to our subjects of interest, mainly early CAE-susceptible smokers, has not been investigated. There has remained the need to demonstrate that PBV is sensitive to the scale of PBF heterogeneity used by Alford et al (3) to differentiate emphysema susceptible from non-susceptible smokers and to demonstrate that changes in PBV track physiologic conventional physiologic responses to alterations in pulmonary vascular resistance (pulmonary arterial pressure). To address our main hypothesis, that smoking-associated HPV, in the midst of lung inflammation, is reversible process, we translate PBV protocols to human imaging. Scan protocols are designed to assess both lung structure (presence of emphysema and central vascular geometry) and function (PBV), before and after a pharmaceutical intervention targeted to the pulmonary vasculature, seeking to explore the notion that pulmonary heterogeneity is a reversible process in CAE-susceptible smokers.

We do this through the following aims:

1) **Develop DECT imaging techniques to quantitatively evaluate regional PBV changes under varying hemodynamic conditions, in an animal model of HPV**, to determine the sensitivity of DECT-based PBV measures and provide a framework for evaluating PBV response to sildenafil, a pulmonary vasodilator.

2) **Evaluate the PBV response of CAE-susceptible smokers and CAE non-susceptible smokers to sildenafil** (pulmonary vasodilator used in the treatment of

pulmonary hypertension, known to reverse HPV). Determine if the resulting increased perfusion heterogeneity in CAE-susceptible smokers is a result of increased pulmonary vasoconstriction, in the face of parenchymal inflammation, or early, undetected, patchy destruction of lung tissue.

3) **Develop techniques to objectively evaluate the central pulmonary arterial response to sildenafil between non-susceptible (NS) and susceptible (SS) smokers**. We use these imaging techniques of vessel structure, coupled with our functional imaging results from Aim 2, to determine if the increased peripheral vasoconstriction (due to HPV) in the parenchymal bed causes enlargement of central arteries in SS subjects and if sildenafil, by reducing PBV heterogeneity in SS subjects, reduces this upstream dilation of central vessels.

Our imaging studies and detailed analysis provides a quantitative imaging framework for development of multi-center imaging studies aimed at characterizing sub-populations of COPD patients and utilizing novel imaging techniques to study early disease as well as quantifying the effectiveness of potential new therapies designed to halt or reverse the progression of this disease. Such studies, based upon the protocols developed in this thesis, are now funded by the National Institutes of Health within the context of SPIROMICS (28) and MESA Lung (71).

CHAPTER 2: OVERVIEW OF THESIS

In Chapter 3, we introduce and outline the clinical relevance of COPD, focusing on centri-acinar emphysema. We discuss the role of hypoxia, lung inflammation, and peripheral pulmonary vascular disease in the pathophysiology of smoking-associated COPD. With the goal of using image-based biomarkers to help assess at-risk- sub-populations of smokers, we provide background of methods to assess regional pulmonary blood flow (PBF) and pulmonary blood volume (PBV) using CT imaging techniques.

The first aim of this work, discussed in Chapter 4, utilizes a pig model of hypoxic pulmonary vasoconstriction (HPV) to develop a DECT imaging protocol and analytical framework for assessing regional pulmonary perfused blood volume (PBV and PBV heterogeneity). . Our pig model was designed to simulate hypoxia-induced changes in peripheral vascular tone known to occur in smoking-associated disease. Our experimental protocol consists of an interval of exposing animals to normoxic and hypoxic gas mixture, as we measure changes in hemodynamics with and without sildenafil, a pulmonary vasodilator, to establish which DECT-based PBV measures are sensitive to changes in pulmonary artery pressure.. This study highlights that with the careful implementation of imaging protocols (i.e. correct time-to-scan, maintenance of steady contrast enhancement, control over breath-hold levels, etc.), DECT-based PBV measures can assess normal physiological changes to pulmonary hemodynamics associated with an hypoxic intervention. In addition, the quantitative DECT PBV measurements along with quantitative measurements of the central arterial tree establish the upstream consequences (central pulmonary arterial tree dilation) of altered peripheral pulmonary vascular resistance. These peripheral and central pulmonary artery-based metrics will provide the sought-after vascular phenotypes (before and after treatment) of CAE-susceptible smokers studied in Chapters 5 and 6.

The second aim (Chapter 5) of this thesis applies the DECT PBV imaging method to characterize a population of CAE-susceptible (SS) and non-susceptible (NS) smokers without CT visible disease, to test the hypothesis that patchy distribution of blood flow in the lung (i.e. increased perfusion heterogeneity), putatively in response to patchy inflammation, is due to increased pulmonary vasoconstriction (mediated by HPV) and can be reversed with sildenafil treatment. To do this we perform DECT-PBV imaging in these subjects, utilizing the imaging protocol outlined in Chapter 3, before and after administration of sildenafil, a vasodilator shown to have clinical efficacy (77) in COPD-associated pulmonary hypertension.

Because of contrast-related image artifacts incurred from the dual energy PBV reconstruction, we perform analysis to look at how selected sampling of the lung is important in enhancing differences in these two groups while avoiding the sampling of noise-prone regions. We evaluate our PBV measures for the whole lung, lobes, and small region of the lung to find the most sensitive (low noise) regions for our analysis. We introduce noise-reducing iterative reconstruction and thicker slices to compare their effects on our measured inter-subject CV differences. Finally, using our desired sampled regions, we show that sildenafil reduces PBV heterogeneity in SS smokers and not NS smokers, without changing mean PBV. This change in PBV heterogeneity is analyzed in the selected lung regions with the lowest contrast-related noise.

With the finding that PBV heterogeneity is reduced with sildenafil in SS smokers, we explored the relationship between peripheral vascular changes in the parenchyma and measurable upstream changes in central arteries to test the hypothesis that The final aim of this thesis (Chapter 6) extends the vascular structural analysis, initially developed in the pig studies in Chapter 4, from whole lung measurements to region-specific arterial cross-sectional measurements to compare vascular structural differences in NS and SS smokers in Chapter 4. We provide a framework for sensitive CT-based assessment of central arteries, utilizing the anatomical correspondence with central airways to measure airway normalized cross-sectional area (CSA_{norm}). We discuss the selection and sampling methods used in locating central arteries, comparing the effects of lung volume and contrast enhancement on vessel measurements, and compare the differences in arterial morphology between non-susceptible (NS) and emphysema-susceptible (SS) before and after sildenafil to show that upstream central arterial dilation in SS subjects, likely due to the increased peripheral vasoconstriction, is reversible with sildenafil, coinciding with the decrease in PBV heterogeneity.

The final chapter discusses objectives for future functional imaging studies coupling DECT with direct indices of lung inflammation using single photon emission tomography (SPECT). We draw from lessons learned from early animal studies and discuss some of the technical challenges of quantifying inflammation with SPECT and incorporating them with regional assessment of PBV. We also discuss some potential solutions to these challenges with more sensitive imaging techniques, such as positron emission tomography (PET).

The work outlined in this thesis is important for further characterizing the vascular phenotype to inflammatory lung diseases, such as COPD, utilizing advanced imaging methods translatable to the clinic. The lack of sensitive biomarkers makes predicting and mapping the progression of early COPD a difficult process. Non-invasive CT measures of pulmonary vascular function/dysfunction, such as DECT-based PBV measures, are important for determining lung health and as biomarkers in outcomes assessment, such as before and after a drug intervention.

CHAPTER 3: BACKGROUND

3.1 PULMONARY CIRCULATION

Structure of the Pulmonary Vessels

The main purpose of the lungs is to facilitate gas exchange, including the absorption of oxygen and the elimination of carbon dioxide. The pulmonary circulation consists of conducting vessels, extending from the main pulmonary arteries (~25-30 mm diameter) down to medium and small (~100 µm) diameter muscular arteries and pre-capillary arterioles (10-50µm) (152) , which serve as a conduits for the transport of deoxygenated blood to the capillaries, where gas exchange, including absorbing oxygen (O_2) and eliminating carbon dioxide (CO_2), occurs. From the capillaries, oxygenated blood is collected into venules and then into larger pulmonary veins, which finally feeds into the left atrium. This is a low-pressure system, with an average atrial pressure of 10-15 mmHg (174). In normal individuals, the entire cardiac output from the left side of the heart matches the cardiac output entering the lungs. In order to avoid a build-up of pressure in the pulmonary circulation, there is a vast network of capillaries within the lung with a large total cross-sectional area, which effectively reduces the resistance to flow. In healthy lungs, this large capillary network is well matched to the large surface area of the lung required for gas diffusion across the alveolar-capillary membrane, a single layer consisting of alveolar epithelium, capillary endothelium, and the surrounding tissue matrix (166, 174, 175).

Although the resistance to flow is lower in the pulmonary circulation compared to the systemic circulation, the resistance can be increased by small pre-capillary resistance arterioles. These arterioles constrict in response to a variety of factors and redistribute blood to various portions of the lung. In diseases that affect gas exchange, such as chronic obstructive pulmonary disease (COPD) (92), pulmonary vascular resistance can be elevated, leading to syndromes, such as pulmonary hypertension, where the small vessels are thickened and/or narrowed and there is enlargement of large central vessels (59, 102, 181).

Pulmonary Blood Flow and Regulation

The pulmonary circulatory system was initially thought of as a passive reservoir, a conduit for blood to be transported from the right to left heart. It is now apparent that the pulmonary vasculature is a highly active and responsive system (30). The prime stimulus for pulmonary artery reaction is oxygen. Compared to other vascular networks, such as those found in skeletal muscle or in kidneys, the pulmonary circulation responds to low oxygen (i.e. hypoxia) by constricting small pre-capillary arterioles. These arterioles are lined with oxygen-sensing smooth muscle cells (27, 166) that contract with hypoxia. The overall effect is the redirection of blood to more oxygenated areas of the lung. Since perfusion ($\dot{Q}$) and ventilation ($\dot{V}$) are tied together, maintaining $\dot{V}/\dot{Q}$ matching is crucial for proper gas exchange. This mechanism is known as hypoxic pulmonary vasoconstriction (HPV) (72, 116, 153).

Normally, the HPV mechanism serves to avoid large $\dot{V}/\dot{Q}$ mismatches. During lung inflammation, the release of nitric oxide and other inflammatory mediators attenuates the effects of HPV, disrupting normal $\dot{V}/\dot{Q}$ matching and impairing proper gas exchange (40, 79). The excessive release of these mediators can damage lung tissue and disrupt the alveolar-capillary barrier (131), leading to further loss of lung surface area required for gas exchange. HPV varies with species, with rabbits and dogs having the weakest response, and pigs being the strongest responders (2, 41, 154). In humans, the HPV response is strong and can be sustained for hours. Individual responses vary with lung inflammation, systemic vascular disease, and intrinsic variability in pulmonary arterial response to hypoxia (116, 117)

Alterations to $\dot{V}/\dot{Q}$ matching can occur by other mechanisms. Intrapulmonary shunting is when blood is diverted away from normal capillary gas exchange routes. These shunts can be anatomical, such as intrapulmonary arteriovenous shunts (IPAVs), or functional, such as a positive pressure recruitment and shunting of blood to atelectatic or collapsed lung (19). It was shown a few years ago, using bubble contrast echocardiography that IPAVs could be recruited during exercise and hypoxia and impairs gas exchange. While these shunts usually close with age, increases in peripheral pulmonary vascular resistance, due to HPV and smoking-induced changes in peripheral vessels, may potentially reopen these shunts and contribute the worsening hypoxemia experienced in COPD (21, 155).

3.2. CLINICAL SIGNIFICANCE

Chronic Obstructive Pulmonary Disease (COPD)

COPD is a common inflammatory lung disease, affecting the airways, lung parenchyma, and vasculature. Clinically, the symptoms of airway obstruction, such as wheezing, chest tightness, cough, and dyspnea, are common to COPD and other obstructive diseases, such as asthma, but the etiology and pathological features are different. COPD is primarily due to smoking, which accounts for more than 90% of COPD cases worldwide (104, 123). Smoking leads to irritation and inflammation of the lung parenchyma and airways in response to the noxious stimuli, which, in turn, can degrade lung tissue, a process known as emphysema. In addition, the irritation to small airways can lead to thickening and narrowing of the airways and increased mucous production, which cause airway obstruction and symptoms of dyspnea and cough. This progressive narrowing of airways is known as chronic bronchitis (160) and can lead to irreversible airway narrowing. This is in contrast to most asthmatics, who also have a component of airway narrowing but typically respond to treatment (16, 37). Treatment for COPD is limited to symptom management, with both short or long acting bronchodilators in combination with anti-inflammatory therapies designed to reduce airway inflammation and decrease the resistance to airflow (104, 135).

Both features of COPD (emphysema and chronic bronchitis) can lead to impairments in lung function. The Global Initiative on Chronic Obstructive Lung Disease (GOLD) defines COPD progression as a gradual increase in airflow limitation (i.e. the ability to get air out of the lungs). The classification of GOLD stages is based on spirometric assessment of airway obstruction, as shown in Table 1. During expiration, small airways collapse and with narrowing lead to a decrease in forced expiratory volume. The forced expiratory is measure during a 1 sec interval of exhalation, which is denoted FEV_1. This is normalized to the functional vital capacity (FVC) to account for differences in lung volume and respiratory effort. An $FEV_1/FVC < 0.70$ classifies GOLD stage 1 (mild) COPD and this ratio decreases with increasing GOLD stage. Diagnosis with spirometry is usually performed pre and post bronchodilator, as airflow obstruction is not fully reversible with bronchodilation in COPD. However, spirometry alone is unable to completely differentiate between COPD and asthma as there are mixed populations with both reversible airway disease in COPD and irreversible airway disease in asthma (123, 136, 148).

Other spirometric tests include flow volume loops (78) and plethysmographic measurements of lung volume. Flow-volume loop provides visual assessment of obstruction by observing a concave bulge in the exp*i*ratory phase of the curve. From these curves, maximum expiratory flow at 50% FVC (MEF) or within 25-75% of the expiratory phase ($MEF_{25\text{-}75}$) can be used as an indicator of small airway obstruction (Figure 1). Body-box plethysmography is a method of measuring a subjects' lung volume (FRC) using the pressure difference in a sealed box as the person breaths in and out and changes the volume in the box. The determines total lung capacity (TLC) and residual volume (RV) using deep inspiration and expiration breathing maneuvers (29). The ratio of RV to TLC is elevated in COPD patients due to expiratory flow limitations and lung hyperinflation. These whole lung functional measurements have been used in clinic, but with significant variability among disease populations, even among GOLD stages, and with considerable overlap between asthma and COPD phenotypes, distinguishing between groups is still challenging (14, 17, 90).

Pathological Features of Emphysema

One of the primary pathological consequences of smoking-associated COPD is the development of emphysema, defined as enlargement of airspaces due to chronic destruction of lung alveoli. In centri-acinar emphysema (CAE), a subtype of emphysema, chronic inflammation leads to destruction of respiratory bronchioles and vessels leads and degradation of surrounding tissue. On CT, this is seen as dilation of a pulmonary lobule, with loss of surrounding tissue (Figure 2). These dilations usually present as small, scattered, low attenuated areas ("holes") that coalesce into larger areas as the disease progresses. Small pulmonary vessels are usually visible surrounding these dilated air-spaces in normal appearing tissue (47, 161). The loss of lung tissue can lead to low oxygenation and retention of carbon dioxide due to trapped expired air.

Smoking-associated CAE frequently presents in the upper lobes. The reason for this is unknown but West et al. described differences in intra-pleural pressure and high regional stresses in the lung apices as a contributing factor to the mechanical weakening of the alveoli (158, 173). These high apical trans-pulmonary pressures were supported by video-fluoroscopy which was used to evaluate regional parenchymal strain in an upright animal model (69). Other explanations include regional differences in blood flow and zonal differences in lymph flow in the lung apices during smoking-associated inflammation (161).

While CAE is a common component of COPD, only about 25-30% of smokers develop CAE. Environmental exposure to pollutants and genetic predisposition to CAE are additional risk factors and have been recently investigated through the use of genome-wide association studies. The imbalance between proteases and anti-proteases are involved in the pathogenesis of emphysema. For example, genetic variation in matrix metalloproteinases (MMPs) and anti-inflammatory cytokines, such as TGF-β, have been reported in smoking-associated CAE (81, 96, 113). MMPs degrade extracellular matrices between alveolar cells and are elevated in patients with emphysema. TGF- β and related proteins are anti-inflammatory and try to maintain normal alveolar structure. Disruption of these signals can lead to exaggerated tissue destruction (29).

Pulmonary Vascular Dysfunction in Early COPD

There has been increased interest in the role of pulmonary vessels in smoking-associated lung inflammation in early COPD. Smoking and inflammation lead to a reduction in vasoactive mediators, such as nitric oxide, which help vessels relax. Cigarette smoke can also cause localized tissue hypoxia-which can damage small pulmonary arteries (143). Recent evidence suggests that endothelial dysfunction and pulmonary arterial-remodeling occurs early in the pathogenesis of smoking-associated COPD (9, 10). Peinado et al. (124) demonstrated that an influx of inflammatory CD8+ T cells, in the pulmonary arteries of smokers, was associated with impairments to vessel structure and function. In the pulmonary arteries of smokers without disease, pathological lesions, such as thickening of the intimal and muscular layers of the vessel wall, could be identified in smokers with early disease (Figure 3), suggesting that vascular changes precede emphysematous changes (124, 127, 143)

Clinical evidence supports the role of endothelial dysfunction in early COPD. Barr et al. (11) observed that smokers with mild to moderate COPD had impaired flow-mediated dilation (FMD) of brachial artery, which was associated with lower FEV_1 and a higher percentage of emphysema in former smokers. Chronic cigarette smoking is associated with increased arterial stiffness and increased CT percentage of emphysema in former smokers (99, 103, 108), suggesting that inflammation and associated vascular remodeling continues, despite smoking cessation, and contribute to lung function decline.

3.3 QUANITATIVE MDCT IMAGING OF THE LUNG

MDCT Technology

The development of rapid and safe imaging tools has allowed non-invasive methods to assess the structure and function of the lung. These imaging tools have been used to study the pathophysiology of airway and parenchymal lung disease and provide a sensitive image-based assessment of early progression (74, 145, 179). Early volumetric assessment of the lung via CT imaging methods were introduced via the use of a one of a kind system known as the Dynamic Spatial Reconstructor, consisting of a 20 ton gantry, 14 x-ray guns and a juxtaposed hemi-cylindrical fluorescent screen. (67, 75). Advances in spiral CT, introduced by Willi Kalendar and colleagues in the early 1990s, allowed for volumetric imaging of the lung in a single (albeit long) breath hold within a clinical setting (87). The increase in the number of detector rows, known as multi-detector row CT (MDCT), increased acquisition speed from 1s per rotation to 0.37s per rotation for rapid volumetric imaging with contiguous slice spacing and better resolution (74). Advances in MDCT have brought volumetric CT imaging times down to realistic breath-hold durations.

Recent MDCTs utilize 64- and 128-detector rows in second and third generation scanners produced near isotropic spatial resolution (0.6 mm x 0.6 mm in-plane) and temporal resolution of less than a second. In ECG-gated imaging, acquisition and reconstruction can be performed with a temporal resolution ~20msec, fast enough to image at multiple phases of the cardiac cycle (7). The accelerated pitch and table motion of the newest generation scanners, such as the Siemens Definition Flash, allows for whole lung and whole body imaging within a few seconds. Improvements in detector technologies, such as reducing electronic noise and minimizing cross talk between detectors, has improved signal-to-noise ratio to allow diagnostic quality images at a much lower radiation dose (119, 187) .

Recent advancements in multi-spectral CT, such as dual energy CT (DECT), has led to improvements in resolution and a wider lung coverage, which is highly beneficial for functional imaging applications of the lung, such as DECT ventilation and perfusion (see Section 3.3) of the whole lung. Multi-spectral imaging uses more than one set of x-ray sources and detectors (Siemens) positioned around the gantry for simultaneous acquisition at multiple energies, or the use of a single x-ray gun imaging chain pair with the x-ray gun rapidly switched between two energies (General Electric). Energy-sensitive "sandwich" detectors (Phillips Medical) use two layers of detectors, a top layer detector (closest to the source) that absorbs low energy X-ray photons and the bottom layer (furthest from the source) that detects higher energy X-ray photons (46). A copper or tin filter further separates the two layers so more low energy photons are absorbed (i.e. effective energy increases) prior to reaching the bottom detector (8), allowing for better energy separation.

The advantages of the two x-ray gun solution, used in the Siemens scanners, are that tube current can be adjusted for each x-ray tube, resulting in similar noise levels for multi-energy images. Low dose protocols have been explored with comparable image quality to single energy scans but with improved X-ray filtering (46). Some of the challenges of multi-spectral CT include spectral separation of energy sources, which is required for accurate differentiation of materials, such as iodine enhanced blood vs. tissue (100, 130). Developments in photon-counting detectors with photon binning, based on the energy of the incoming X-ray photon, allow for simultaneous acquisition of energies without any spectral overlap, eliminating some of the noise problems associated with current dual energy imaging (110, 144).

Quantitative Volumetric Image Analysis

With the development of high-resolution MDCT and volume-controlled (48) scanning protocols, robust algorithms have been developed to extract structures of the lung from expiratory and inspiratory volume scans (40). Volumetric CT is an accurate way to assess lung volumes and regional lung density. Segmentation of structures, such as airway and vascular trees, lungs, and lung lobes, can be used to quantify lung volumes and regional density (167). The x-ray attenuation (expressed in Hounsfield units: HU), representing tissue densities, can be used to extract air and parenchymal tissue fractions from the lung. Quantitative measures, such as low-attenuation areas (LAA), which measure the percentage of voxels below a defined density threshold, can used to measure "emphysema-like" lung or areas of air trapping. Density thresholds of -950 and -910 HU are used to characterize severe and moderate emphysema on inspiratory scans and -856 HU are used to characterize air trapping on expiratory scans (120, 188).

CT-based airway measurements have provided valuable insight into the variability of airway dimensions due to disease. An airway centerline is extracted from airway tree masks and CT images and radial tracings from the centerline are used to find the airway wall and lumen boundaries in order to compute various airway measures, including cross-sectional area and wall-thickness, at anatomically defined airway branches (133, 167). These measurements have been widely used to show smoking and gender-related differences in airway dimensions and helped characterize asthma and COPD phenotypes based on their airway changes with increasing functional impairment (18, 39, 92).

Essential to this process of reproducible airway and parenchyma assessment is proper lung volume control during scanning (48, 83). To account for inter- and intra-subject differences in volume, image registration has been essential for proper matching of lung regions when evaluating the effects of treatments, studying longitudinal changes, and merging functional and structural image data. The rigid and non-rigid transformations are the two most common registration algorithms. For deformable registration of the lung, a mass-preserving image registration was developed to account for large air volume changes. The registration is based on the assumption that tissue volume changes are minimal with lung expansion and that a voxel-change in density is due to an increase/decrease in air fraction (185, 186). This method has worked well for matching TLC and FRC images, assessing regional lung mechanics (24), and used as an image-based biomarker to differentiate airway vs. emphysema-dominant disease in COPD (50).

3.4 IMAGING REGIONAL PULMONARY PERFUSION

Measuring Regional Pulmonary Perfusion

Early studies for measuring pulmonary perfusion focused on gas exhalation and multi-compartment modeling. West et al. and colleagues developed a technique of measuring concentrations of various exhaled insoluble gases infused in a peripheral vein. For each gas, the concentration in the mixed venous and arterial blood and mixed expired air is used to measure the retention and excretion of gases and derive the $\dot{V}/\dot{Q}$ distribution. This method, known as the Multiple Inert Gas Elimination Technique (MIGET), measures whole lung and regional $\dot{V}/\dot{Q}$ distribution (169, 170). Using this technique, West et al. ascribed regional (or zonal) differences in $\dot{V}/\dot{Q}$ based on gravitational differences in blood flow (i.e "West zones"), as blood would preferentially distribute to dependent (low $\dot{V}/\dot{Q}$) zones because of lower trans-pleural and higher hydrostatic pressures. These zones vary with lung position. For example, in the recumbent (i.e. supine) position, the non-dependent lung is above the heart with the dependent zone is below the heart (169, 176).

The use of radionuclide imaging provided better spatial discrimination of perfusion distribution. Glenny et al. used fluorescent microspheres (FMS) injected into the capillary bed to measure microvascular blood flow in resected lung samples. They found that a major component of perfusion heterogeneity in the lung was due to the structure and branching pattern of the pulmonary vascular tree, which was further enhanced by HPV, which redistributed blood from cranial to more caudal regions (58, 66).

Despite the high spatial resolution of FMS, there was a need for less destructive methods to measure pulmonary blood flow (PBF). Schuster and colleagues developed PET/CT imaging techniques to measure PBF in-vivo in large animal models, which agreed well with previous microsphere techniques (114). Their technique used a constant infusion of radioactive ^{15}O-water and based on a single-compartment model, measured the free distribution of labeled ^{15}O in the blood to estimate regional PBF. The limited resolution of these early PET imaging systems (8-10mm) limited regional assessment of PBF heterogeneity to the lung lobes (62, 114, 168). In a model of acute lung injury, Shuster et al. showed that HPV was inhibited in inflamed lung lobes which had an overall effect of altering blood flow heterogeneity and worsening the $\dot{V}/\dot{Q}$ mismatch (62, 168).

Dynamic Perfusion MDCT

Contrast enhanced high resolution CT imaging and quantitative image analysis have helped transform CT from a tool purely a structural assessment of the lung to quantifying functional measures. The spatial resolution of current MDCT scanners has aided in sensitive quantification of regional PBF. The 4D-dynamic, perfusion CT method utilizes a sharp bolus injection of intravenous contrast. In MDCT, a slab of the lung can be temporally imaged to determine regional PBF and mean transit time (MTT) using indication dilution theory. The theory is based on regionally tracking a central bolus of contrast with time and measuring the attenuation changes in the lung due to contrast in sequential CT images (acquired in axial mode). Based on the height of the time-intensity curve of regions of interest (ROIs) in the lung parenchyma and main pulmonary artery, the PBF and MTT can be derived (70, 178). PBF is the measured rate of delivery of contrast (i.e. blood) in units of milliliters per minute or grams per minute or is normalized to mean PBF of the whole lung, in order to track regional lung variation in PBF throughout the lung slab (25, 178). Similar methods of measuring regional pulmonary perfusion have been adapted for myocardial and cerebral blood flow studies using CT (53, 138, 177) and MRI (20, 64, 151). The MDCT-based perfusion imaging has been used to assess regional PBF has been validated in various animal studies (25, 40, 70, 178, 182). Using perfusion-MDCT, Hoffman et al. demonstrated that in areas of the lung with localized lung inflammation, regional HPV response is blunted and hypothesized that in smokers with parenchymal lung inflammation, the inability to block HPV in areas with inflammation may be a precursory event to developing centri-acinar emphysema (40, 74). Remy-Jardin et al. found a regional association between lung areas with ground-glass infiltrate, representing diffuse parenchymal inflammation, and development of emphysema in asymptomatic smokers with normal pulmonary function tests (PFTs) (134). Evidence for an altered pulmonary perfusion distribution in current asymptomatic smokers came from Alford et al. (3). Using dynamic perfusion CT in two smoking cohorts with normal pulmonary function tests (PFTs), Alford et al. observed that in smokers with a minimal CT evidence of emphysema (“emphysema-susceptible smokers”), perfusion heterogeneity was higher compared to normal PFT smokers without CT evidence of emphysema. The association between early emphysematous lesions and more rapid decline in lung function suggests that these perfusion CT findings and represented quantitative measures serve as sensitive image-based biomarkers linking pulmonary vascular dysfunction and inflammation to early emphysema progression.

Dual Energy CT Perfused Blood Volume (DECT PBV)

Advancements in dual energy CT (DECT) in recent years has made it possible to perform functional imaging studies of the whole lung. DECT utilizes MDCT technology so has the similar spatial resolution as conventional MDCT, and shown great clinical potential for assessing perfusion and ventilation changes in various lung diseases (118, 122, 165). The principle of dual energy (and by extension, multi-energy or multi-spectral) imaging is based on the idea of material separation based on reconstruction of multi-energy images. Materials, such as iodine and calcium, have mass attenuation coefficients that vary with the energy spectrum, as shown in Figure 4a. Iodine content found in intravenous iodinated contrast has better material separation compared to calcium and water due to the additional K-edge effect of iodine, attributed to the photo-electric absorption of photons at low (approximately 30keV) energies (89, 144).

DECT reconstruction generates material-specific images based on basis-material decomposition (38), which assumes the attenuation coefficient for a mixed material (for example iodine and blood in the lung) is a weighted sum of attenuation coefficients of two basis materials. The mass fraction equation is described as follows:

$$\mu_L{}^* f_L = \mu_{1L}{}^* f_{1L} + \mu_{2L}{}^* f_{2L}, \text{ and}$$

$$\mu_H{}^* f_H = \mu_{1H}{}^* f_{1H} + \mu_{2H}{}^* f_{2H},$$

where μ_L, μ_H and f_L, f_H represent attenuation coefficients and mass fractions for the two combined materials at high (H) and low (L) energies, respectively. Similarly, $\mu_{1H}, \mu_{2H}/\mu_{1L}, \mu_{2L}$ represent the attenuation coefficients for basis materials 1 and 2 and $f_{1H}, f_{2H}/f_{2L}, f_{2H}$ represent the mass fractions for each basis material. To calculate the material-specific images of for each material, the decomposition (inverse) equation is solved for materials f:

$$\vec{f} = \overrightarrow{A^{-1}}\vec{\mu} \quad ,$$

where A is the composition matrix of attenuation coefficients $\vec{A} = \begin{pmatrix} \mu_{1L}I & \mu_{2L}I \\ \mu_{1H}I & \mu_{2H}I \end{pmatrix}$ and I is the identity matrix. For multispectral (i.e. three or more sources and detectors) with N-energies and M materials, the composition matrix $\vec{A}$ would be extended to N x M, consisting of N linear mass fraction equations to generate M material-specific images (98).

For contrast-enhanced DECT images, iodine and water are chosen as basis materials. Utilizing an appropriate contrast injection and scan protocol, iodine equilibrates with blood in the lung parenchyma and in the process of image decomposition, the iodine distribution in the lung is calculated, which serves as a measure of pulmonary perfused blood volume (PBV). Similarly, if iodine distribution is known and water is the other basis material, another material can be measured. These virtual unenhanced image (VNC) images represent iodine that has been virtually "subtracted" from the contrast-enhanced image. Figure 4 shows an example DECT PBV and a VNC image from patients with two types of lung disease. The PBV image (Figure 4b) shows areas of consolidation, where compression of pulmonary vessels has limited regional perfusion. In the VNC image (representing water-density image or images where iodine is virtually removed) in Figure 4b, we can see a lung mass with similar lung intensity as a conventional single energy CT in (d). VNC images can be helpful in characterizing soft-tissue structures, like lung masses. Smoothing of the images is usually required for both PBV and VNC images as the reconstruction can lead to increased image noise compared to single energy scans.

Noise-suppression methods with iterative reconstruction (IR) algorithms have helped to improve material separation. The choice of the low and high energies is key to discriminating certain materials (49, 162) but the noise of the images can vary with size of the patient (61). Second generation DECT systems, such as the Siemens Definition Flash, typically use a 140 kVp high energy x-ray source with tin filter and a and a low energy source (80 or 100 kVp, kVp is peak kilovoltage).

Typical scanning protocol to obtain higher contrast enhancement utilizes the 80 and 140 kVp, but for larger patients a 100 kVp low energy source may produce images with lower noise (94). The addition of photon-counting detectors, which can bin photons base on their energy, will help better separate materials at a much lower radiation dose and with better signal-to-noise ratio (33, 98, 137).

Table 1. Global Initiative for Chronic Obstructive Lung Disease (GOLD) Classification for the staging of COPD. Spirometry measurements are post-bronchodilator responses and in COPD subjects will demonstrate an airflow limitation that is not fully reversible.

	Stage	Spirometry
Mild COPD	I	$FEV_1/FVC < 70\%$ & $FEV_1 \geq 80\%$
Moderate COPD	II	$FEV_1/FVC < 70\%$ & $50\% \leq FEV_1 < 80\%$
Severe COPD	III	$FEV_1/FVC < 70\%$ & $30\% \leq FEV_1 < 50\%$
Very Severe COPD	IV	$FEV_1/FVC < 70\%$ & $FEV_1 < 30\%$

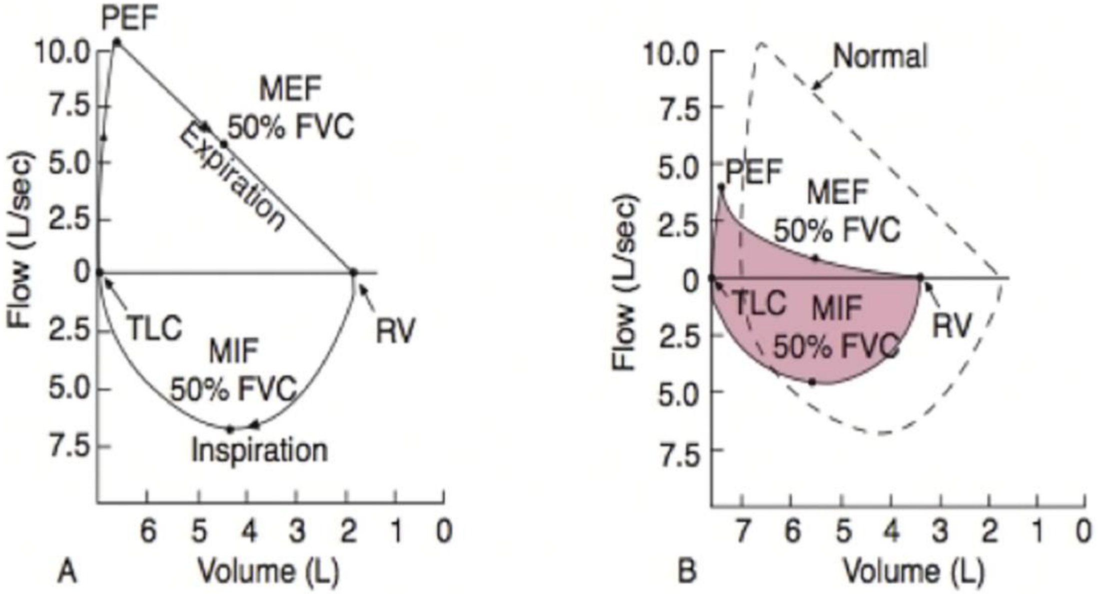

Figure 1: Flow-volume loop in a normal subject (a) and a subject with COPD (b) in red. Maximal expired flow (MEF) and volume of expired are reduced and total lung capacity is increased due to air trapping. This type of loop helps in the diagnosis of obstructive airway diseases, such as COPD and asthma.

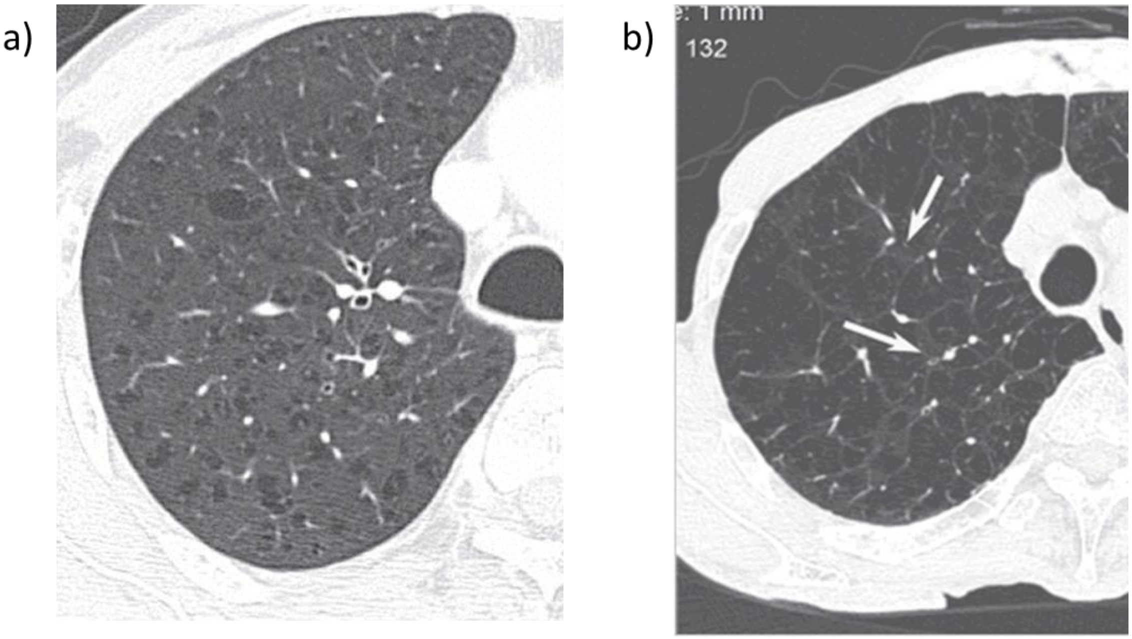

Figure 2: (a) Example of a HRCT of a patient with early centri-acinar emphysema (CAE) in the upper lobes, showing dilated airspaces (low attenuation areas). (b) A patient with advanced CAE, showing diffuse disease and loss of normal tissue except around small vessels (arrow). Also visible are the septal wall thickening, where normal tissue is compressed by dilated airspaces. Adapted from (161).

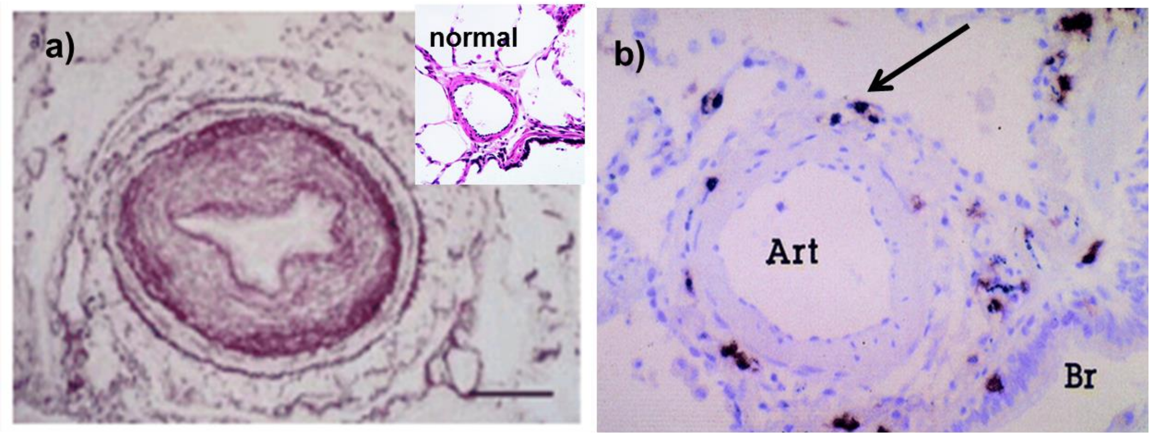

Mild COPD smoker **CD8 T cells in the vessel wall**

Figure 3: Biopsy of a small pulmonary artery from a smoker with mild COPD, showing intimal thickening and narrowing of the vessel lumen. Shown in the inlet is a normal pulmonary artery of similar size, with no wall thickening. (b) Inflammatory cells, such as the stained $CD8^+$ T cells (arrow) are observable in the thickened vessel wall (Art, arterial, Br, bronchiole). Adapted from (124).

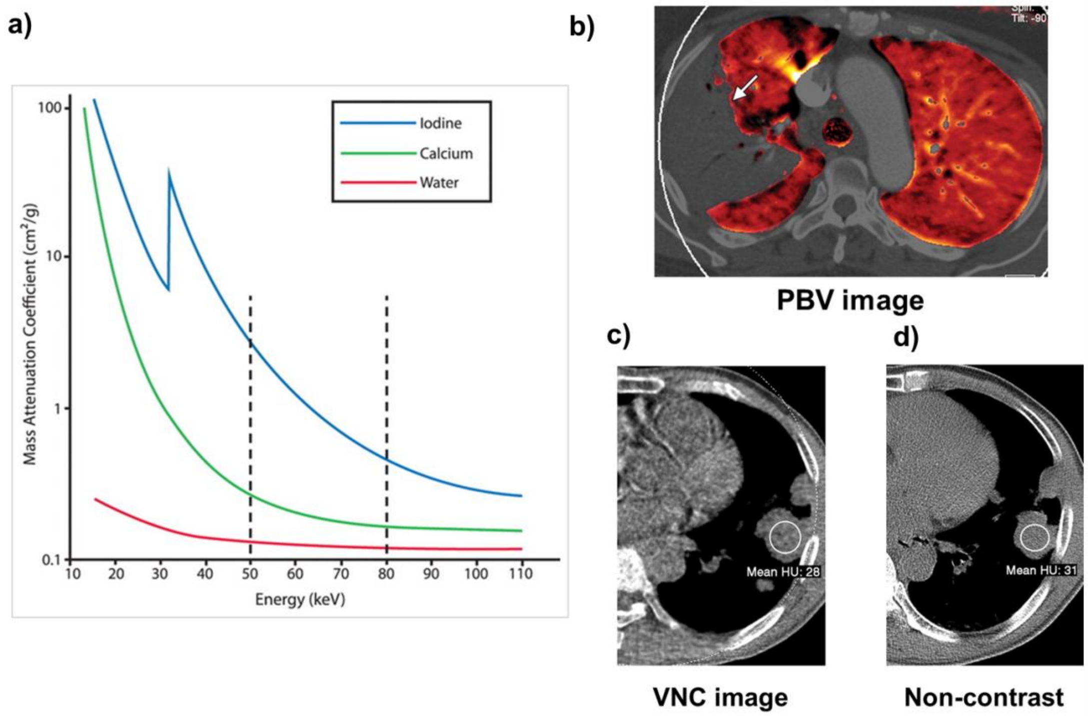

Figure 4: (a) Mass attenuation coefficients for iodine (blue), showing a larger difference at 50 and 80 kV compared to calcium (such as in bone) and water. This is due to the added K-edge effect due to photoelectric absorption of photons (b) Example DECT PBV image from a patient with consolidation (arrow), showing areas where there is a lack of perfusion. Example VNC (c) and non-contrast (d) images from a patient with a lung mass, showing that VNC images can produce similar mean intensity as the non-contrast images. Adapted from (89).

CHAPTER 4: ANIMAL STUDIES: MEASURING PBV AND PBV HETEROGNEITY IN A MODEL OF HYPOXIC PULMONARY VASOCONSTRICTION

4.1 RATIONALE

Dual energy multi-detector CT (DECT) perfused blood volume (PBV) is a functional imaging method that is gaining importance in the clinical assessment of lung diseases (22, 109) This imaging technique has also circumvented many of the technical difficulties associated with conventional perfusion CT methods, including central line placement, cardiac-gating to measure contrast kinetics, and prolonged breath holds, making its transition to clinical and multi-center studies (25, 35). However, there have been few studies done in patients with pulmonary disease and those studies that have published DECT PBV results have largely focused on relative measures (low or high PBV enhancement) and failed to quantify how these measures relate to underlying pulmonary physiology, since patient populations have diverse cardiac and/or pulmonary conditions (115, 118, 142).

As Fishman and Milnor et al. explained nearly 40 years ago, alterations to pulmonary blood flow, and by extension PBV, are a direct effect of hemodynamic changes from left and right heart (45, 112). Therefore, there is added value in developing quantitative methods to help measure pulmonary blood volume and evaluating them in context of the underlying pulmonary physiological changes in patients. To validate the DECT PBV measures, Fuld et al. showed that regional DECT-based PBV measures served as a surrogate measure for dynamic, contrast-enhanced perfusion CT measures (mean transit time and pulmonary blood flow) in an animal model of varying airway pressure and regional pulmonary perfusion (50). Two measures, mean PBV and PBV coefficient of variation (131), a measure of spatial heterogeneity, are of particular relevance to studying pulmonary vascular dysfunction in early COPD. As Alford et al. (3) showed with her CT perfusion study in smokers, perfusion heterogeneity is increased in smokers with early centri-acinar emphysema (CAE). If this increased perfusion heterogeneity is due to patchy inflammation and increased peripheral vasoconstriction (mediated by hypoxic pulmonary vasoconstriction, HPV), we are interested in adapting the initial DECT PBV studies by Fuld et al. (50)to human studies of CAE-susceptible smokers, studying pulmonary vascular response to sildenafil.

With our motivation of extending this initial DECT work of Fuld et al. (50), we developed an imaging protocol and analysis method for measuring regional PBV changes in a pig model of HPV. With the known physiological alterations caused by HPV, including increases in mean pulmonary artery pressure, we evaluated the sensitivity of our regional lung PBV measures to changes in pulmonary artery pressure in our model to determine which measures would be suitable to evaluate the regional response to sildenafil in our human studies in Chapter 5.

4.2 METHODS

Animal Preparation

The University of Iowa Animal Care and Use Committee approved all animal studies. Six laboratory-bred pigs were pre-anesthetized intramuscularly with ketamine (20 mg/kg), xylazine (2 mg/kg), and acepromazine (0.2mg/kg) and anesthetized during surgery with 3-5% isoflurane by nose cone inhalation. A tracheostomy was performed, an endotracheal tube was placed for mechanical ventilation, and carotid arterial and external jugular catheters were placed for blood pressure monitoring, drug administration and IV contrast injection. During scanning, anesthesia was maintained with intravenous infusion of propofol (0.1-0.2 mg/kg/min). A paralytic agent (0.1-0.2 mg/kg IV bolus of pancuronium or 1-1.5mg/kg IV bolus of rocuronium) was given to prevent spontaneous breathing during scanning. Supplemental oxygen was provided during surgery but the animal was switched to room air (FiO_2 = 21%) ventilation during the course of imaging. Tidal volumes were kept at 10-12ml/kg with occasional deep inspirations to 25 cm H_2O airway pressure in order for alveolar recruitment. Arterial blood pressure (ABP), oxygen saturation, and airway pressures (P_{awy}) were continuously monitored and recorded during the hypoxic and normoxic interventions. Cardiac output (CO) and pulmonary artery pressure (PAP) were measured using a Swan-Ganz transpulmonary thermodilution catheter (Edwards LifeSciences, Irvine CA) after each intervention. Arterial and venous blood gases were measured using a portable blood gas analyzer (Irma TruPoint).

CT Imaging

Imaging was performed on a second-generation dual-source, dual energy CT scanner (Somatom Definition Flash, Siemens Medical). The scanner consisted of a low energy (Tube A: 100 kvP, where kVp = peak kilovoltage) and high energy (Tube B: 140 kVp) x-ray sources. Tube currents were adjusted for each X-ray source was adjusted so radiation output would be similar between sources. The total CT dose index ($CTDI_{vol}$), a radiation dose equivalent measure, for each DECT scan was 11.7 milliGrey (mGy), similar to a clinical DECT scan. Images were acquired while the animal was supine and breath held with a peak airway pressure (P_{awy}) of 5cm H_2O. We chose to image with the animals in the supine body posture due to surgical convenience and to mimic clinical imaging studies. A positive end expiratory pressure (PEEP) of 5cm H_2O was applied to the ventilation circuit with occasional recruitment breaths to avoid progressive atelectasis in the lungs. PBV imaging was carried out at this airway pressure to avoid flow reductions in the gravitationally non-dependent lung, which occur at higher $P_{awy.}$ A weight-based (2cc/kg) amount of iodinated contrast (Isovue 370, Bracco Diagnostics, Inc) was injected in the external ear vein at an infusion rate of 4ml/s. Prior to imaging PBV, a test bolus scan was performed using a 30 mL of contrast, injected in the ear vein. The bolus measured the time for the contrast to equilibrate with the blood pool in the lung. We used a region of interest in the right atrium to measure the intensity change as contrast entered the right side of the heart (before entering the lungs), using a threshold of 100 Hounsfield units (HU). The time that the contrast bolus took to reach the atrium, from start of the test bolus to the peak intensity was between 10-12 seconds for each animal. This was used as the delay before the start of acquisition. Total imaging time, was approximately 20 seconds, including the scan delay from the test bolus.

Assessing PBV Changes to Alveolar Hypoxia and Sildenafil

We altered regional PBV by lowering alveolar oxygen in the breathing circuit and inducing hypoxic pulmonary vasoconstriction (HPV). Nitrogen gas was added to the oxygen-gas mixer; and FiO2, measured in the inspiratory wing of the ventilation circuit, was titrated between 12-15% (hypoxic breathing). An increase of PAP of at least 5 mmHg was used to confirm activation of HPV. After approximately ten minutes of hypoxic breathing, a second PBV scan was performed, while maintaining hypoxia. The animals were then switched over to room air for 10 min to recover, after which a decrease in PAP was measured. We attempted to reverse hypoxia-induced increase in pulmonary physiology with sildenafil (10mg IV), a phosphodiesterase-5 inhibitor known to reverse HPV in humans (13, 77). The animals breathed room air for 30 min while sildenafil was administered and then were switched over to hypoxic air for ten minutes for the final DECT PBV scan under hypoxia.

Measuring Regional PBV

The dual energy decomposition algorithm was used to generate the raw PBV map representing the iodine density distribution in the lung (23) Mean PBV was normalized to iodine concentration in the pulmonary artery (PA) to account for differences in contrast amount (PBVnorm). We sampled the PA in first and second-generation branches, since this represented areas of full contrast mixing entering into the lung. As there were differences between animals in the amount of contrast used for each scan (and therefore the amount of iodine and the change in intensity in the PA), we tested if PBV values measured in the PA closely matched true iodine concentration. We imaged a series of syringes filled with varying concentrations of iodinated contrast (0-35 mg/mL), as shown in Figure 5a, to simulate the concentrations we would measure in the PA. As seen in Figure 5b, the measured iodine concentration, computed from the three-material basis decomposition, closely matched the true iodine concentration (in mg/ml). When we looked at the PA PBV values for the five animals, they correlated with the measured concentration of the syringe phantoms (Figure 5c). Thus, when we report normalized PBV (PBVnorm) in the parenchyma, we are reporting it as a percentage of pure iodinated blood.

Figure 6 outlines the process for obtaining regional PBV and coefficient of variation (CV), a measure of the spatial heterogeneity of blood flow, from DECT images. The PBV images were normalized to iodine concentration in the PA, and divided into 30 by 30 by 40 voxel regions, approximating 2mm^3 voxels, and PBV and CV was computed for each region. Histograms of these CV regions were used to measure the CV statistics, including mean and mode of the CV. Curve fitting was performed using a two component Gaussian distribution CurveFit Toolbox Matlab v. 7.14, Mathworks, Inc.). Additionally, lung PBV and CV were evaluated in the ventral-to-dorsal direction by dividing the lung into thirds and computing average PBV and CV in the gravitationally non-dependent (ND), middle (M), and dependent (D) lung zones.

CT-Based Assessment of the Central Pulmonary Vascular Tree

Since hypoxia-induced vasoconstriction works predominantly in the peripheral arterioles in the pulmonary circulation, we surmised that global alveolar HPV would lead to enlargement of central arterial tree via peripheral vasoconstriction, and could be detected using quantitative imaging techniques of the central arterial tree. We measured central pulmonary arterial volume from segmented pulmonary vascular trees. We used Apollo software (VIDA Diagnostics; Coralville, Iowa) to obtain initial vessel segmentations from the 140 kVp single energy images; this initial segmentation was refined using a vessel smoothing operation to preserve vessel boundaries (51). The vessel masks, including arteries and veins, were used to measure total pulmonary vascular volume (TPVV). Additionally, the pulmonary arteries were separated from the pulmonary vascular tree using an algorithm to separate iso-intense objects (51). A user placed seed points (~30-40) in the main branches of the pulmonary artery (A) and vein (V) and the two objects (arterial and venous trees) were grown iteratively while still preserving the boundary between them. Figure 7 diagrams the process from initial seed point placement in the vessel segmentation to arterial tree separation, utilizing the vessel segmentation. The A/V separated tree was then used to measure total pulmonary arterial volume (TPAV) from the 140 kVp image.

Image and Statistical Analysis

Physiological data, including ABP, O_2 saturation, end tidal CO_2, and heart rate was measured continuously over the duration of study. PAP was measured 10 min prior to the designated intervention (hypoxia or sildenafil) and CO was measured during normoxia, hypoxia and sildenafil and averaged from triplicate readings.

Whole lung PBV, mean CV, as well as regionalized PBV and CV in the nondependent and dependent lung and the CV mode (computed from the regionalized CV map) were averaged for the five animals and expressed as a mean ± standard deviation (SD). PBV and CV comparisons (normoxia vs. hypoxia, pre and post sildenafil) was compared using one-way ANOVA with repeated measures and a post-hoc analysis (R v. 3.1.1) to adjust for multiple comparisons, using a P value of 0.05 for significance. Regression analysis of PBV, CV, and TPAV and changes with PAP changes was performed using R statistical toolbox (R v. 3.1.1).

4.3 RESULTS

Physiological Data

Table 2 shows physiological and hemodynamic data for the five animals studied. Because, by design, we reduced alveolar FiO2 until we observed an increase in pulmonary arterial pressure, the mean hypoxia-induced mean increase in PAP of 6 mmHg was significant ($p<0.05$). Post sildenafil, the mean PAP changes also increased (9mmHg), which were surprisingly greater than the pre sildenafil hypoxia-induced PAP increase but not significantly different. While sildenafil did not reverse the hypoxia-induced increases in PAP in these animals, the primary goal of this study was to track the relationship between changes in hemodynamic measures and the changes in regionally assessed DECT PBV and CV measures.

The ABP decreased after sildenafil ($p<0.05$) but recovered to pre sildenafil baseline level during the last PBV scan. The SpO_2 remained above 90% during hypoxia pre sildenafil. After sildenafil, SpO_2 fell to 85% but was not significantly different from pre sildenafil SpO_2. Compared to the start of the study, arterial pO_2 significantly decreased (30 mmHg) and end-tidal CO_2 increased (48 ppm) during the last hypoxia scan (Table 2).

HPV Causes Reciprocal Changes in DECT-Computed Regional PBV and CV

Hypoxia caused a near-significant ($p=0.06$) decrease in PBVnorm that was evident more- in the gravitationally dependent lung. Figure 8 (top panel) illustrates the regional PBV decreased with hypoxia, here shown in the gravitationally dependent (dorsal) portion of the lung. Table 3 summarizes the PBV changes with hypoxia, showing a similar magnitude of decrease in PBV in both dependent and whole lung.

Figure 9a shows an example of the regional distribution of CV in the lung, represented as a CV map. A visibly heterogeneous pattern of regional CV is observed throughout the lung, suggestive of patchy HPV-related perfusion distribution. We analyzed whole lung CV and CV in the non-dependent (ventral) and dependent (dorsal) lung. The mean CV for the whole lung demonstrated a near-significant increase ($p=0.06$); although the non-dependent (ND), with higher noise and standard deviation, did not significantly differ from baseline; the CV in the dependent lung (Table 3) significantly increased with hypoxia ($p<0.05$).

Sildenafil Increased Baseline PBV but Does Not Reverse HPV-Induced Increase in PBV Heterogeneity

Both PBV and PBVnorm significantly increased with sildenafil. Figure 8 (bottom panel) shows regional PBV enhancement with sildenafil, compared to baseline normoxia. The mean CV did not change with sildenafil during normoxic breathing. Re-exposing animals to hypoxia (i.e. post-sildenafil hypoxia), caused a similar decrease in PBV and increase in mean CV as pre-sildenafil hypoxic exposure, more so in the dependent lung ($p<0.05$) (Table 3). The CV mode, representing the majority of CV regions in the histogram represented by Figure 9a, displayed a right shift towards greater CV after hypoxia pre and post sildenafil. This is represented by the histogram in Figure 9b.

DECT-Based PBV and CV Are Sensitive to Changes in PAP with Hypoxia

Since sildenafil did not completely reverse HPV but rather increased baseline PBV, we pooled the pre and post sildenafil data to look at how PBV and CV changed with PAP pressure changes during hypoxia. Figure 10a-b shows the relationship between DECT PBV measures and PAP. The normalized PBV (Pearson's rho = -0.67, $p<0.01$) negatively correlated with PAP but the non-normalized PBV did not (Pearson rho = 0.08, p= n.s.). As expected, the DECT-computed CV and TPVV positively correlated with the increased PAP due to hypoxia (Pearson's rho = 0.49, $p<0.05$) (Figure 10c-d). Additionally, regression analysis of the change in mean CV with the change in mean PAP revealed a strong inverse correlation (Pearson's rho = 0.91, $p<0.01$) (Figure 11a). There was no relationship between PAP and PBVnorm change pre or post sildenafil (data were not significant and are not shown).

Hypoxia-Induced PAP Increases Associate with Central Arterial Enlargement

The TPVV positively and significantly correlated with the PAP increase with hypoxia (Pearson's rho = 0.49, $p<0.05$). We looked specifically at central arterial volume change, since HPV predominantly affects pre-capillary arterioles (65), to determine if measurement of TPAV would be sensitive to changes in PAP. Similarly to CV, there was as positive correlation between TPAV change and PAP change (Pearson's rho = 0.67, $p<0.05$) (Figure 11b). The vascular volumes (TPVV and TPAV) increased both with hypoxia but only the TPAV increase was significant (Figure 12), suggesting that measures of central arterial enlargement (i.e. arterial central volume increase) reflects downstream (arteriolar) vasoconstriction due to hypoxia.

4.4 DISCUSSION

This study highlighted that use of DECT-based PBV and PBV heterogeneity (131) as a sensitive measure to study changes in regional PBV and PBV heterogeneity accompanying changes in pulmonary artery pressure in a relevant animal model of HPV. Under a careful PBV imaging protocol, with control for contrast delivery and scan timing, we showed that DECT- based PBV and PBV heterogeneity strongly associated with PAP increase during hypoxia. The PAP increased 6-7 mmHg pre and post sildenafil, confirming activation of hypoxic vasoconstriction (HPV). The negative association between PBVnorm and PAP and the positive correlation between PAP and mean CV suggest HPV reduced distal parenchymal blood flow and increased PBV heterogeneity.

The DECT PBV and CV are two measures of blood volume distribution that are similar to regional PBF measures outlined by Chon et al (25, 178). Fuld et al. demonstrated a direct correlation of DECT-derived PBF and PBV (50) under normal range of perfusion. In this study, we showed that changes in these regional lung measures captured the known physiological and hemodynamic changes with hypoxia. Certain measures, such a PBV, required normalizing to pulmonary iodine concentration to account for contrast accumulation in the lung. Our time-to-scan was coordinated to match the time for steady-state iodine equilibration within the pulmonary blood pool. While it was expected that PA intensity would increase with the addition of contrast for repeated scans, we observed that PA intensity did not vary greatly between scans in the same subject. Rather, PA intensity differed between animals, which is why we chose it to normalize PBV in the lung. Lung volume differences between scans, which could have affected the distribution of PBV (and therefore CV), were negligible as lungs were positively ventilated and recruited between scans to avoid atelectasis.

Coefficient of variation (131) has been used widely to quantify blood flow heterogeneity (15, 57). CV can vary with image noise, particularly near the heart border, where contrast-related artifacts are present in the ventral lung. This may explain why CV in the non-dependent (ventral) lung did not show any significant differences. The CV mode, representing the majority shift in heterogeneity, was less-susceptible to image noise and demonstrated similar changes to hypoxia and sildenafil as the dependent lung zone.

HPV-induced changes in PAP reflect changes in total pulmonary vascular resistance (84). It is a heterogeneous process, with multiple regions of the lung simultaneously constricting and dilating. The change in CV was more sensitive to HPV-induced changed in PAP than PBV. The inverse relationship between the change in CV and change in PAP suggests that animals had a varied response to HPV, but that in animals with a more robust HPV response (and greater PAP increase), there was a uniform constriction of peripheral pulmonary vessels. Since lungs were uniformly exposed to hypoxia, it is possible that uniform vasoconstriction throughout the lung would minimally effect overall CV. Figure 13 illustrates this with an example from two animals with similar PBV change with hypoxia; one animal had a large increase in PAP with hypoxia and a minimal change in CV (uniform CV distribution) and another animal had a moderate PAP increase and a large shift in CV (more heterogeneous CV distribution). With regional lung inflammation or edema, the change in the regional distribution of PBV (and CV) would likely alter this relationship, by regionally inhibiting or enhancing the HPV response (40, 76, 168).

We are the first to report the direct correlation between PAP and DECT-based CV. A previous study by Miura et al (115), using DECT PBV imaging, did not observe a relationship between PBV heterogeneity and pulmonary artery pressures, which could have been due to several factors. The study did not account for subject-specific differences in contrast timing or because a saline chaser was used during scanning, which could have affected regional PBV signal. They also utilized data from both the first generation Siemens DECT scanners, which had considerable reconstruction artifacts from beam hardening and scatter (61, 89).

Treatment with sildenafil, a phosphodiesterase inhibitor, had limited efficacy in our model to reverse HPV and reduce PAP. Studies on the effects of sildenafil on pulmonary vasodilation in pigs have been limited. Sildenafil partially reverses HPV in dogs (44) but because it causes systemic hypotension in animals and humans, we limited our dose to 10 mg IV (~0.3 mg/kg). This was similar to the dose given by Tessler et al. in newborn pig model of HPV (163). The increased end tidal CO_2 and increasing acidosis during the last PBV scan may have enhanced HPV response in these pigs and blunted sildenafil's effects on reversing PAP. Our main goal was to track changes in PBV and CV with changes in PAP rather than show physiological inhibition of HPV with sildenafil.

We also chose to image supine to simulate clinical imaging studies. Hlastala et al. observed that HPV response depends on lung position in pigs, with the supine position having more heterogeneous HPV response throughout the lung compared to the prone position (66, 154). Our intention was not to show physiological inhibition of HPV with sildenafil but to track changes in our regional PBV measures with alterations in baseline vascular tone and regional perfusion, evidenced by the increased mean PBV and decreased CV.

This similar response to hypoxia pre and post sildenafil allowed us to pool our TPAV data. Our observation that the greater the PAP increase with hypoxia, the greater the increase in TPAV suggest that changes to central arterial geometry is a sensitive measure to reflect downstream changes to vascular resistance in this model. Enlargement of pulmonary arteries has been associated with COPD with resting pulmonary hypertension, resulting from pulmonary vascular disease and increase in pulmonary vascular resistance (82, 172). The combined regional PBV heterogeneity and TPAV measures were helpful in linking hypoxia-induced structural and functional alterations occurring within the lung.

4.5 SUMMARY

DECT PBV imaging helps visualize both structure and functional changes in the lung (97, 122, 165) with high spatial resolution. Studies showing the direct correlation between DECT-derived measures of PBV and simultaneously measured physiologic variables are limited. Changes in PBV distribution due to hypoxia are a dynamic process, incurring both temporal and spatial changes to blood flow (4), vascular compliance, etc.; however, DECT-based PBV/CV provide a snapshot of these changes and we demonstrate that functional measures, particularly PBV heterogeneity and structural measures (TPAV) is sensitive to PAP changes in a simplified but clinically relevant model of HPV.

Our analysis suggests that geometric measures of central arteries coupled with PBV, as an index of peripheral vascular function, may be sensitive markers of early rather than later pulmonary vascular dysfunction in lung diseases. In the next two chapters (Chapter 5 and 6) we apply the imaging and analysis methods, outlined in Chapter 4, to CAE-susceptible and non-susceptible smokers to determine if PBV heterogeneity, a marker of early vascular dysfunction, is reversible with sildenafil. We expand on the idea that central artery analysis can differentiate between these two cohorts. By developing a more sensitive and direct measurement of central arteries, we provide evidence to support that in CAE-susceptible smokers, upstream dilation of central arteries likely reflects the increased peripheral pulmonary vasoconstriction and is reversible with sildenafil. From these initial findings in a simplified animal study, the next two chapters link structural and functional changes in this unique cohort of early progressed smokers.

Table 2: Physiological vitals during each intervention. Mean PAP is reported as an average of 2-5 min interval recordings when the Swan-Ganz catheter was placed in the pulmonary artery. CO is average of triplicate readings after each intervention. ABP, mean arterial blood pressure; CO, cardiac output; EtCO2, end tidal CO2; HR, heart rate (beats per minute); PAP, mean pulmonary arterial pressure; SpO2, pulse oxygen saturation; pO2, arterial partial pressure oxyen; pCO2, arterial partial pressure carbon dioxide.

N = 5	Pre sildenafil		Post sildenafil	
	normoxia	hypoxia	normoxia	hypoxia
SPO_2 (%)	96.9 ±2.4	90.7±8.6	94.1±2.9	84.5±12.8
HR (bpm)	86.8±8.2	104.3±17.7	109.3±29.0	113.3±32.5
ABP (mmHg)	93.4±8.3	86.9±14.9	76.9±10.4	83.8±15.7
PAP (mmHg)	18±3.7	25.2±3.7*	16.6±3.4	$25.4\pm5.7^{\#}$
CO (L/min)	4.6 ±2.2	4.6 ±3.0	5.8±3.2	6.0 ±3.2*
$EtCO_2$	37±4.7	41±5.3	42±8.4	48±7.9*
pO_2 (mmHg)	201.7 ±192.9	68.8 ± 64.8	72.8 ±26.5	31.0±4.4*
pCO_2 (mmHg)	39.1±6.6	42.8±10.3	43.6±10.2	56.3±7.4*
Ven pO_2 (mmHg)	55.8±10.8	30.7±10.5*	52.3±8.8	29.3±11.3*
Ven pCO_2 (mmHg)	45.7±16.2	50.5±10.3	52±13.2	57.9±14.0

Table 3: DECT-based PBV and CV measures for the whole lung and in the gravitationally dependent (D) and non-dependent (ND) lung region. PBV, raw, non-normalized PBV signal; PBVnorm, normalized PBV; *p<0.05 vs. pre-sildenafil normoxia; [#]p=0.06, vs pre-sildenafil normoxia; [&]p<0.05, vs. post sildenafil normoxia; p-value adjusted for multiple comparisons.

N = 5	Pre sildenafil		Post sildenafil	
	normoxia	hypoxia	normoxia	hypoxia
PA HU	287.1	300.4	291.3	297.7
PBV (HU/cm^3)	80.0±8.4	78.2±6.0	96.5±9.4*	98.3±22.9
PBVnorm	0.17±0.07	0.15±0.07[#]	0.20±0.08*	0.16±0.07
PBVnorm (ND)	0.11±0.05	0.09±0.05	0.12±0.06	0.11±0.06
PBVnorm (D)	0.22±0.08	0.20±0.08*	0.26±0.10*	0.21±0.10[&]
Mean CV	0.37±0.05	0.43±0.09[#]	0.39±0.07	0.42±0.06
Mean CV (D)	0.22±0.04	0.26±0.06*	0.22±0.04	0.24±0.04
Mean CV (ND)	0.50±0.07	0.55±0.14	0.51±0.08	0.54±0.07
CV mode	0.13±0.02	0.16±0.02*	0.11±0.02*	0.13±0.02

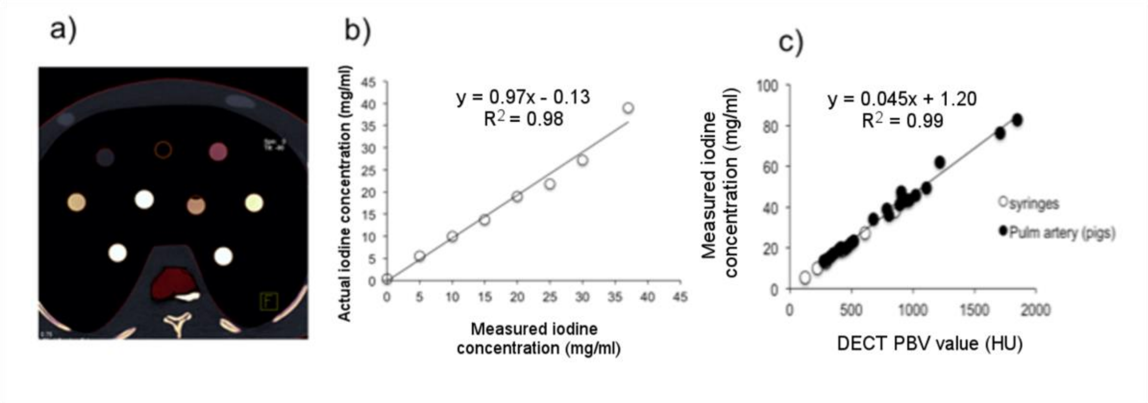

Figure 5: DECT Iodine calibration using syringe phantoms. (a) Screenshot of DECT-computed iodine concentrations in the various syringes filled with iodine ranging from 0 (water) to 35 mg/ml. (b) DECT measured iodine concentration agreed well with true concentrations (R^2 = 0.99). (c) Sampled pulmonary artery from the 4 DECT scans per animal, showing linearity between measured iodine concentrations and PBV value (HU).

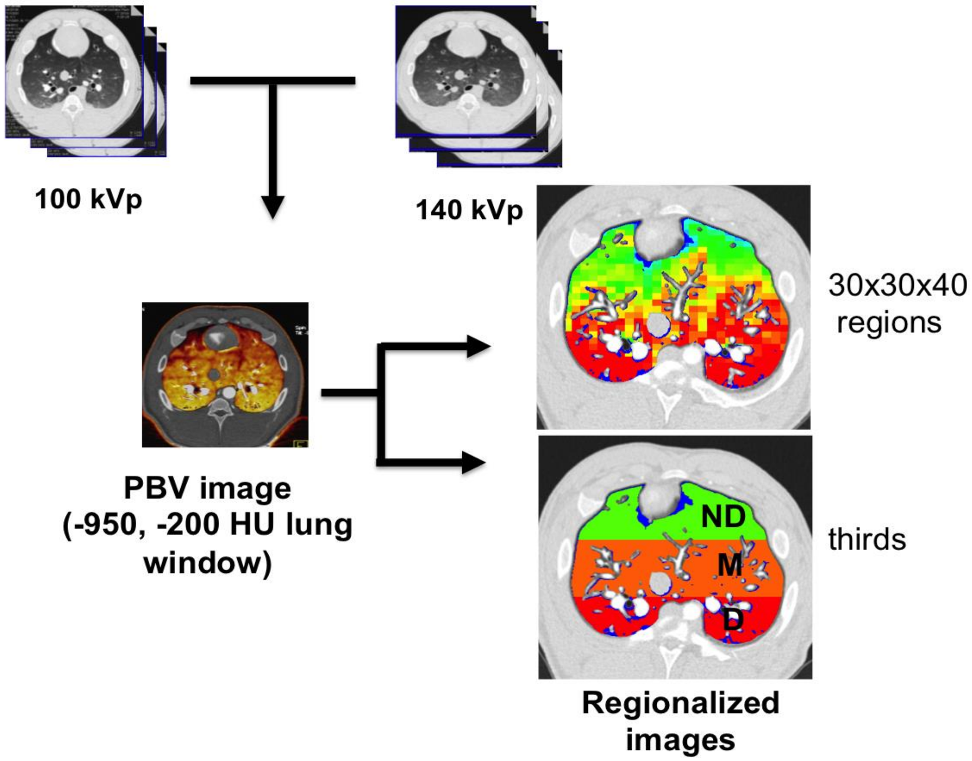

Figure 6: Schematic describing the process of generating and analyzing PBV images. DECT images 100 kVp and 140kVp, with equal enhancement of arteries and vein. The two images were run through Siemens Syngo DECT workstation to compute PBV images. We used Siemens' suggested values for soft tissue HU and contrast material (CM) ratio (lung window: -950 to -200 HU, CM=2.24, soft tissue = 55 HU). PBV images were then regionalized, using in-house software, into 30x30x40 regions to compute regional PBV and CV and then regionalized into thirds (ventral-dorsal direction) to measure gravitationally dependent and non-dependent PBV and CV.

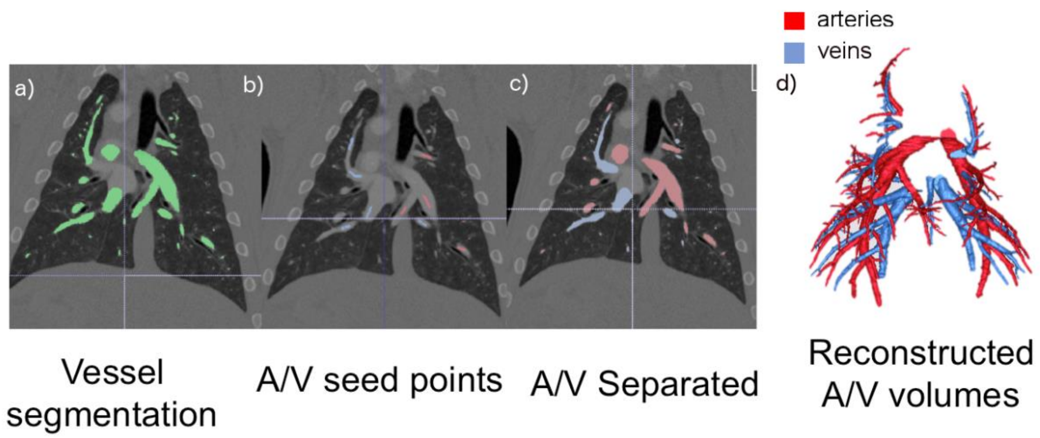

Figure 7: Diagram describing artery (A) and vein (V) separation process. (a) The segmented vascular tree is generated from the 140 kVp single energy image using Apollo software (VIDA Diagnostics; Coralville, IA) and extended using vessel smoothing operation to preserve vessel boundaries. (b) Artery and vein seed points (blue and red) were placed in the central vessels. (c) A and V were separated using morphological algorithm in (39). (d) Reconstructed A and V trees were used to compute TPAV and TPVV (veins + arteries).

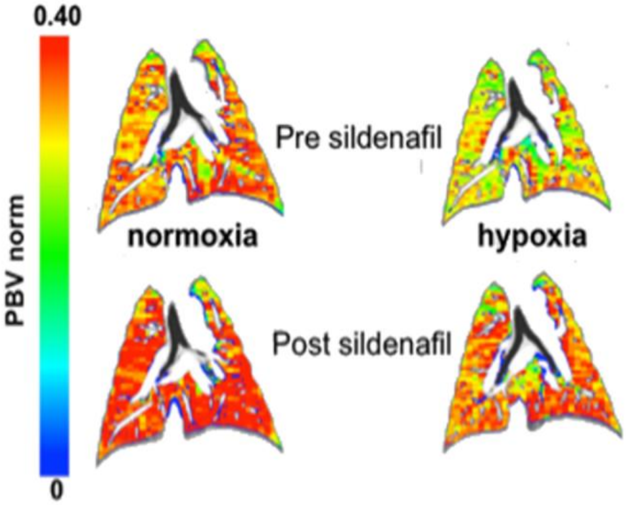

Figure 8: Regional DECT-based PBV changes with hypoxia and sildenafil. Example DECT PBV images, normalized to pulmonary artery intensity and regionalized into 30x30x40 voxel regions. This coronal slice was taken in the more dependent (dorsal) region of the lung, with the animal supine on the scanner. While sildenafil did not reverse HPV-induced PAP increase, it did increase PBVnorm compared to baseline.

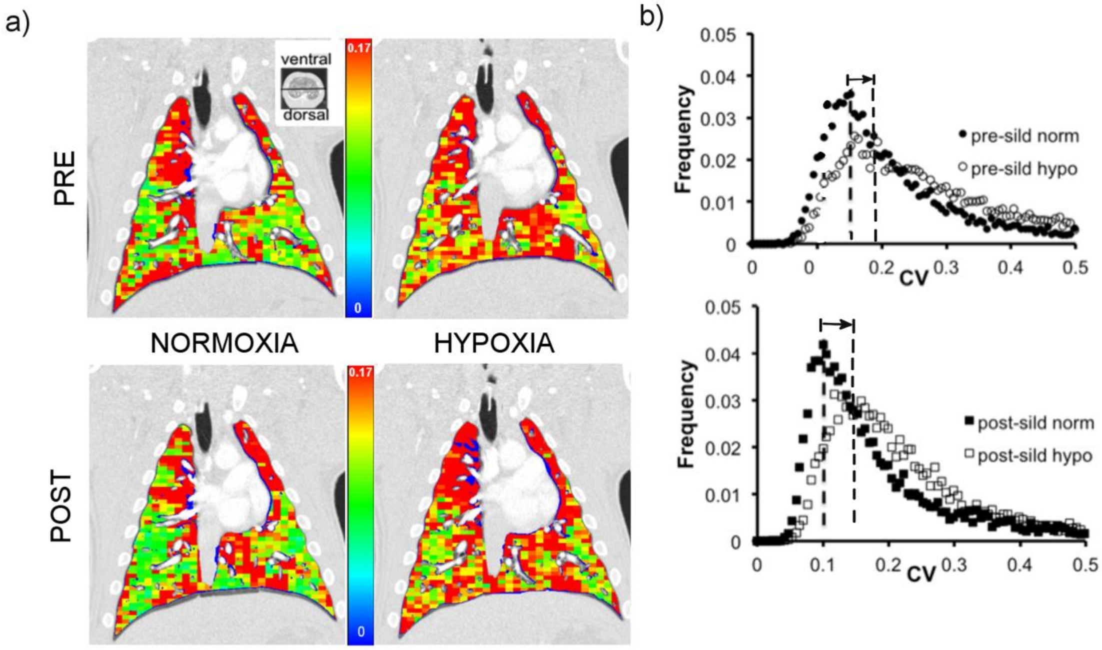

Figure 9: Regional DECT-based CV changes with hypoxia and sildenafil**.** (a) Example of regionalized CV image (30x30x40 regions, ~2mm^3) sliced in coronal view. Horizontal black line on gray-scale image shows relative location of slice in ventral-dorsal direction. (b) Histogram of the regionalized CV image used to compute CV mode. Hypoxia increased CV mode pre and post sildenafil (arrow showing left to right shift in CV mode).

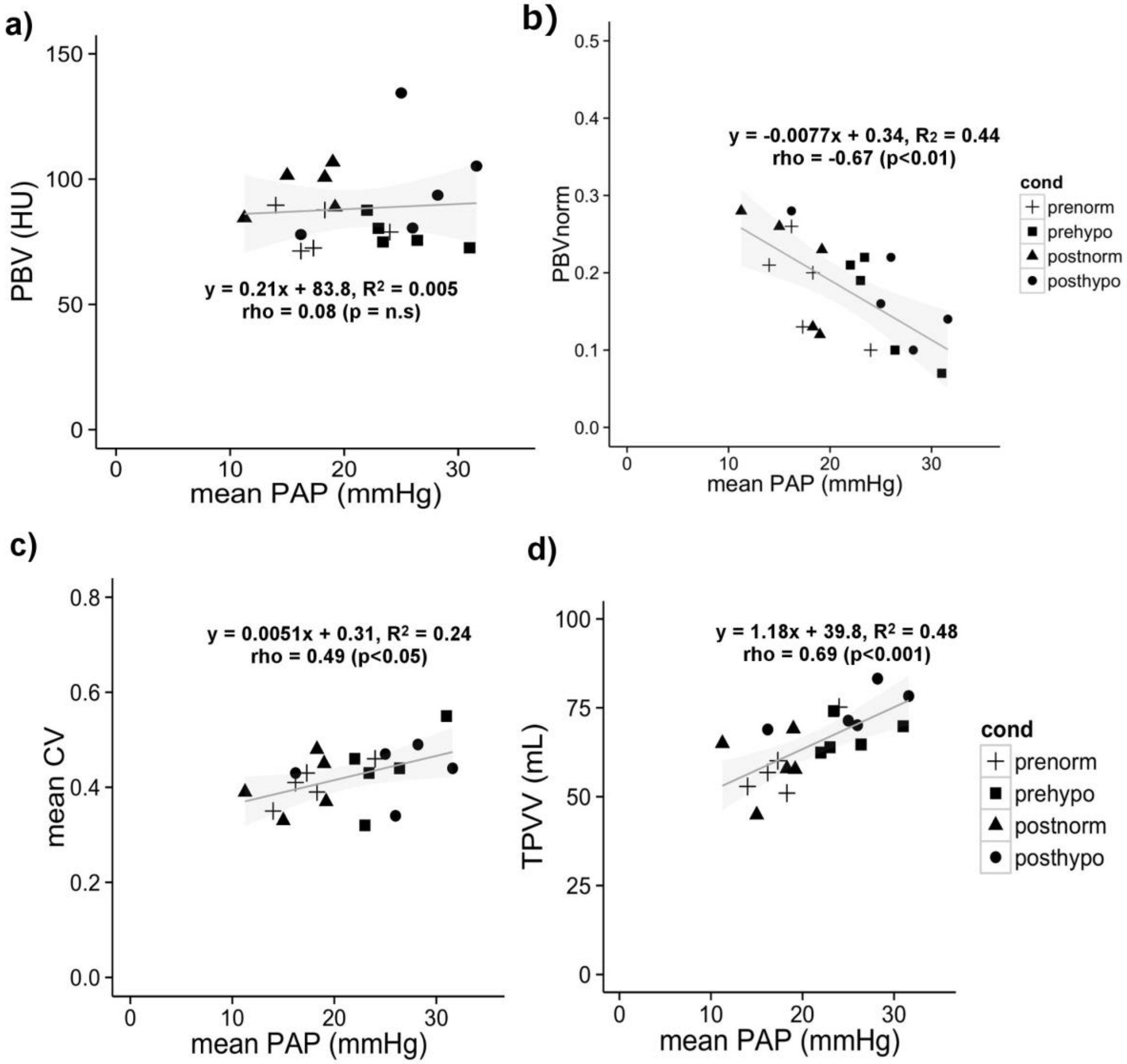

Figure 10: Relationship between PBV, CV, and PAP. (a) Non-normalized PBV did not correlate with mean PAP but in (b) we see the PBVnorm correlated inversely ($p<0.01$) with PAP increase (n.s = not significant). Mean CV (c) and TPVV (d) both positively correlated with PAP increase, suggesting hypoxia-induced increases cause a direct increase in PBV heterogeneity and central vascular volume.

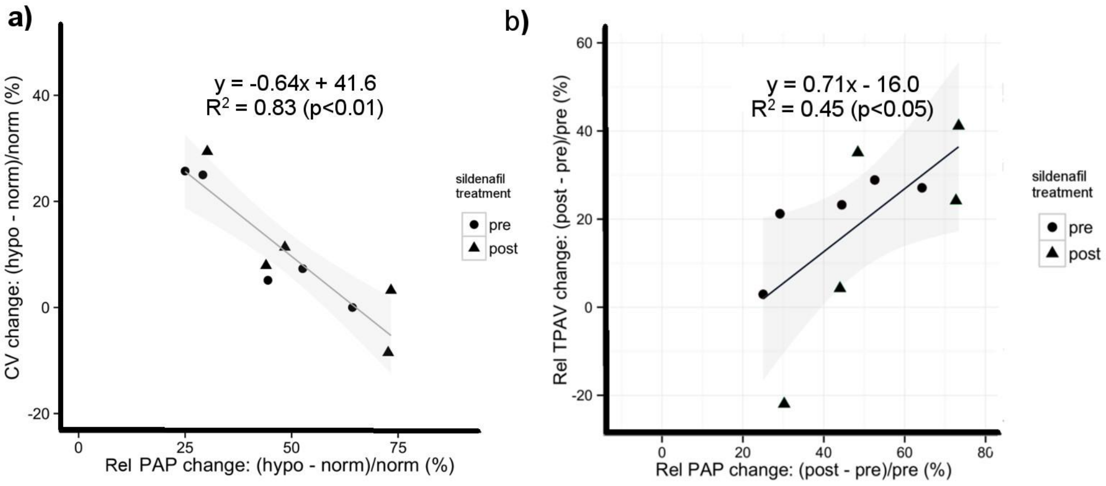

Figure 11: Sensitivity of CV and TPAV changes to HPV. (a) The CV change inversely correlated with PAP change, suggesting that in animals with more robust HPV activation, pulmonary vasoconstriction was more uniform throughout the lung, leading to smaller overall change in CV. Similarly, in (b), the TPAV increase directly correlated with increased PAP, demonstrating that greater hypoxic response (i.e. peripheral vasoconstriction) is reflected in upstream arterial enlargement.

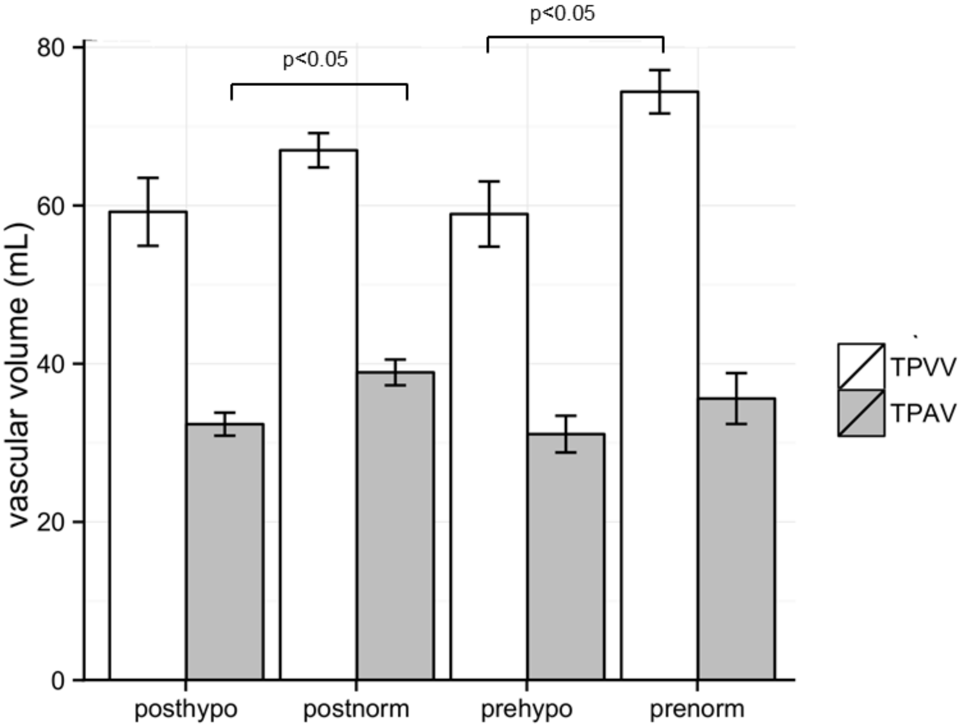

Figure 12: Whole lung vascular measurements. (a) TPVV and TPAV both increased following hypoxia; but only TPAV increase was significant pre sildenafil. After sildenafil, the TPVV and TPAV decreased towards baseline. Upon re-exposure to hypoxia, the TPVV increased but TPAV did not (TPVV = total pulmonary vascular volume; TPAV = total pulmonary arterial volume).

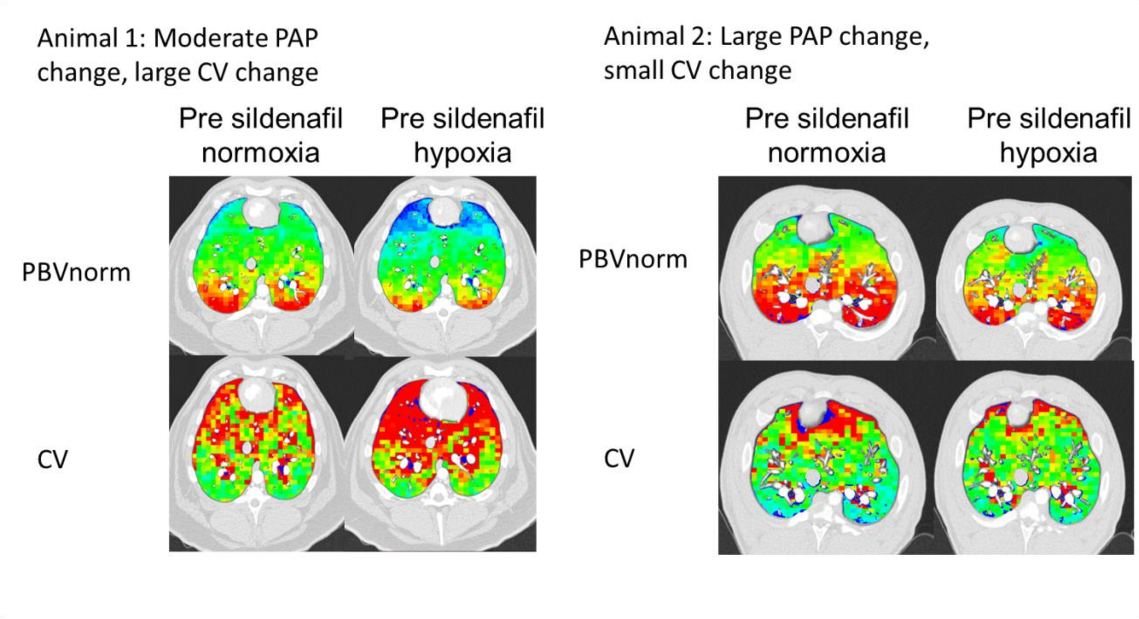

Figure 13: Example of two animals with different regional PBV responses to hypoxia. Both animals had similar PBV change but in animal 1 (left), the CV for the whole lung increased for a moderate increase in PAP; for animal 2 (right), hypoxia caused a large increase in PAP but the regional and whole lung CV did not change.

CHAPTER 5: HUMAN STUDIES: PBV HETEROGENEITY IS REDUCED WITH SILDENAFIL IN CAE-SUSCEPTIBLE SMOKERS

5.1 RATIONALE

X-ray computed tomography (CT) is providing quantitative maps of lung destruction and airway remodeling (74) in large multi-center studies (COPDGene, MESALung, SPIROMICS, etc) seeking to assess sub-phenotypes of chronic obstructive lung disease (COPD). However, identifying these anatomic alterations is insufficient to identify initial causal factors of emphysema, critical to the development of new therapeutic interventions. We present here a multi-spectral CT method (Dual Energy Computed Tomography: DECT) for the assessment of regional pulmonary perfused blood volume (PBV) and PBV heterogeneity, a surrogate for pulmonary blood flow (PBF) with a goal of establishing a novel phenotype based upon a difference in the vascular response of the lung periphery to a single dose of sildenafil. Sildenafil inhibits phosphodiesterase-5, the enzyme responsible for hydrolyzing cGMP, enhances the vasodilator effects of endogenous nitric oxide and is known to block hypoxic pulmonary vasoconstriction (HPV)(95).

Pulmonary vascular changes have been characterized early in the history of COPD (123, 181). More recently it has been observed that, with inflammation, there is an enhanced delivery of progenitor cells to sites of lung injury (80, 128). Thus, it is clear that the normal response of the lung to constrict local vasculature in poorly ventilated regions and shunt blood to better-ventilated regions would be counterproductive to the smoking-associated repair process. There is evidence suggesting that, in humans, HPV is normally blocked in the presence of inflammation (62, 147), allowing the maintenance of perfusion to inflamed regions. In animals, pulmonary vascular abnormality *precedes* emphysema with tobacco smoke exposure (43, 149, 180), suggesting that alterations to the HPV mechanism. Using dynamic, contrast-enhanced CT to assess regional PBF, we have demonstrated that smokers with normal pulmonary function tests, but small visually detectible signs of localized centri-acinar emphysema (CAE) have an increase in the coefficient of variation (CV) of CT-based regional PBF and mean transit time, two measures of spatial blood flow heterogeneity (3).

We have hypothesized that this is due to the inability of CAE susceptible smokers to maintain perfusion to patchy regions of inflammation, putatively due to a failure to block HPV. If increased vascular tone in an inflamed region is a critical event in the etiology of emphysema, this would have greater consequences in the lung apices where PBF is further compromised due to gravitational effects, explaining the predominance of apical pathology in smoking related emphysema.

In this study, we have sought to demonstrate that the previously observed increased heterogeneity of PBF in CAE susceptible normal smokers is reversible and not simply an index of early destruction. We utilize the DECT PBV imaging protocol, developed in Chapter 4, and expand on our_regional assessment of PBV heterogeneity to demonstrate the altered vascular response to sildenafil in CAE-susceptible (SS) and non-susceptible (NS) smokers.

5.2 METHODS

Subject Characteristics

The University of Iowa institutional review board approved the study and written consent was obtained from all subjects prior to entering the study. Subject were identified for recruitment being SS or NS based on the presence or absence of centri-acinar emphysema (CAE) and ground glass infiltrate on prior volumetric scans, as shown in Figure 14for a typical NS and SS subject. These scans were acquired from NIH-sponsored multicenter studies (COPDGene and SPIROMICS) and evaluated by an experienced cardiothoracic radiologist (JDN). Criteria for enrollment included: 1) age between 30-60 years, 2) current smoker with at least ½ packs per day (ppd). Exclusion criteria included: known history of heart or kidney disease, diabetes, body mass index (BMI) greater than 32, a positive pregnancy test, contrast allergies, abnormal kidney function (creatinine > 1.0) and recent history of upper respiratory infection or chronic respiratory impairment. SS subjects with visible airway or lung parenchymal disease, other than emphysema, were excluded. Pre-bronchodilator spirometry, lung diffusing capacity (DLCO) measurements and vital capacity (VC) measurements were performed prior to imaging. Pulmonary function and volume measurements were acquired via a V6200 Body Box (Sensor Medics). Spirometry quality followed the American Thoracic Society and European Respiratory Society guidelines (111). After scanning, SS and NS subjects were re-confirmed by visual evaluation by an experienced cardiopulmonary radiologist (JDN). SS subjects were identified as having small regions of predominantly apical centri-acinar emphysema (CAE) or distal lobular emphysema with or without findings of respiratory bronchiolitis that included the presence of upper lobe predominant non-branching ground glass centrilobular nodules or upper lobe predominant patchy ground glass opacities. The NS subjects did not have any evidence of either emphysema or respiratory bronchiolitis.

CT Scanning

Subjects were imaged in the supine body posture at defined lung volumes, using a computer-controlled, lung volume controller with a flow-based pneumo-tachometer (described by Fuld et al. (48), previously validated by Iyer et al. (83)). Vital capacity (VC) was measured while the subject was supine in the scanner with the lung volume controller. We used %VC to determine lung volumes (total lung capacity: TLC, and functional residual capacity: FRC) to ensure subjects with different sizes, attained similar lung inflation. In addition, volume control helped minimize lung volume differences between pre and post sildenafil PBV scans.

Subjects received one single energy non-contrast scan while lung volume was held at 90% VC (approximating TLC) and two dual energy scans (DECT) for the assessment of perfused blood volume (PBV), with the lungs held at 20% VC (approximating FRC). Because changes in lung volume alter the regional distribution of parenchymal perfusion (50) it was important to assure that the subject was close to the same lung volume pre and post-sildenafil so that changes in PBV distribution were related to sildenafil effects and not an effect of altered lung volumes.

Subjects were imaged via a second-generation dual energy 128-slice multi-detector row CT (MDCT) scanner with 64 active channels (Siemens Definition Flash, Siemens Healthcare, Forscheim, Germany) and two x-ray sources and detector pairs positioned 90° apart to allow simultaneous imaging of CT image pairs at two energies (Figure 15a). The scanning protocol consisted of: 1) a spiral non-contrast volumetric CT scan at total lung capacity (TLC: 90% vital capacity) to assess lung parenchyma, 2) a test bolus scan at 20% vital capacity using 30 ml of iodinated contrast (Isovue 370, Bracco Diagnostics), to establish start of acquisition after steady state contrast mixing, and 3) two DECT-PBV scans with the patient breath-held at 20% vital capacity and scanned one hour apart (before and after sildenafil). Details of the scan protocols, including effective radiation dose, are given in Table 4.

TLC Non-Contrast Scanning

This scan was performed to assess lung parenchyma and quantitative "emphysema-like" lung. A spiral or helical acquisition mode was used with 0.5 mm overlapping slice thickness. TLC images were reconstructed using B35f medium-soft kernel with near isotropic voxel spacing (0.5-0.6 mm in-plane, 0.5mm slice thickness).

Test Bolus Scan

Contrast was injected and a series of consecutive axial CT scans were acquired at the level of the left atrium (FRC). These CT scans were obtained at 20% vital capacity. A region of interest (ROI) was drawn in the left atrium on the axial CT scans to compute a time versus contrast density curve. The delay was computed for each subject and averaged 15 seconds. To simplify quantitative PBV imaging in the future, we recommend using the mean ± one standard deviation of the delay times observed in this study, rather than performing a test bolus on every subject. Thus, 15 seconds + 2 seconds = 17 second delay between onset of contrast delivery and onset of DECT PBV scanning. A contrast density threshold of 100 HU was used to trigger the start of scanning.

DECT PBV Imaging

Two contrast-enhanced (0.5 ml/kg of contrast, up to 100 ml per scan) DECT PBV scans were obtained at 20% VC. We chose to image at a lower lung volume to avoid compression of the microvascular bed in the non-dependent lung regions at high lung volumes. The baseline DECT PBV scan was obtained first and then a second scan 1hr after oral administration of 20mg of sildenafil. All contrast injections were performed via an antecubital vein using a 20 gauge needle and flush port with an injection rate of 4cc/s administered with a programmable dual-head contrast injector (Medrad Inc, Bayer AG). We did not use a traditional saline “chaser” at the end of the contrast injection but rather maintained contrast flow until the end of the scan. A saline chaser during the final portion of the scan would risk diluting contrast and thus violating the assumption of a steady state blood enhancement needed for quantitation of PBV. A maximum of 230 mL of contrast was allowed for contrast scanning, 30 mL for test bolus, and up to 100 mL for each DECT PBV scan.

The DECT images were acquired using 80kV and 140 kV x-ray guns (100 mAs and 85 mAs, respectively), resulting in a maximum effective dose of 11.5 mSv per scan and a z-coverage (22-30cm) adjusted to cover the whole lung. Blood pressure, heart rate and oxygen saturation were monitored during the scanning protocol and 1hr after the final DECT scan. Non-contrast TLC images were used to compare the were reconstructed using B35 medium-soft kernel and contrast-enhanced DECT images were reconstructed using D30f medium-soft dual energy kernel, both with near isotropic voxel spacing (0.5-0.6 mm in-plane resolution, 0.5 mm slice spacing). Subject vital signs, including heart rate, ECG, arterial pressure, and oxygen saturation (SpO2) were continuously monitored (Philips IntelliVue) during the study. No adverse events due to contrast or sildenafil administration were observed.

DECT Image Analysis

Lung (right and left), lobe masks and pulmonary vascular tree was segmented from CT images (Apollo pulmonary workstation software, VIDA Diagnostics, Iowa City, IA) from the non-contrast TLC and contrast-enhanced PBV scans (using the 140 kVp image). The lung masks for the TLC images were used to measure mean lung density, tissue fraction (%), air fraction (%), and emphysema index for thresholds of -950 (EI_{-950}). DECT PBV images were analyzed in a similar manner as outlined in Chapter 4.2. An 80/140kVp dual source decomposition method was used to extract PBV images, as shown in Figure 15c, allowing for better contrast separation (50).

Lung masks and airway tree masks were used to extract the PBV signal from the lung only and remove noisy signal coming from the chest wall or trachea. Central pulmonary vessels were extracted from the 140 kVp images and the PBV signal from these large vessels was removed, resulting in an image of parenchymal PBV (Figure 15d). The PBV signal was normalized to the iodine concentration of pure blood represented in the main pulmonary artery (PA). This normalization was to account for contrast differences in the lung pre and post sildenafil and between subjects, as explained in Chapter 4.

Pre and post sildenafil images were co-registered using laboratory-developed registration software (185) in order to compare spatially similar lung regions. We used the 140 kVp images from our pre and post DECT scans as our target and moving volumes and a b-spline deformable registration to smoothly register the whole lung. The displacement field, encompassing this deformation from moving to target volume, was then used to register the post sildenafil PBV images to the pre-sildenafil PBV images, as shown in Figure 15e. As all the analyzed pre and post image pairs had a volume difference within 10%, the amount of deformation was small.

For the whole lung, we computed variance (standard deviation), mean PBV, and CV pre and post sildenafil (Table 6). Images were then regionalized into 30x30x40 regions (average region size: ~0.3-0.5 cm3) in order to compute mean PBV, mean variance, and coefficient of variation (CV), a measure of spatial heterogeneity, for each 30x30x40 region Figure 15d. We also investigated gravitational effects of sildenafil in the supine position by dividing the lung into thirds in the ventral-dorsal direction and computing CV for each third of the lung. We measured the post pre CV differences for registered regions for SS and NS subjects. Data was filtered to remove regions with large PBV (i.e. near large vessels) and high noise regions (i.e. near the lung apex).

Regional PBV Heterogeneity Analysis

Our PBV heterogeneity (CV) comparison between NS and SS subjects was dependent on minimizing the influence of image-related noise caused by PBV reconstruction, which affect regional CV. Due to the contrast bolus in the subclavian vein, the PBV image suffered from beam-hardening artifacts predominantly in the lung apices. In order to reduce the influence of image noise on our analysis of the PBV C, we used the lobe masks (RUL, RML, RLL, LUL, LLL) processed from the FRC (140 kVp) images, to find regions of the lung with the smallest PBV CV. Lobar PBV CV was analyzed in the pre and post sildenafil PBV images separately as well as the post-pre CV differences for both NS and SS subjects. We then compared lobe-by-lobe CV differences between NS and SS subjects. Additionally, we explored the use of noise-reducing iterative reconstruction software (SAFIRE) and increased slice thickness to determine which set of parameters were sensitive to differentiating the PBV CV response to sildenafil between NS and SS subjects.

Statistical Analysis

Data for PBV and PBV-CV difference pre and post-sildenafil was represented as a mean ± SD for the whole lung, lung regions. A one-way ANOVA (R v. 3.1.1 statistical toolbox) followed by post-hoc analysis using Bonferroni method was used to determine statistical differences between NS and SS subjects, with a P value less than 0.5 considered significant. Subject's age and pack years were adjusted in multi-variate analysis to compare CV and CV differences between groups. Paired t tests assessed differences in the dependent vs. non-dependent regions.

5.3 RESULTS

Twenty-two subjects were enrolled to have DECT PBV imaging during breath-holds at spirometrically monitored functional residual capacity (20% vital capacity) before and one hour after oral administration of sildenafil (20 mg). Three-subjects were excluded prior to imaging because of blood pressure or asthma medications. The remaining 19 smokers were characterized as NS or SS based on CT-presence of visually determined CAE (3), evaluated by an experienced chest radiologist (JDN).

Subject Characteristics

Lung volume differences, quantitatively assessed via an Apollo workstation (VIDA Diagnostics, Coralville, Iowa) for the DECT scan (pre and post) pairs were demonstrated to be well controlled in 17/19 subjects. For two subjects (1 NS and 1 SS) lung volume difference (post – pre) were greater than 500 ml. These two subjects were eliminated from further analysis because of known lung volume effects on regional PBV (48). NS and SS demographics and physiologic findings for the remaining 17 subjects are provided in Table 5.

SS subjects were significantly older (9 years) and had a greater number of pack years. Both groups, on average, started smoking at the same age. Thus, the greater pack years in the SS group were likely age-based. Spirometric measurements, including vital capacity and FEV_1/FVC, did not differ between NS and SS. Both were at the high-end of the lower range of normal (70-80 percent predicted). The lung diffusing capacities (DLCO, % predicted) were significantly lower in SS compared to NS subjects. All subjects were cotinine confirmed smokers. C-reactive protein (CRP: an index of systemic inflammation) did not differ between groups. CRP in one NS subject was considerably higher (6.4) than subjects from both groups. (except for this one subject, all others had a value <1) If the one subject with a value of 6.4 is eliminated from the statistical analysis, the CRP was borderline greater ($p<0.06$) in the SS subjects.

Non-Contrast MDCT Performed at Full Inspiration Pre-Sildenafil

In addition to visual inspection of CAE, CT-based density measures served to evaluate "emphysema-like" lung. The emphysema index, (% lung voxels below -950 Hounsfield Units) was not significantly different between groups despite the presence of CAE in SS subjects. Both groups were within the range of normal (68). Mean lung densities were higher, as expected, than normal non-smokers (83) and did not differ between groups. This is consistent with the presence of smoking-associated peripheral lung fluid accumulation putatively associated with inflammation in both groups.

Comparing PBV Heterogeneity Across Lobes

We utilized lobe masks to compare lobar CV differences between groups. Due to beam-hardening artifacts in the lung apices, from concentrated contrast in the subclavian, we observed that the CV was highest in the RUL, as expected, for both NS and SS subjects, whereas the lower CV was in the lower lobes for both groups (Figure 17). Iterative reconstruction and thicker (1.5mm) slices did not change this trend. The lobar CV change, shown in Figure 18, showed distinctly different patterns between groups, with a positive CV change in NS subjects (top panel) and a negative change in SS subjects (bottom panel). The SAFIRE (iterative reconstruction kernel) and increased slice thickness (1.5mm) seemed to enhance these differences between groups, with more of the lobes, particularly the less noisy lower lobes, showing a significant difference. It is interesting to note that, although the RUL had a larger CV in SS subjects pre and post sildenafil, the change in CV (pre to post sildenafil) was larger in the SS subjects and significantly different from NS subjects, regardless of reconstruction kernel or slice thickness.

Sildenafil Decreases PBV Heterogeneity in SS Subjects without Affecting Whole Lung PBV

The distribution of PBV was measured for the whole lung with variance (standard deviation and CV) and regional CV's, a measure of spatial PBV heterogeneity. Table 6 shows that the variance and CV changed without affecting PBV. In SS subjects, there was a decrease in variance with sildenafil whereas in NS subjects there was a slight increase. This difference in whole lung response to sildenafil was significant ($p<0.05$ for SD, $p<0.01$ for CV). Figure 16 shows that the change in CV and change in PBV were related in SS subjects ($R^2 = 0.89$, $p<0.01$), showing that as PBV decreased with sildenafil, so did the CV; whereas in NS subjects, there was no association between PBV and CV and most subjects clustered together ($R^2 = 0.03$, p=n.s).

As demonstrated in Figure 19a, we divided the lung (minus the apical regions with artifacts from contrast in the subclavian vein) into thirds by vertical height (ventral to dorsal in the supine subjects) and compared the PBV-CV's for each region between SS and NS subjects. For all regions, PBV-CVs trended greater in SS compared with NS subjects, and the greatest SS vs. NS difference was found in the non-dependent lung regions. The gravitationally non-dependent lung (compared with the dependent) had the greatest ($p<0.01$) heterogeneity pre-sildenafil for both the SS (0.42 ± 0.09) and NS (0.37 ± 0.03) subjects. For each subject, post-sildenafil lungs were warped into the shape of the pre-sildenafil lung. Each lung image was divided into 30x30x40 voxel regions (~0.3-0.5ml) and PBV heterogeneity for each region was assessed and then the regional PBV-CV's for the post-sildenafil were mapped into its pre-sildenafil shape through image warping (185). A map of the regional distribution of CV's is shown in Figure 19b for a representative SS and NS subject. The baseline differences in regional heterogeneity between the NS and SS subject is striking with a clear increase in regional CV for the SS smoker. Histograms of regional CVs are superimposed on each other for the pre and post PBV data for these two subjects in Figure 19c. The CV mode shows a significant left shift in the SS subject. As a group, the shift in the CV histogram mode was significantly different ($p < 0.05$) for SS (-0.02±0.02) vs. NS (+0.01±0.02).

Following sildenafil, the PBV-CVs significantly ($P<0.05$) decreased in SS subjects by 0.03 (-4.8%) and increased in the NS subjects (+7.5%). Mean PBV (normalized to iodine content in the pulmonary artery) did not differ between groups, averaging 0.16 ± 0.04 and 0.17 ± 0.04 in NS and SS, respectively. Thus, reduction in CV for the SS subjects represents a re-distribution of blood flow to the lung and not an over-all increase in pulmonary perfusion. As shown in Figure 19, sildenafil significantly decreased heterogeneity in all lung regions (dependent, middle and non-dependent) of SS subjects. In contrast, the CV change, pre to post-sildenafil, was not significant in NS subjects for any lung region.

5.4 DISCUSSION

In this study, we introduce the use of multi-spectral CT (DECT) to provide quantitative, functional and structural measures of the central and peripheral pulmonary vasculature; demonstrating the presence of a unique phenotype associated with SS vs. NS subjects. We show that the previously established (3) elevated PBF heterogeneity in SS subjects is reversible with sildenafil and thus not simply a result of early lung destruction but rather evidence of a peripheral vasoconstriction unique to CAE susceptible subjects. In both the SS and NS subjects the PBV-CV was significantly greater in the non-dependent lung regions consistent with prior observations of Alford et al. (3) using a dynamic perfusion CT methodology. In addition, the PBV-CV trended higher in the SS subjects vs. the NS subjects (p=0.06 and p=0.08 for dependent vs. non-dependent lung regions, respectively), suggesting greater vasoconstriction in the non-dependent lungs of SS subjects.

We initially measured whole lung PBV heterogeneity using standard deviation and CV of the PBV signal. Although we found SD and CV changes were significantly different between NS and SS subjects, we ultimately decided to explore regional CV because it was normalized to the mean PBV signal. As we saw in Figure 16, PBV tended to change with sildenafil in the SS subjects more than NS subjects. We believe this is because whole lung PBV does not change with sildenafil but rather redistributes to areas with low perfusion (i.e. vasoconstricted lung). Normalizing to PBV allowed us to minimize PBV differences before and after treatment. By normalizing, the CV tended to show stronger statistical differences between groups. In addition, the goal of our PBV heterogeneity comparison was to minimize the influence of image-related noise, which affected both PBV and variance.

While PBV has been shown to be a strong surrogate for true parenchymal perfusion (50), the measurement method, as implemented in this study (Siemens Flash scanner, no iterative reconstruction methods, and relatively low dose imaging) coupled with the relatively small sample size likely explain these trending but non-significant results. The noise in the PBV measurement is expected to diminish with newer generation scanners and the introduction of improved iterative reconstruction software to dual energy imaging (119). The noise effects on the PBV response to sildenafil was less of a concern since we carefully controlled lung volumes and matched PBV image pairs before and after sildenafil.

Our lobar analysis of CV demonstrates that the upper lobes had the highest CV and therefore contained most of the noisy signal. Although we chose reconstruction without iterative reconstruction, the results show iterative reconstruction and thicker slices would enhance, rather than diminish, the existing CV differences between groups. It is interesting to note that the upper lobes (particularly RUL) had a higher CV in SS subjects compared to NS subjects at baseline despite the presence of contrast-related artifacts in both groups. Also, the change in CV was greater (more negative) in SS subjects, suggesting that even with added noise, there was a measurable decrease in PBV heterogeneity with sildenafil.

We attributed the higher CV at baseline not just to increased noise but physiological variability due to greater resistance of blood flow and/or increased parenchymal damage. We intentionally avoided the apical lung because of the added noise and because of increased prevalence of emphysema; so that relatively "normal" lung could be sampled to show that the reversibility of blood flow heterogeneity is a phenomenon related to intrinsic differences in vascular response between groups and not a result of vascular dysfunction due to loss of parenchyma.

It is important to recognize that, while our SS population is selected based upon visual CT evidence of CAE, the NS cohort is selected based upon an absence of evidence for CAE. It is possible for NS subjects to be incorrectly classified simply because they were studied earlier in the pathologic process (the SS subjects were older by an average of 9 years). A larger population study would be useful and could provide the ability to age match the two groups. However, age was accounted for in the multi-variate analysis model and did not contribute to group differences.

The signaling pathway(s) that subsequently mediate pulmonary arteriolar vasoconstriction is controversial, but a strong contender is the attenuation of the nitric oxide – cyclic GMP pathway (6, 116). Decreased expression of endothelial NO has been found in primary pulmonary arterial hypertension and in pulmonary hypertension associated with diseases, such as COPD (36, 55, 125). It was recently shown that increasing nitric oxide production, such as a soluble guanylate cyclase stimulator, blocked the development of pulmonary hypertension and emphysema in cigarette smoke-exposed animal models and human lung tissue (171) . In healthy subjects, sildenafil has been shown to inhibit hypoxic vasoconstriction (54). A recent study by Blanco et al. (13) demonstrated that, in patients with COPD associated pulmonary hypertension, sildenafil (20 mg and 40 mg) improved hemodynamics at rest and during exercise. This effect was accompanied by the inhibition of HPV that impaired arterial oxygenation at rest (but not exercise). An important result of our study is that given a similar dose of sildenafil in SS subjects, sildenafil improved pulmonary blood flow without impairing a pulse oximeter-derived measure of oxygenation. While the de-oxygenation associated with restoration of flow to poorly ventilated lung regions has been interpreted as a negative outcome of Blanco et al. (13), it is possible that such restoration of flow could have longer-term benefits as long as the subject can tolerate the reduction in the regional ventilation/perfusion relationship.

The decrease in PBV heterogeneity with sildenafil was not accompanied by an increase in mean lung PBV. Alford et al. (3), using a more difficult to implement method of dynamic CT, similarly observed that increased heterogeneity of PBF in SS subjects was not associated with a difference in mean perfusion to the lung of SS, NS and non-smokers, suggesting that sildenafil redistributed parenchymal blood flow from areas with low CV's to areas with high CV's, presumably representing a restoration of perfusion to regions of lung injury experiencing putative hypoxic pulmonary vasoconstriction. Perfusion to injured lung regions is important to the inflammatory response cascade including delivery of progenitor cells promoting parenchymal repair (128, 129).

5.5 SUMMARY

In summary, the key finding of this study is that increased perfusion heterogeneity (assessed via DECT-based PBV), in otherwise normal appearing lung, is reversible with sildenafil, suggesting a nearly functional mechanism interrelating parenchymal destruction with increased pulmonary vasoconstrictor tone during smoking-related lung inflammation, and suggesting that pulmonary vasculature is target for early intervention.

By disinhibiting constricted vessels, sildenafil likely decreased heterogeneity by redistributing PBV to regions of inflamed lung parenchyma. We present in the next chapter, evidence to support the notion that peripheral vasoconstriction in SS subjects, contributing to the increased perfusion heterogeneity, leads to upstream enlargement of central arteries, which can be detected by sensitive imaging method of central arteries. Our structural analysis of vascular tree also will support the notion that this peripheral constriction is reversible with sildenafil.

Table 4: Imaging parameters for the three scan types. Each subject had a non-contrast scan, a test bolus scan, and two DECT PBV scans.

Protocol / Lung Volume	Tube peak kilovoltage (kVp)	Tube current (mAs)	Effective Dose (mSv)	Pitch	Slice thickness (mm)	Scan type
Non-contrast (90%VC)	120	115	3.6	1.0	0.75	Spiral
Test bolus (20%VC)	120	45	0.5	--	10	Axial
DECT (20%VC)	80/140	100/85	5.0	0.5	0.75	Spiral

Table 5: Subject characteristics for non-susceptible (NS) and susceptible (SS) smokers. Results are expressed as mean ± SD unless noted otherwise. Spirometry and DLCO is reported as percent predicted. BDI, baseline dyspnea index; BMI, body mass index; CRP, c-reactive protein; DLCO, diffusing capacity of the lung for carbon monoxide; EI, emphysema index; FEV1, forced expiratory volume in 1 second; FVC, forced vital capacity; MLD, mean lung density; no., number of subjects; SpO2, oxygen saturation; *p<0.05 vs. NS subjects.

Characteristic	**NS**	**SS**
N	7	10
Gender (% male)	14	20
Age (years)	41 ± 10	50 ± 6*
BMI (kg/m^2)	26.2 ± 3.7	25 ± 4.5
Heart rate: pre-sildenafil (bpm)	74.8 ± 6.3	70.4 ± 9.9
Heart rate: post-sildenafil (bpm)	73.8 ± 10.4	71.7 ± 12.9
Blood pressure (mm Hg)		
Systolic BP (mmHg): pre-sildenafil	120 ± 15.5	113 ± 13.6
Diastolic BP (mmHg):pre-sildenafil	69.9 ± 9.9	68.8 ± 6.0
Systolic BP (mmHg): post-sildenafil	116 ± 15	114 ± 14
Diastolic BP (mmHg):post-sildenafil	67.3 ± 8.7	68.5 ± 8.6
SpO$_2$: Pre-sildenafil	99 ± 1.0	99 ± 0.92
SpO$_2$: Post-sildenafil	99.1 ± 0.69	99 ± 1.1
CRP (mg/L)	1.4 ± 2.21	2.23 ± 2.61
Pack-years	20 ± 13	**32 ± 9***
Age started smoking (years)	16 ± 4	16 ± 3
BDI	11.9 ± 0.38	10.1 ± 2.0
FEV$_1$ (%)	120 ± 16	115 ± 18
FVC (%)	116 ± 10	118 ± 28
FEV$_1$/FVC (%)	80 ± 4.8	78 ± 6.9
DLCO pre-Sildenafil (%)	113 ± 22	**85 ± 14***
TLC air volume (L) (CT)	4.96 ± 0.40	4.81 ± 0.71
Tissue volume (L) (CT)	0.97 ± 0.15	0.97 ± 0.081
EI$_{-950}$ (%)	0.36 ± 0.25	0.43 ± 0.31
MLD (HU)	-830.7 ± 17.3	-820 ± 19.5

Table 6: Whole lung difference in standard deviation (SD), PBV, and CV pre and post sildenafil for NS and SS subjects. NS subjects had a slight increase in SD and CV post sildenafil whereas in SS subjects, SD and CV decreased; *p<0.05; #p<0.01.

	NS		SS		Δ (post – pre)	
	PRE	POST	PRE	POST	NS	SS
SD	0.056±-0.012	0.067±-0.015	0.065±-0.012	0.063±-0.013	0.012±0.0045	-0.001±0.017*
PBV	0.17±-0.033	0.18±-0.032	0.17±-0.038	0.18±-0.045	0.013±0.01	0.006±0.041
CV	0.33±-0.028	0.38±-0.054	0.39±-0.091	0.36±-0.065	0.045±0.036	-0.022±0.044#

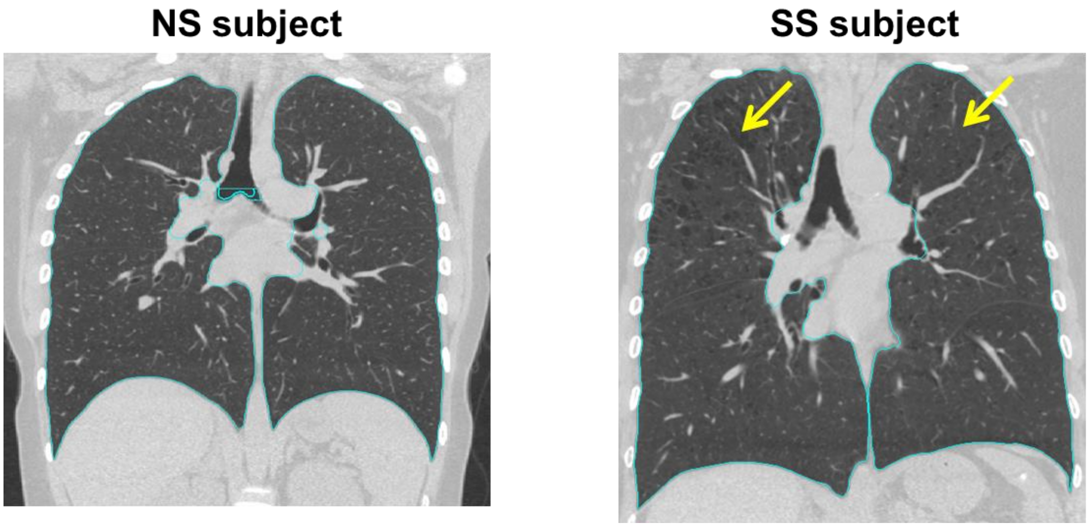

Figure 14: TLC scans from an NS and SS subject, showing areas of visible centri-acinar emphysema in the apical lobes (arrows) in the SS subject.

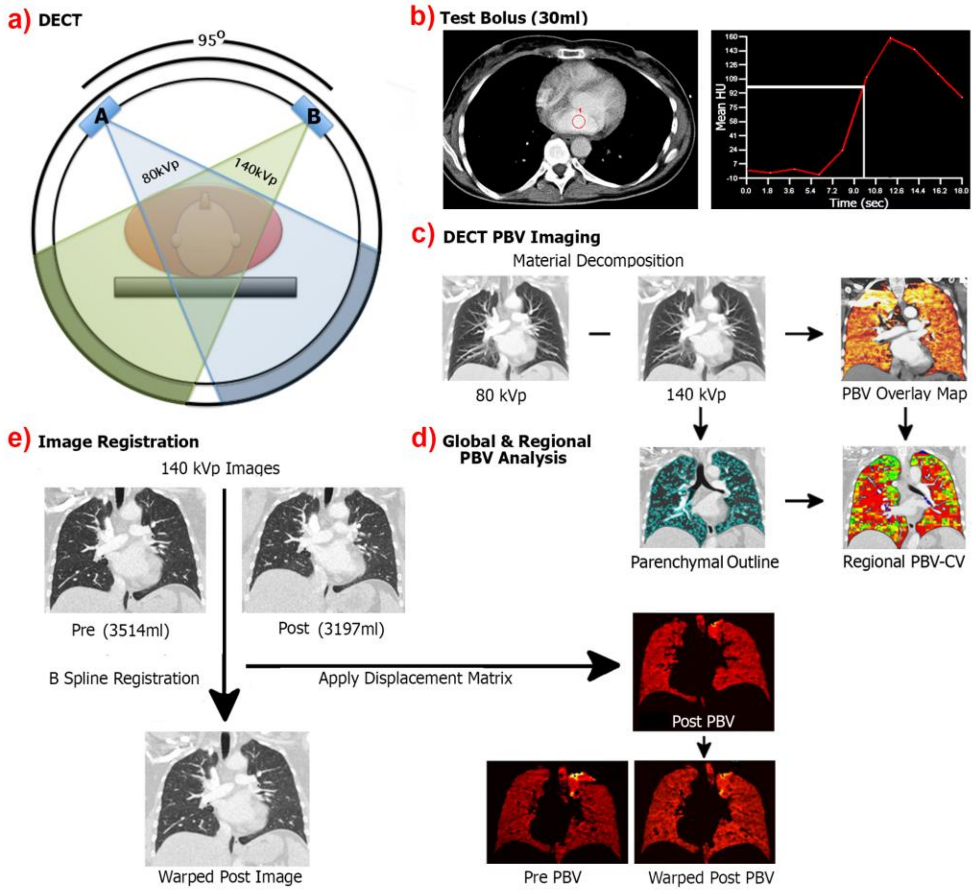

Figure 15: Diagram illustrating the process of PBV imaging from acquisition, data collection, processing, and comparison of regional PBV measures. (a) DECT PBV imaging is performed using 80 kVp and 140 kVp energies, detectors 90º apart, acquiring low and high energy contrast-enhanced CT images. (b) Test bolus: a ROI is placed in the left atrium and the time to peak intensity is the delay required for start of acquisition. The intensity in the left atrium has to exceed 100 HU in order to image. Contrast is injected before this delay and during scanning in order to equilibrate with parenchymal blood. (c) 80 kVp and 140 kVp images used to reconstruct PBV images (d) Regional PBV analysis, showing lung mask outlining only the lung parenchyma. Large vessels and airways are excluded. e) Process of image registration: images are warped from 140 kVp images (post is moving image that is warped to the fixed or pre image). The displacement for this registration is used to warp the post PBV image to the pre. This is to ensure same regions are compared pre and post sildenafil.

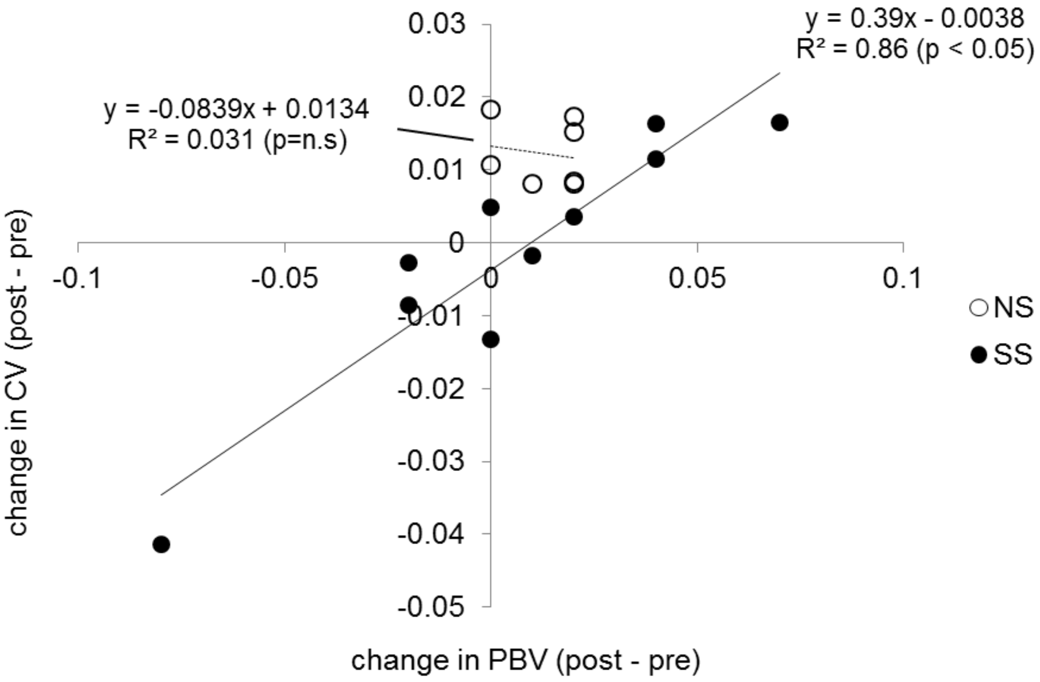

Figure 16: Change in PBV vs. change in CV for NS and SS subjects, showing a linear relationship in SS subjects (R^2 = 0.89, $p<0.05$) and no relationship in NS subjects (R^2 = 0.031, p=n.s). CV tended to decrease with sildenafil in SS subjects and did not change in NS subjects.

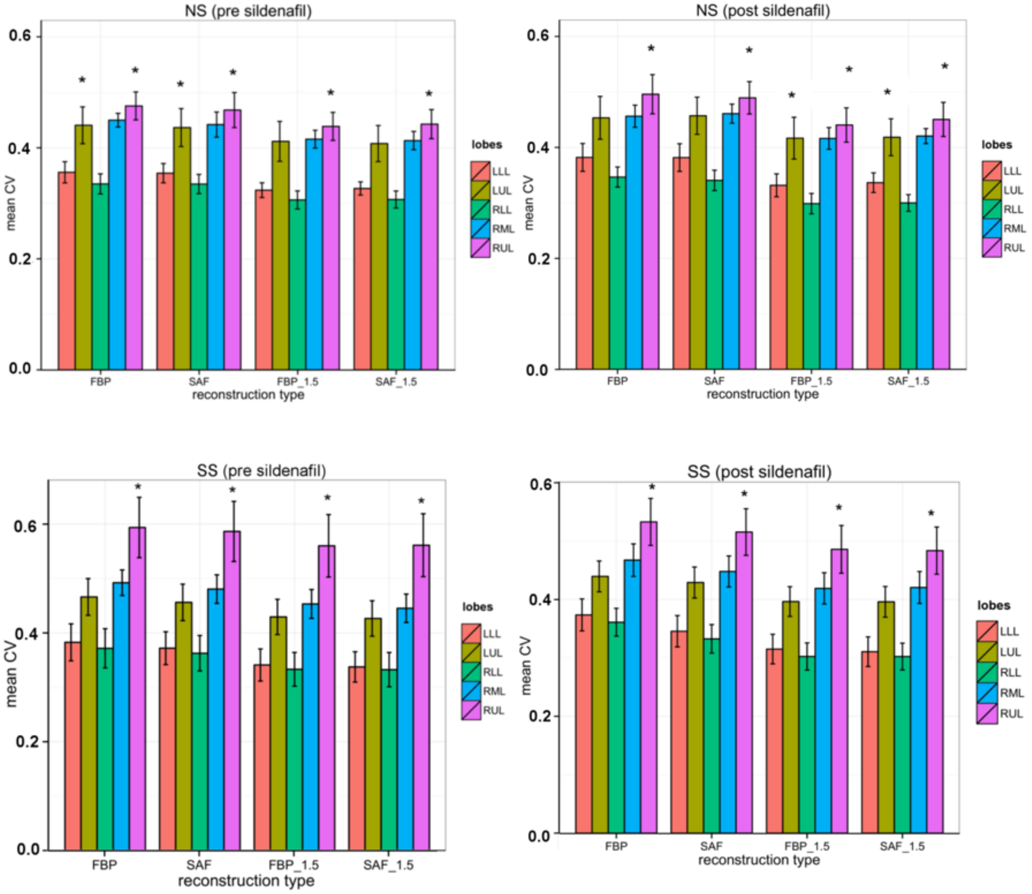

Figure 17: Lobar CV analysis for NS (top panel) and SS (bottom panel) subjects, showing that the RUL had the largest CV and the RLL had the lowest (* $p<0.01$ for RLL vs. RUL, NS and SS groups separately). Other lobes did not show statistical differences. There was very little difference in this trend pre and post sildenafil, or with the use of iterative reconstruction kernel (FBP vs. SAF) and increased slice thickness (0.75mm vs. 1.5mm).

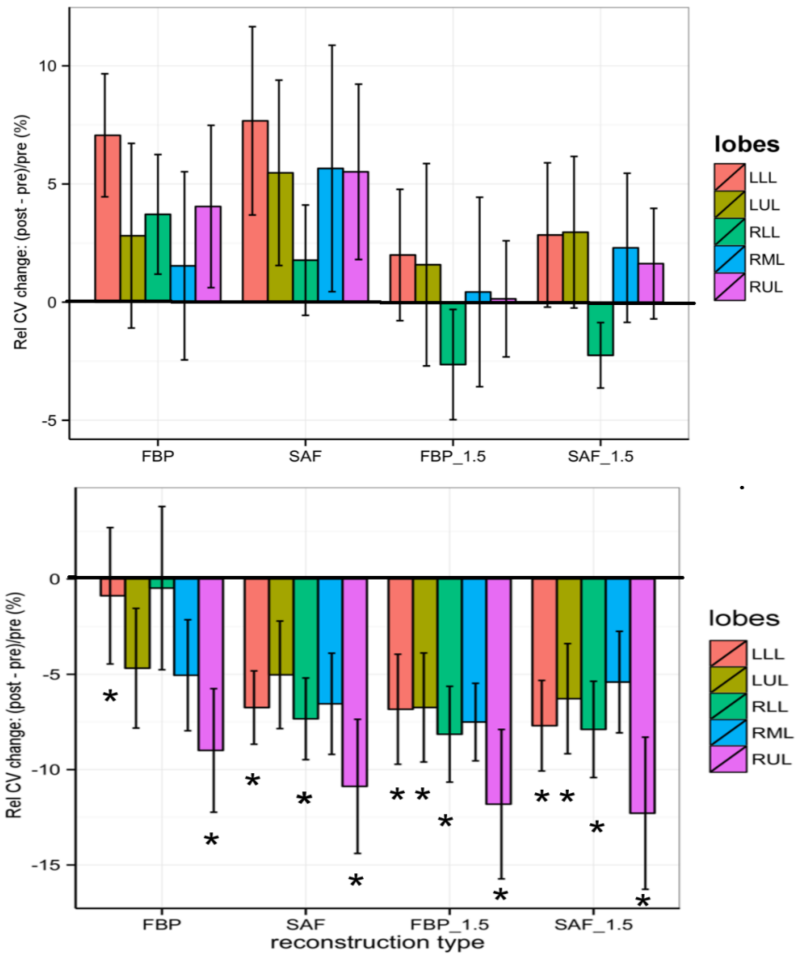

Figure 18: Change in CV for each lobe, showing distinctly different pattern in NS and SS subjects. In the NS subjects, CV increased post sildenafil whereas in SS subjects it deceased with sildenafil. The use of noise-reducing iterative reconstruction (FBP vs. SAF) and increased slice thickness (0.75mm vs. 1.5mm) enhanced these differences between groups. (*p<0.01, NS vs. SS).

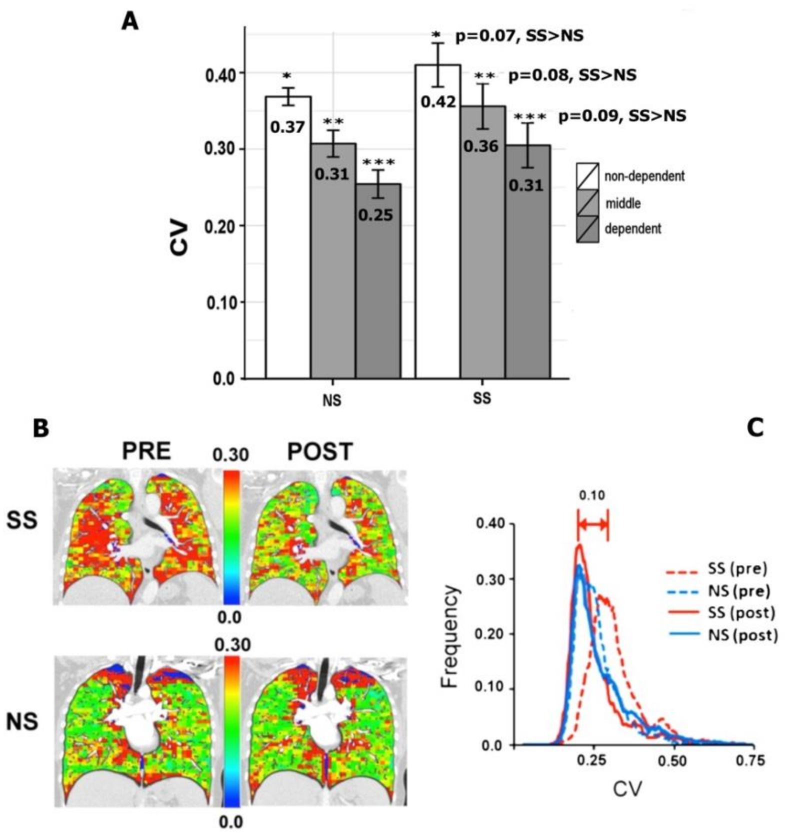

Figure 19: (a) The whole lung was divided into dependent, middle and non-dependent thirds by vertical height and the PBV-CV's were calculated for each of these regions. For each region, PBV-CV's trended greater for the SS subjects. For both SS and NS subjects, the PBV-CVs were significantly ($P<0.01$) greater in the non-dependent vs. dependent lung regions. (b,c) For each subject post-sildenafil lungs were warped into the shape of the pre-sildenafil lung. PBV heterogeneity for each region was assessed and then the regional PBV-CV's for the post-sildenafil were mapped into its pre-sildenafil shape. Note the higher CVs pre-sildenafil in this SS subject compared to the pre-sildenafil NS subject. Post-sildenafil there is little change in the color distribution pattern of the NS subject while the color distribution of the SS subject shifts to more closely match the NS subject. **(c)** demonstrates the histogram plots for the whole lung of each of these 4 image data sets. Note the significant shift (0.10) in the mode of the SS histogram pre vs. post sildenafil with the post-sildenafil histogram modes coming into alignment. This same shift was found in the full population of SS vs. NS smokers and was found to be significant ($p<0.05$).

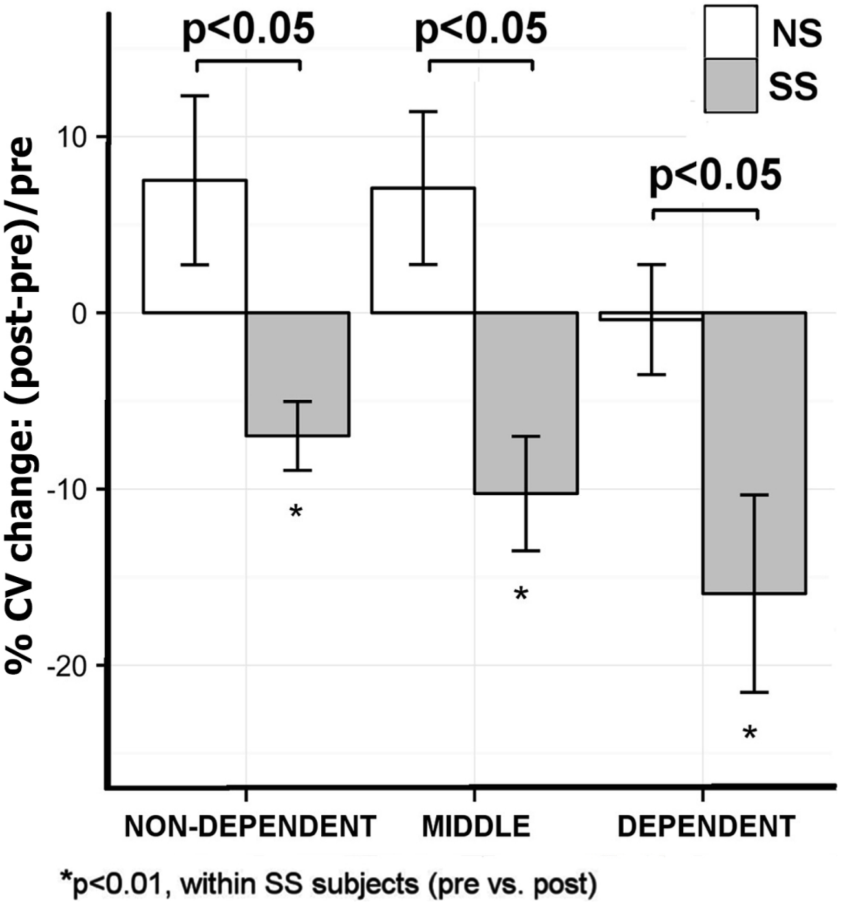

Figure 20: Regional and whole lung PBV heterogeneity measures pre and post sildenafil. The lungs of each NS (open bars, ± standard error) and SS (shaded bars, ± standard error) subject were divided by vertical height into the non-dependent (ventral), middle and dependent (dorsal) regions. The relative % change (Post-Pre)/Pre in CV in response to sildenafil for the SS subjects significantly fell within each lung region while there were no significant changes in CV for any of the lung regions of the NS subjects. This SS vs. NS difference in the CV response to sildenafil was significant for all lung regions.

CHAPTER 6: ASSESSING PULMONARY VASCULAR STRUCTURAL CHANGES WITH SILDENAFIL IN CAE-SUSCEPTIBLE SMOKERS

6.1 RATIONALE

There is growing evidence that pulmonary vascular dysfunction plays a role in the progression of smoking-associated emphysema (9, 10). Several recent imaging and clinical studies have observed that abnormalities in the pulmonary vasculature are associated with CT emphysema and disease progression. Wells and colleagues observed that enlargement of the main pulmonary artery, observed on CT, was an independent predictor of morbidity and mortality and postulated that the increased pulmonary vascular resistance and centralization of blood flow, in the presence, of lung inflammation, is responsible for arterial enlargement and the deterioration of lung function (82, 172).

Estepar et al. analyzed the whole pulmonary vascular tree, including arteries and veins, from CT images and observed a decrease in cross-sectional area (CSA) of small vessels in patients with severe COPD. This decrease positively correlated with CT emphysema and negatively with pulmonary artery pressure suggesting that small-scale vascular changes are related to large scale parenchymal and hemodynamic changes (42)

Along with these findings and based on our functional imaging findings in Chapter 5, supporting the notion of increased perfusion heterogeneity in SS smokers, we hypothesized that central vessels would be enlarged in individuals with early emphysema, due to downstream peripheral vasoconstriction and this enlargement could be reversed with sildenafil treatment. Due to difficulties in measuring small peripheral vessels, we sought to measure central arterial morphometry to determine if they could help differentiate CAE-susceptible and non-susceptible smokers as well as their individual response to sildenafil.

We developed on two central measures of vascular structure, the whole lung total arterial volume (TPAV), which utilized the separated arterial tree. Previous studies have used the total pulmonary vascular volume (TPVV), including arteries and veins, and found a correlation with functional lung measures. As vascular dysfunction is largely attributed to smoking-associated arterial remodeling (126), we focused on differentiating central arterial geometry and its changes with sildenafil in in CAE-susceptible smokers.

As lung volume can affect the detection of small vessels (and therefore TPVV and TPAV), we outline a more detailed method to measure the cross-sectional area of central pulmonary arteries using the anatomic correspondence between arteries and central airways in order to standardize measurements across lung volume. These arterial measurements were tested in our CAE-susceptible and non-susceptible cohort to determine if these measurements were more sensitive than TPVV in detecting structural changes in lung vessels of CAE-susceptible smokers and test whether the vascular response to sildenafil could be detected, as well as help explain the physiological differences between NS and SS using the relationship between vascular structure and functional PBV measures.

6.2 METHODS

Whole Lung Arterial Volume Measurements

For this study, we included the same cohort of 10 SS and 7 NS subjects from the previous PBV imaging study presented in Chapter 5. To extract central pulmonary arteries, we followed the similar image processing steps as the animal studies in Chapter 3 (see Methods). Briefly, central pulmonary vessels were extracted from CT images, then the segmentation was refined using a fuzzy connectedness operation to extend the vessel boundaries (85). Figure 21 shows an example of how extending vessel boundaries to preserve peripheral vessels but extends the mask coverage of central vessels. The central pulmonary vascular tree was separated into arteries and veins, using the algorithm by Saha et al. (141), and total pulmonary vascular volume (TPVV) and total pulmonary arterial volume (TPAV) were measured.

We focused on the right lung and excluded the left lung arteries due to confounding effects of cardiogenic motion on the detection of small vessels. We used the lobe masks, generated from the contrast-enhanced FRC images (pre and post sildenafil) to further subdivide the arterial tree into upper, middle, and lower lobe vessels. We used these lobe masks also to exclude large pulmonary vessels (such as the pulmonary arteries in the mediastinum) and only include vessels within the lung parenchyma. We found that, because of reconstruction artifacts in the right upper lobe associated with high concentrations of iodine in the subclavian vein and because of cardiogenic motion artifacts in the right middle lobes, TPVV and TPAV in the right lower lobe (RLL) best represented the state-of-the-lung, without confounding factors, in SS and NS subjects. Because lung volumes vary between subjects and vascular volumes vary along with lung volume (the pulmonary vascular bed is space filling), we normalized the whole lung and lobar TPVV and TPAV to whole lung or lobe masks, respectively, to obtain a percentage (denoted herein as $TPVV_{norm}$ for total vascular volume and $TPAV_{norm}$ for total arterial volume percent in the lung or lobe).

The lung can be divided into central ("core") and peripheral ("peel") segments of the lung. The "peel" in our case represents the outer 15 cm of the lung periphery and the "core" represents the remaining central portion of the lung. Lung diseases, such as COPD typically progress in small, peripheral regions of the lung, so core and peel measures of emphysema have helped mapped the distribution of disease and association with physiological and clinical variables (32, 74). Adapting this method, we divided the separated arterial tree into the central and peripheral arteries using the core and peel (outer 15mm of the lung) lung masks, as shown in Figure 22. Similar to the whole lung and lobar TPAV, we normalized the core and peel arterial volumes to their respective core and peel lung volumes.

Establishing Airway-Arterial Anatomic Correspondence

Horsfield and colleagues in the 1970s first described the unique pairing of the arterial and airway branches in the human arterial tree (152). We build on this correspondence to reconstruct matching arterial segments to anatomically labeled airways. We chose the lower lobe airways and vessels for our measurements (corresponding to RB10 and LB10) because vessels and airways were easier to identify in the FRC images and we aimed to minimize the influence of contrast-related artifacts and cardiogenic motion on the detection of small pulmonary arteries. Of particular importance is the fact that these two vessel and airway segments traverse the lung in a direction perpendicular to the scanning plane compared with other vessel and airway segments. These airway branches have been used to identify important disease features in COPD (34, 56).

The segmented airway tree (Apollo Workstation, VIDA Diagnostics) is skeletonized using a novel arc skeletonization algorithm (86) and matching arteries are identified using a spatial proximity measure of the vessel skeleton and its local orientation. The arteries associated with these airway paths are manually identified from CT images and seed points are placed along the vessel segment. A minimum of three points is used to reconstruct the arterial segment: a parent, branch point, and child branches. This is equivalent to two generations of the arterial tree.

Branch Point Selection Criteria

We utilize the major branching pattern of the airways to select points along the vessel tree. At a lower lung volume, such as in FRC images, the airway and vessel branches are easier to identify because they are regularly spaced with a difference of a few voxels between airway and vessel branches. However, at higher lung inflation, such as TLC, several minor airway and vessels branches can be detected. In this case, we determine the associated artery based upon proximity and parallel orientation to the major airway. The major airway follows the major longitudinal axis of the anatomical airway branch. An artery may branch several times before an airway branches. In this case, we ignore these minor arterial branches and only label the arteries that parallel its associated airway. Figure 23 shows a reconstruction of the airway and arterial segment (parent and child) and how major and minor branches are identified (subpanels a, b and c). In FRC images, minor branches (shown in yellow) project off the main airway path and are not orthogonal to the imaging plane. The bifurcations (*) and minor branches are filtered during the measurement process since they may lead to overestimation of CSA. For the RB10 and LB10 path, we constrain our parent-child branch analysis to two generations distal to this major bifurcation (i.e. we reconstructed two generations of vessel tree distal to the RB10).

Artery CSA Measurement and Normalization to the Airway

Cross-sectional area (CSA) of selected arterial branches in the lower lobes of the right and left lung (RB10 and LB10) was measured from accurate reconstruction of the arterial tree from the 140 kVp FRC CT images. The branches were chosen according to their association with anatomically defined airway segments (Fig. 4a) and a semi-automated algorithm using manually placed seed points in the target arterial segment was used to compute arterial CSA.

The centerline of the target arterial segment was computed by joining the user-selected end points with the minimum cost-path (26). The arterial CSA measure was computed over the central one-third section of the computed centerline. At a given point (the red-cross on Figure 24a) on the central section, a stable measure of local arterial orientation was computed using principal component analysis (PCA) of neighboring centerline voxels, in order to reconstruct an orthogonal cross-sectional plane (the yellow plane on Figure 24a). The arterial CSA was measured using a radial sample-line approach (140) (Figure 24b). The erroneous edge points (yellow-crosses) generated by adhering anatomic structures are detected using a coherence analysis (183) and these points are replaced (green-crosses) using interpolation of confident arterial edge points.

Outliers are gradually excluded until the model fit does not change (or gets worse). CSA measurements are measured distal and proximal to the center-point voxel. Outlier measurements were manually filtered using the similar coherence criteria (183) to select the set of CSA measurements for statistical comparison.

The arterial CSA is normalized to the airway CSA, provided by Apollo pulmonary workstation software (VIDA Diagnostics, Iowa City, IA). We normalized the CSA of the arterial segment to the airway lumen area plus the wall area. The airway-normalized arterial cross sectional area (CSA_{norm}) was used to account for inter-subject differences in airway and arterial sizes. Since the arterial and airway branching patterns slightly differed, we normalized a parent and child arterial CSA to the proximal portions of the parent and child airway branches. Final measurement verification was performed by manually locating the proximal airways and its corresponding arterial segment and estimating CSA with digital calipers.

6.3 RESULTS

Central Vessel Measurements: Effects of Lung Volume and Contrast

TPVV (and by extension TPAV), as expected based upon their space filling function, positively correlated with lung volume in both the FRC and TLC images, necessitating normalization to the lung as shown in Figure 25a. When we performed the normalization (Figure 25b), the $TPVV_{norm}$ was significantly larger in the FRC images compared to TLC images (2.98±0.28 % and 3.47±0.3 % for FRC and TLC, respectively, $p<0.01$). After separating data into NS and SS groups, the $TPVV_{norm}$ was larger at FRC compared to TLC for SS subjects (3.68 ± 0.33 % vs. 3.0 ± 0.30 %, FRC vs. TLC, $p<0.01$) but there was no difference in $TPVV_{norm}$ between TLC and FRC for NS subjects (3.21 ±0.38 %, $p<0.01$).

The absolute arterial CSA (not normalized to the airway CSA), shown in Figure 26a, did not differ between TLC and FRC images. For NS and SS subjects, CSA was between 30-50mm^2 for both TLC and FRC images. After normalizing to the airway CSA, the normalized CSA (CSA_{norm}) was significantly larger at FRC compared to TLC for both NS and SS subjects and was larger in SS subjects compared to NS subjects. At TLC lung volume, CSA_{norm} was close to 1.0 and the between group differences in CSA_{norm} were not detected, as shown in Figure 26b.

Since FRC images were contrast-enhanced, we assessed if the presence of contrast within the central vessels affected our CSA measurement. In SS and NS subjects, the CSA was measured in virtual non-contrast (VNC) images, obtained from DECT decomposition. As described in the introductory chapter (Chapter 3, DECT Perfused Blood volume), the DECT decomposition, using water as a basis material, virtually "subtracts" iodine from the original contrast-enhanced images, creating a virtual unenhanced image. At baseline (pre-sildenafil images), the mean intensity in the main pulmonary artery of the VNC images was 70.4 ± 10.9 SD compared to 241.0 ± 43.6 HU in the contrast-enhanced images. This was an approximately 3.5-fold HU reduction in contrast enhancement that was observed in the pre and post sildenafil PBV images. Figure 27 shows that vessel CSA differed by no more than 10% using the VNC or contrast-enhanced images to measure CSA measurements in both the pre and post sildenafil images and they did not differ between NS and SS subjects, suggesting that our measurement of the vessel outer wall was unaffected by contrast enhancement in the vessel lumen and wall.

The Central Arterial Response to Sildenafil Differentiates NS and SS Smokers

With the notion that downstream vascular resistance reflects up-stream changes of vascular geometry, we examined the acute arterial response in NS and SS subjects to sildenafil using our whole lung vascular and detailed CSA measurements. The $TPAV_{norm}$, was measured in the right lower lobe (RLL) and right upper (RUL) of the lung. The right lower lobe $TPAV_{norm}$ in SS subject was significantly greater ($p<0.05$) compared to NS subjects. The peel and core $TPAV_{norm}$ for the right lung did not differ between groups, although the core or central $TPAV_{norm}$ tended to be greater in the SS subjects (3.14 ± 0.41 % and 2.87 ± 0.35% for SS and NS subjects, respectively, $p=0.07$). We plotted the relationship between PBV and the core and peel $TPAV_{norm}$ in the right lung, observing a significant positive correlation between core $TPAV_{norm}$ and PBV and a negative correlation between peel $TPAV_{norm}$ and PBV. In SS, there was no relationship between pre or post sildenafil TPAV and PBV.

Administering sildenafil significantly increased the $TPAV_{norm}$ in both NS and SS subjects and the between-group differences were eliminated, as shown in Table 6. To test the notion that $TPAV_{norm}$ is reflective of downstream resistance, we evaluated the change in $TPAV_{norm}$ vs. the change in PBV pre- vs. post-sildenafil. PBV and $TPAV_{norm}$ changes with sildenafil were inversely correlated in SS subjects ($R^2 = 0.62$; $p<0.01$), while in NS subjects there was little change in PBV in response to sildenafil and no significant relationship ($R^2 = 0.13$; p=n.s.). In Figure 28, NS points are seen clustered around the y axis whereas for SS subjects they cluster about the regression line with a slope of -0.38.

After observing a significant difference between groups in the lobar $TPAV_{norm}$, we focused on a more detailed structural analysis using our airway-normalized CSA in the right lower lobe. CSA_{norm}, algorithmically independent measure to that of $TPAV_{norm}$, was compared between SS and NS subjects pre- and post-sildenafil. An example of the RB10-associated arterial segment, along with its child branches, is shown in the Figure 29a and the reconstructed arterial and airway-normalized CSA is shown in Figure 29b for the parent branches of RB10 and LB10 (i.e. lower lobes). Visually, the CSA of the arteries were larger compared to the airways in SS subjects, as shown in the superimposed artery and airway masks in the inlet of Figure 29b**.** The CSA_{norm}'s for the NS subjects were not significantly different from 1.0 either before or after sildenafil. However, as demonstrated in Figure 29**c**, the pre-sildenafil SS smoker CSA_{norm}'s were significantly greater than 1.0 and significantly greater than the NS subjects. This measurement of CSA was significant even after adjusting for pack years and age (p=0.03). With sildenafil, these SS vs. NS differences in CSA_{norm} were eliminated. Figure 29d shows that sildenafil increased the CSA_{norm} in NS and decreased the CSA_{norm} in the SS subjects, with a change that was significantly different between the two groups ($p<0.01$). Figure 30 shows the relationship between change in CV of the whole lung and change in CSA_{norm} of the RLL after sildenafil. There is a clear separation of the two groups, with a significant correlation in SS subjects (Pearson's rho = 0.79, $p<0.05$); whereas in NS subjects, points were clustered without a significant association between change in CV and change in CSA_{norm}. There was a significant between-group difference for the RB10 path and near-significant (p=0.06) between-group difference for the LB10 path.

6.4 DISCUSSION

In this study, we provide details regarding our development of quantitative measures to assess the central pulmonary vascular structure, focusing on lobar vascular volume (TPVV and TPAV) and a more detailed assessment of arterial cross-sectional area (CSA) as structural biomarkers of pulmonary vascular dysfunction in CAE-susceptible smokers. We show that central pulmonary arterial dimensions (assessed by two algorithmically separate methods: $TPAV_{norm}$ and arterial CSA_{norm}) were significantly larger in the SS population compared with their NS counterparts, consistent with the notion of increased peripheral arterial resistance in the SS smokers (143). This dilation of the central pulmonary arterial tree is consistent with the observations of pre-sildenafil vasoconstriction discussed in Chapter 5. The increased CSA_{norm} in the SS subjects was eliminated with sildenafil, and the change in arterial volume inversely correlated with PBV change. These observations support the hypothesis that CAE-susceptibility is associated with alterations in peripheral vascular physiology and restoration of a more uniform PBV distribution as well as a reduction in peripheral vascular tone may represent a restoration of blood flow to inflamed lung regions.

Measurement of TPVV has previously been used as a structural of pulmonary vascular disease in advanced COPD (1, 42). Alford et al., in a MDCT study of patients with moderate COPD, observed a larger TPVV in current and former smokers compared to controls, after adjusting for body and lung size (see review in (9)). Grout et al.

observed that TPVV inversely correlated with post-bronchodilator FEV_1 and positively correlated with percent emphysema, suggesting that TPVV is a vascular phenotype for emphysema-dominant disease (60). We show that that rather than using whole lung vascular measures (arteries and veins), regional arterial measurements (lobar TPAV and cross-sectional area) provide a more sensitive vascular measure in differentiating cohort of smokers with and without subclinical emphysema. Since emphysema development occurs regionally, occurring predominantly in the upper lobes (181), we proposed looking at regional vascular measures. While whole TPVV and TPAV did not differ between NS and SS subjects, the right lower lobe TPAV was more sensitive to differences between NS and SS subjects. We purposefully avoided sampling the upper lobes because of known artifacts from the subclavian vein as well visible lung destruction, which affect detection of small vessels (106, 107). Our regional analysis of TPAV in otherwise healthy lower lobes supports the previously reported relationship between increased CT percent emphysema and decreased left ventricular filling due to increased peripheral vascular resistance (10).

We normalized TPVV and TPAV to lung volume based on our observed association between vascular volume and lung volume. The effects of lung inflation on vessel caliber are complicated but it is well known that greater inflation compress small vessels and lead to increases in pulmonary vascular resistance (63) but larger lung volume reduce venous return to the right heart, which can affect the amount of blood in the central vessels. This may have been why $TPVV_{norm}$ was lower at TLC compared to FRC in SS subjects. The larger $TPAV_{norm}$ finding in SS suggests additional mechanisms, including greater peripheral vascular resistance. Our examination of arterial CSA_{norm} and

$\text{TPAV}_{\text{norm}}$ in the RLL at FRC supports the notion of larger (dilated) central arteries in SS subjects. We were able to differentiate SS and NS subject using CSA_{norm} better at FRC compared to TLC, suggesting that between-group comparisons of arterial morphometry should be performed at a lower lung volume in order to avoid small vessel compression.

Our normalization of the central arteries to the airways was to account for differences lung sizes between subjects. Few studies have attempted to quantify the normal range of the pulmonary artery to bronchus ratio at the segmental or sub-segmental airways (12, 91). Kim et al, using thin slice CT, observed a range of artery-to-bronchus ratio between 0.53-1.39 (91). Using this as a reference, our NS subjects were within the normal range but CSA_{norm} for SS subjects were at the higher end of normal, even after using the outer airway lumen as the airway CSA. The CSA_{norm} in RB10 showed stronger differences between groups while the LB10 parent branch demonstrated a near significant ($p = 0.06$). The LB10 branch was susceptible to cardiogenic motion artifacts, making it difficult to detect child branches of the airways. We therefore, focused on parent branches for our analysis.

Intravascular contrast had minimal influence on CSA measurements, as there was less than 10% difference between VNC and contrast-enhanced FRC images pre and post sildenafil. The contrast scans tended to underestimate vessel CSA compared to measurements in VNC images, in both NS and SS subjects. Previous studies showed that measurement error increased with less contrast in the vessels due to an inability to differentiate vessel lumen and wall; but these studies relied on using density threshold to make measurements of a vessel mask (159, 189). We based our CSA measurements on reconstructed CT images and a FWHM-based method to estimate the vessel wall, accounting for partial volume effects, which helped minimize error near the vessel wall and is a an appropriate method for measurement of contrast-enhanced images based on prior validation studies (93, 105).

Our method of measuring CSA was sensitive to the vascular changes elicited by sildenafil and the relationship between the change in CSA and CV and the change in TPAV and PBV clearly represents the relationship between local vascular structural alterations and changes in PBV distribution; this further signifies the important vascular structural and functional differences between CAE-susceptible and non-susceptible smokers.

Although dilation of central arteries, due to distal vessel pruning, is associated with advanced COPD (123, 172, 181), we observed dilation of central arteries in our cohort of SS subjects with only limited visible signs of CAE. The reversibility of this arterial dilation with sildenafil in the SS subjects suggests that neither the increased PBV heterogeneity nor the upstream arterial dilation is related to parenchymal destruction (and loss of peripheral parenchymal vessels). Perfusion to injured lung regions is important to the inflammatory response cascade including delivery of progenitor cells promoting parenchymal repair (128, 129). This study advances the use of volumetric CT imaging techniques to measure regional structural and compare to functional relationships in SS and NS smokers.

6.5 SUMMARY

This study advances the use of high resolution CT imaging techniques coupled with dual energy imaging to measure regional structural to functional relationships in SS and NS smokers. We found a larger $TPAV_{norm}$ in the SS subjects and demonstrated that changes in $TPAV_{norm}$ were related to changes in PBV in this same population. This supports the previously reported relationship between increased CT percent emphysema and decreased left ventricular filling and suggests a link between pulmonary vascular dysfunction and emphysema. Although dilation of central arteries, due to distal vessel pruning, is associated with advanced COPD, the absence of visual or quantitative CT-based metrics of parenchymal destruction, other than limited signs of CAE in our SS cohort, and the reversibility of the arterial dilation with sildenafil in the SS subjects suggests that the neither increased PBV heterogeneity and/or the upstream arterial dilation is related to parenchymal destruction (and loss of parenchymal vessels).

Table 7: Normalized vascular volume data (%) reported as a mean ± s.d.; TPVV, total pulmonary vascular volume (arteries + veins); TPAV, total pulmonary arterial volume; All measurements were performed in the right lung; RLL, right lower lobe; RUL, right upper lobe. **p<0.05 vs. NS subjects (pre sildenafil).

volumes	NS		SS	
	PRE	POST	PRE	POST
Lung volume (Liters)	1.95±0.57	1.90±0.60	1.77±0.18	1.76±0.17
TPVV (mL)	76.7±27.5	83.3±31.3	68.5±10.1	75.3±10.7
$TPVV_{norm}$	4.7 ± 0.32	5.6 ± 0.89	5.0 ± 0.50	5.6 ± 0.63
$TPVV_{norm}$ (RLL)	2.34 ± 0.21	2.79 ± 0.45	2.31 ± 0.33	2.55 ± 0.33
TPAV (mL)	36.5±14.3	42.1±17.7	34.6±5.1	38.8±6.8
$TPAV_{norm}$	1.0 ± 0.17	1.16 ± 0.26	1.04 ± 0.11	1.20 ± 0.11
$TPAV_{norm}$ (RLL)	1.91 ± 0.30	2.32 ± 0.50	2.17 ± 0.26**	2.58 ± 0.21
$TPAV_{norm}$ (RUL)	1.65 ± 0.26	2.02 ± 0.43	1.78 ± 0.28	2.32±0.43

Table 8: Pre sildenafil vessel CSA computed from reconstructed CT images and the corresponding airway CSA, reported from Apollo workstation, for the parent branches of RB10 and LB10. The CSAnorm was computed from the parent branches. The (b) airway wall area and lumen area in the parent branch of RB10 and LB10. Values are in mm2 and reported as a mean ± standard deviation.

RB10	Vessel CSA (mm^2)	Airway CSA (mm^2)		CSA$_{norm}$
		WA+LA	WA	
NS	39.5±14.0	36.7±14.7	21.9±6.1	1.10±0.15
SS	40.2±13.7	30.3±8.3	22.1±4.0	1.31±0.29*
LB10	PARENT	WA+LA	WA	CSA$_{norm}$
NS	45.7±9.4	39.8.2±7.1	21.7±8.8	1.13±0.22
SS	42.6±9.3	32.9±7.6*	20.8±5.0	1.30±0.32$^{\#}$

Table 9: Post sildenafil vessel CSA computed from reconstructed CT images and the corresponding airway CSA, reported from Apollo workstation, for the parent branches of RB10 and LB10. The CSAnorm was computed from the parent branches. The (b) airway wall area and lumen area in the parent branch of RB10 and LB10. Values are in mm2 and reported as a mean ± standard deviation.

RB10	Vessel CSA (mm^2)	Airway CSA (mm^2)		CSA$_{norm}$
		WA + LA	WA	
NS	40.4±11.2	37.7±13.9	22.3±8.11	1.11±0.20
SS	32.7±9.7	31.4±9.8	18.2±3.2	1.29±0.34
LB10	PARENT	WA+LA	WA	CSA$_{norm}$
NS	47.1±10.4	39.8±9.4	23.4±6.6	1.21±0.25
SS	41.7±11.9	33.7±8.4	19.9 ± 4.5	1.24±0.30

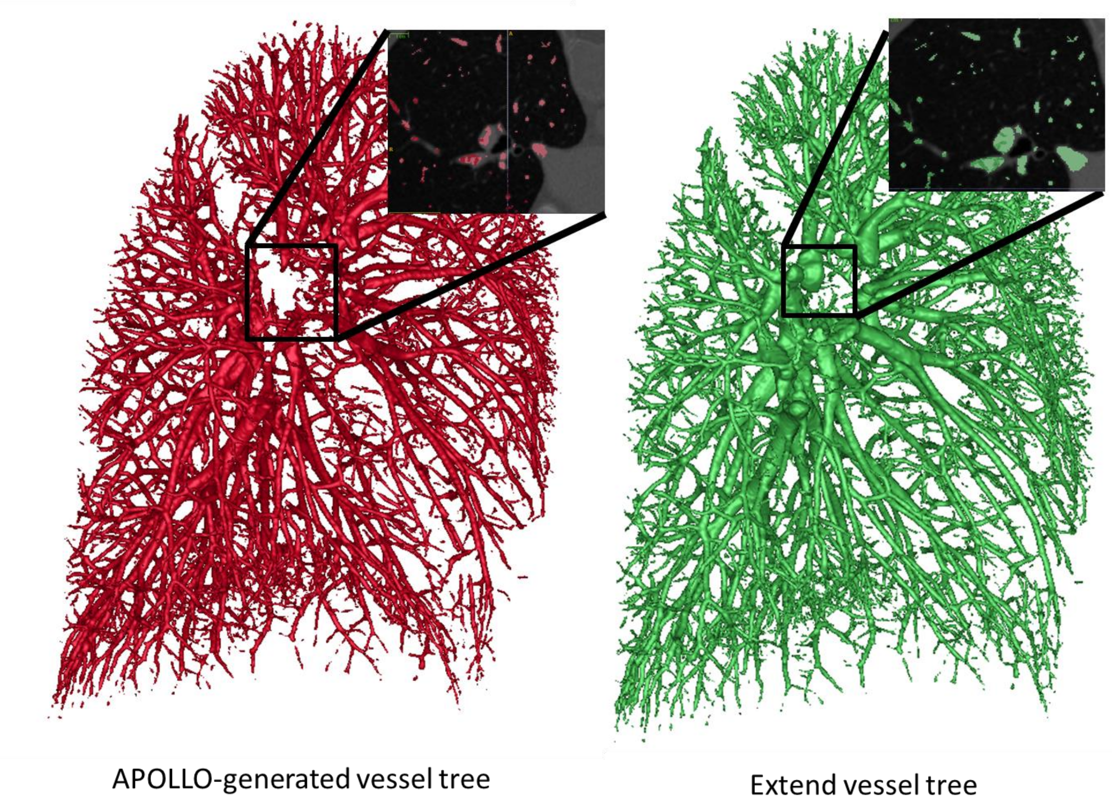

APOLLO-generated vessel tree

Extend vessel tree

Figure 21: Comparison of Apollo-generated vessel tree (left) and the vessel tree after extending the boundaries of the initial Apollo segmentation (right). Vessel extension did not affect peripheral vessels but did increase the mask coverage of central vessels. The cross-sectional subimages show better coverage of vessels near the hilum of the lung after extending the mask.

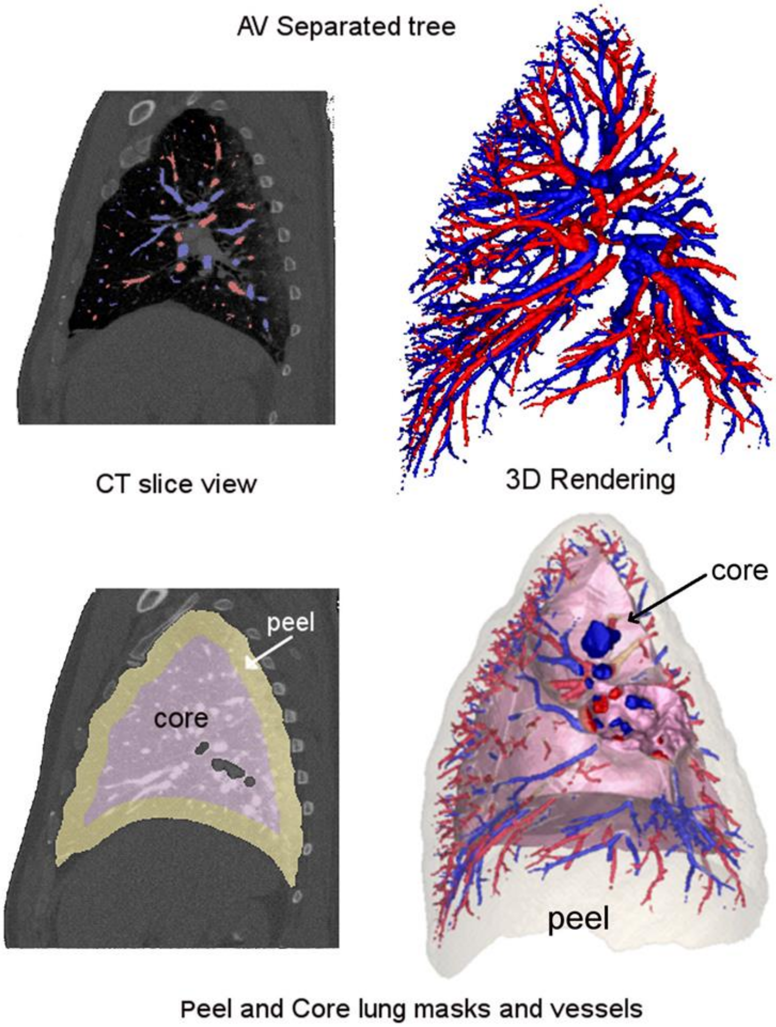

Figure 22: Diagram showing the extraction of the arterial and venous trees and then using the peel (outer 15 mm) lung masks, the peel and core arteries are extracted and normalized to their respective volumes.

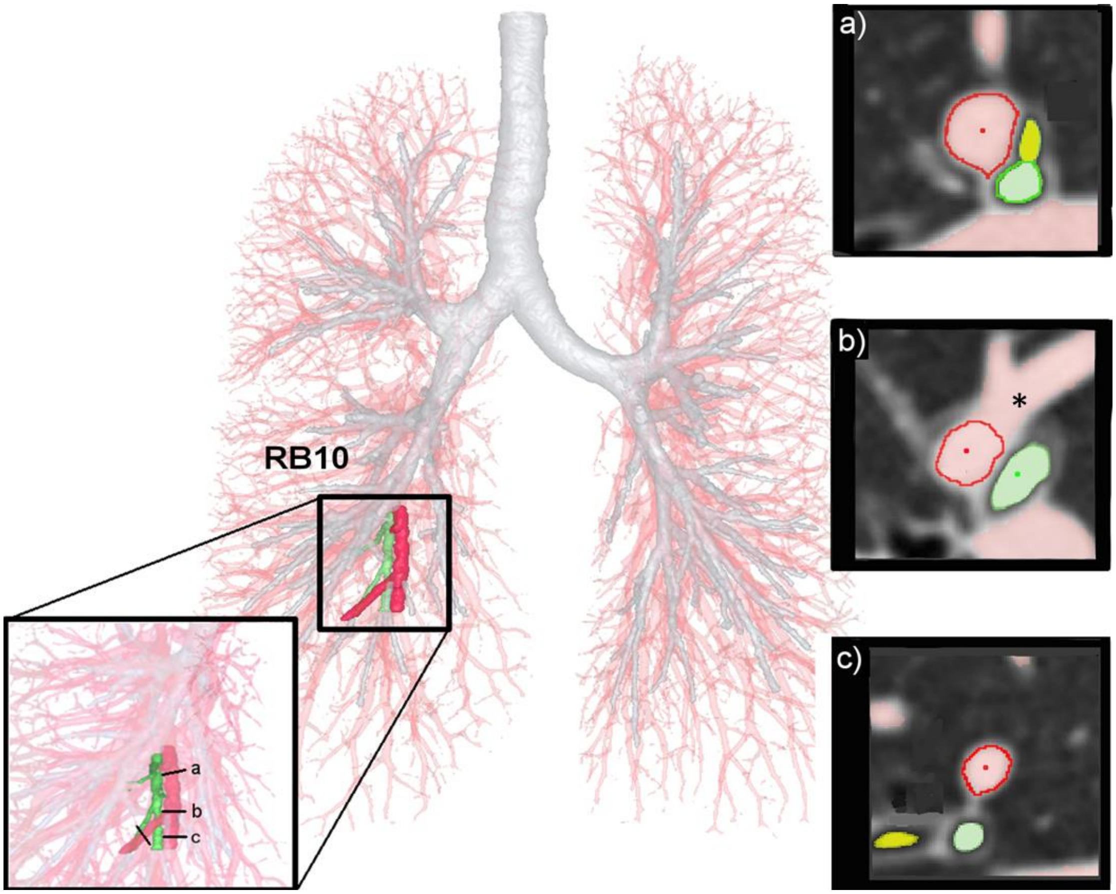

Figure 23: A reconstructed airway (in green) and arterial segment (in red) for the RB10 airway path. In the inlet figure is a magnified view of this reconstructed segment, showing positions where cross-sectional measurements are taken (a, b, and c). In cross-section (a), a minor airway (highlighted in yellow, arrowhead) can be seen. This airway does not follow the major airway and vessel path (highlighted in green and red, respectively) so a seed point is not placed in this yellow are but is placed in the green area. The cross-section (b) shows an artery bifurcation, which is, filtered out during the measurement process so that the actual arterial cross-section (dark red boundary) is measured. The cross-section (c) shows a child branch of the arterial segment in (a) with another minor airway branch in yellow. The corresponding airway and arteries, shown in green and red, are contiguous with the parent branches in (a).

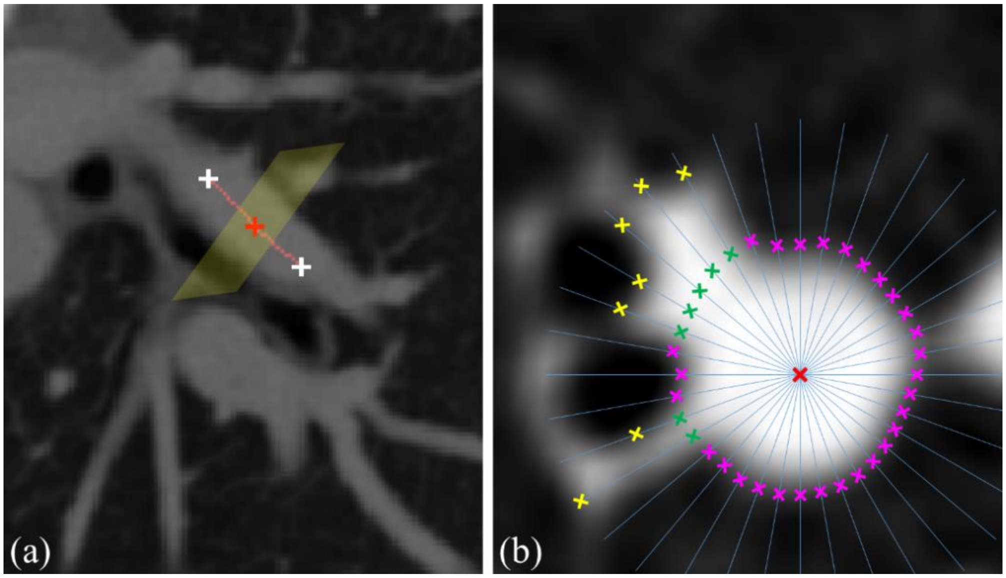

Figure 24: Illustration of arterial cross-section area (CSA) measurement in a CT image. (a) The centerline of an arterial branch is traced as the minimum cost-path joining user selected end points (white-crosses). At a candidate point (red-cross) on the inner one-third segment, the orthogonal plane is used to determine the arterial cross-section area at that point. (b) Initial arterial edge points (purple- and yellow-crosses) are on individual radial lines emanating from the candidate point of (a). The artifactual edge points (yellow-crosses) generated by adhering anatomic structures are replaced by more confident edge points (green-crosses) using coherence analysis and interpolation.

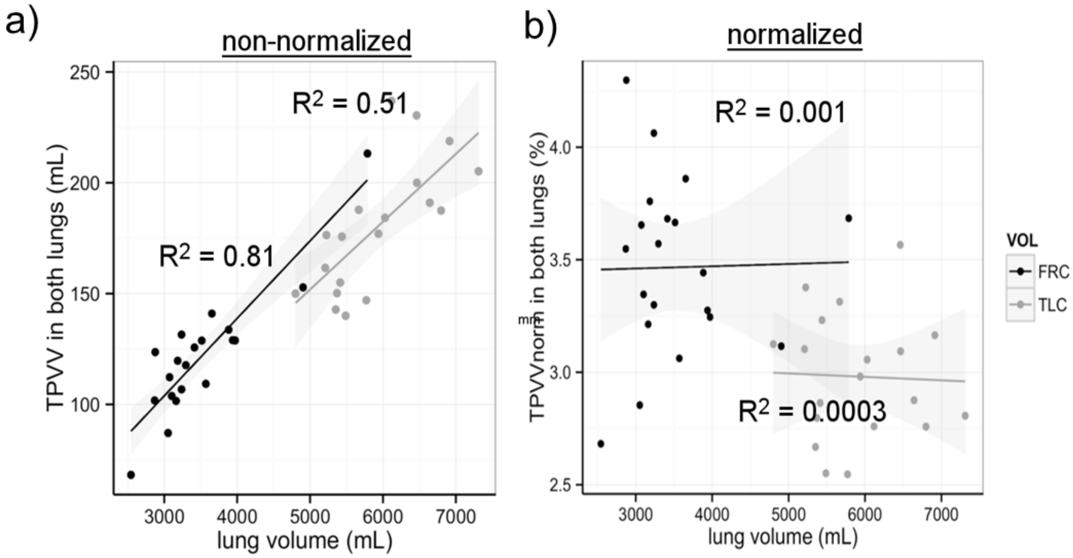

Figure 25: The relationship between lung volume and TPVV for FRC (black dots) and TLC (gray dots) images. FRC images represent the contrast-enhanced baseline (pre-sildenafil) images. After normalizing the TPVV to lung volume (b), TPVVnorm was significantly larger at FRC compared to TPVVnorm at TLC ($p<0.05$).

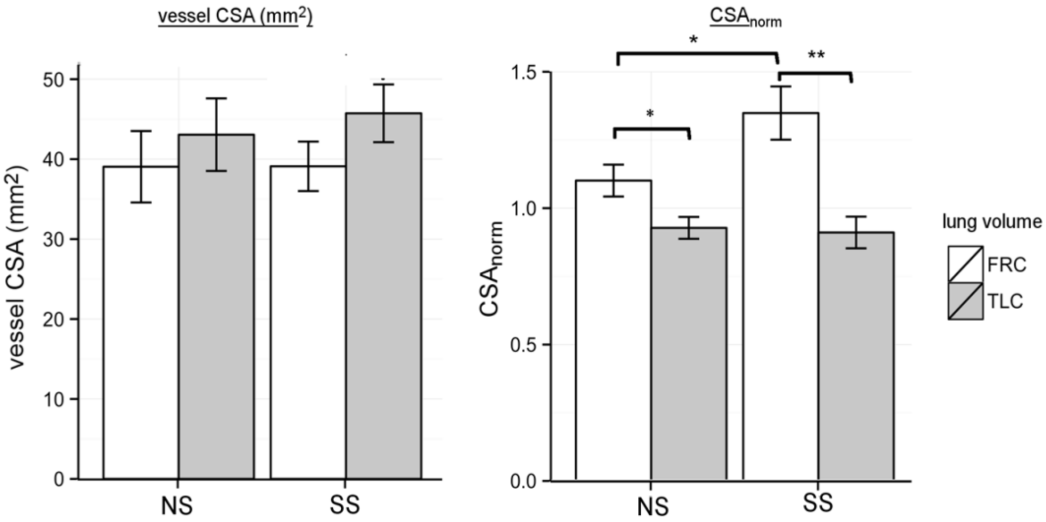

Figure 26: Effects of lung volume on cross-sectional area (CSA) measurements. (left) CSA measured in NS and SS subjects at FRC and TLC for the RB10 path, showing a larger CSA at TLC for SS subjects. (right) CSAnorm (normalized to the airway CSA) shows the opposite relationship, with larger CSAnorm in FRC images compared to at the TLC lung volume; $^{*}p<0.05$, $^{**}p<0.01$.

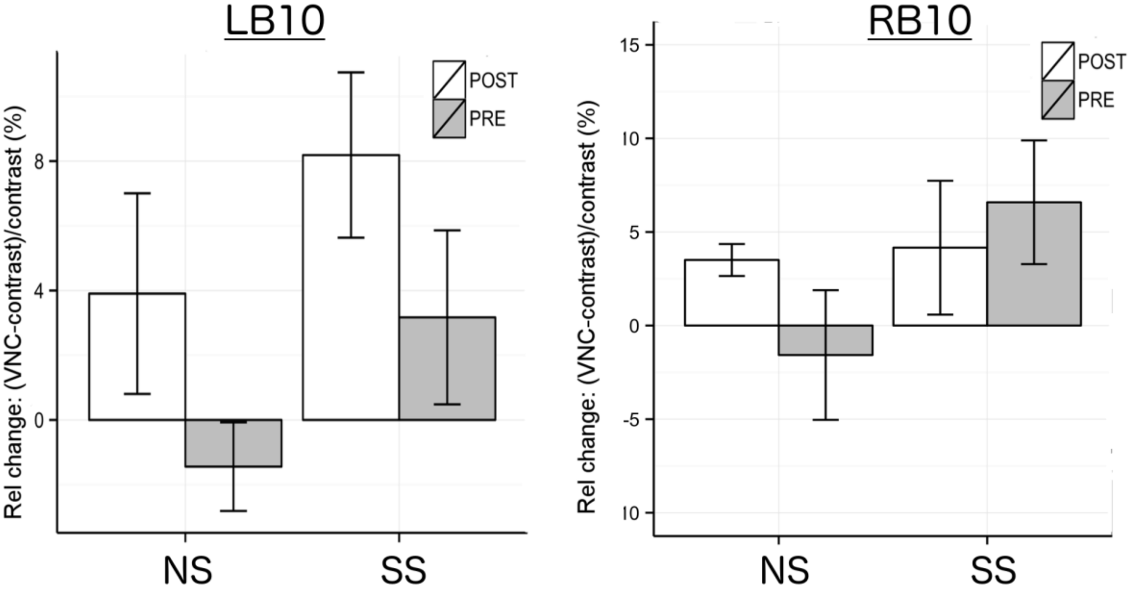

Figure 27: Relative error (change) in vessel CSA between VNC and contrast-enhanced 20%VC images for the LB10 (left) and RB10 (right) branches pre and post sildenafil. Error was small (less than 10%) for both NS and SS subjects.

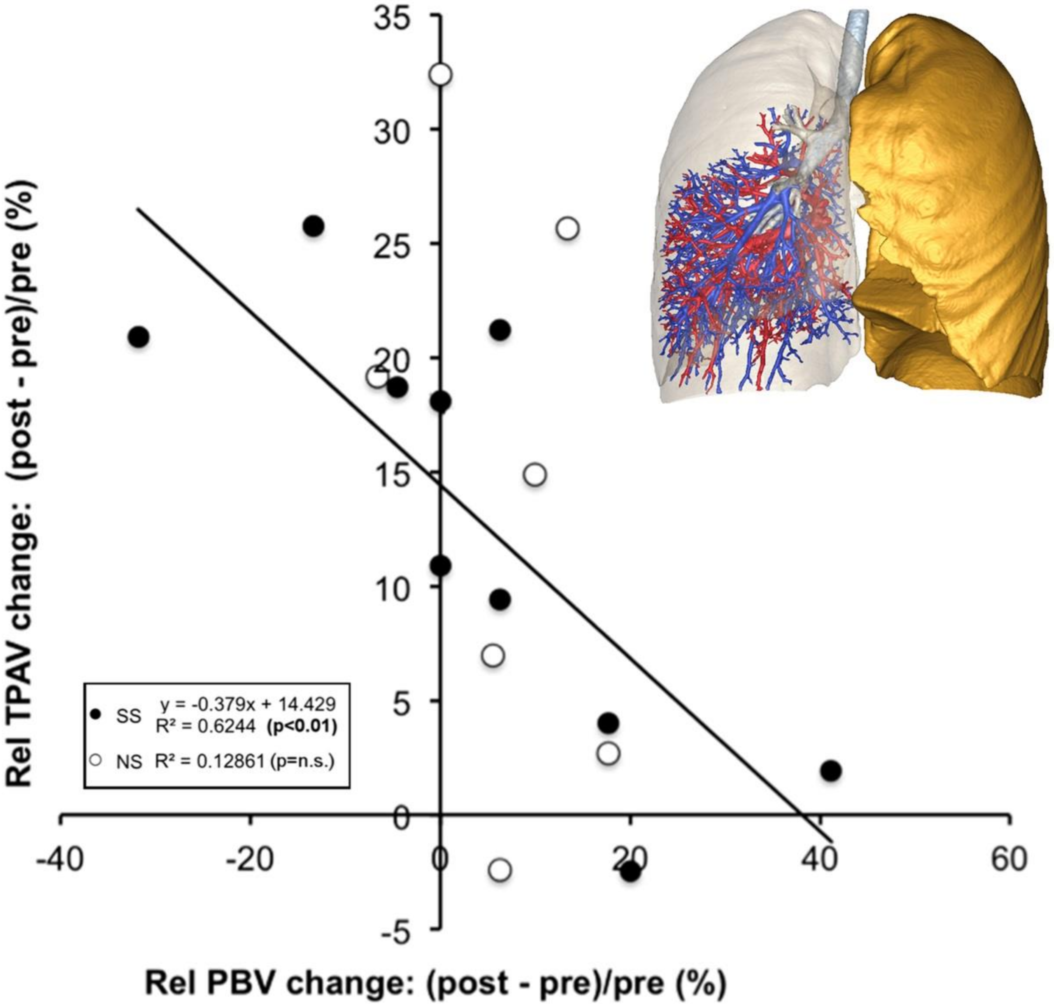

Figure 28: Volumetric CT evaluation of total pulmonary arterial volume pre and post-sildenafil. (a) From the 140 kVp volumetric image, the right lung volume along with the total central pulmonary vascular volume (TPVV) for the right lung was segmented. The lung lobe mask for the right lower lobe was over-layed onto the segmented TPVV and the total central pulmonary arterial volume (TPAV, in blue) was identified and normalized to the whole right lower lobe volume (TPAVnorm). The right lower lobe (RLL) TPAVnorm was identified as largest in SS subjects' pre-sildenafil (b) The relative change in TPAVnorm pre to post sildenafil inversely correlated with the PBV change in SS subjects but not in NS subjects, where this relationship was not significant.

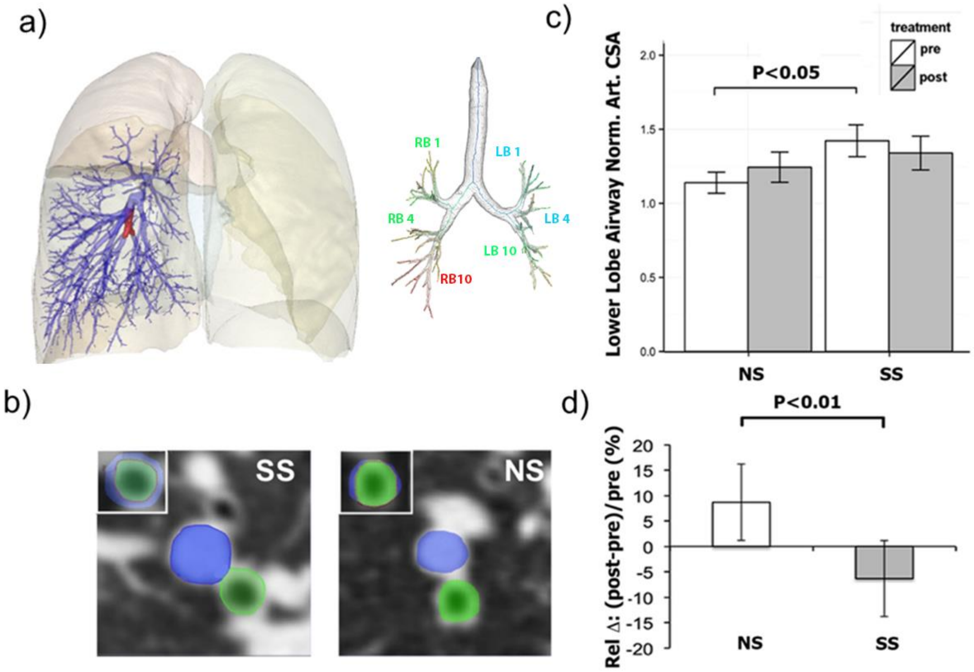

Figure 29: (a) Volumetric CT evaluation of arterial cross-sectional area pre and post sildenafil. Segmental branches of the arterial tree (associated with the RB10 and LB10 bronchial segments shown in the right panel) were sampled in the right and left lung. Shown in red is the RB10 associated arterial segment and its child branches. (b) In the lower left panel, the RB10 airway cross sectional area (52) and associated arterial segment cross sectional are (blue) are demonstrated with their superposition for an SS and NS subject. (c) Arterial CSA normalized to the airway cross-sectional area (CSAnorm) was significantly larger in SS subjects pre-sildenafil and this relationship was eliminated post-sildenafil. (d) Post-sildenafil change in CSAnorm in SS subjects and NS subjects were significantly different (*p<0.01).

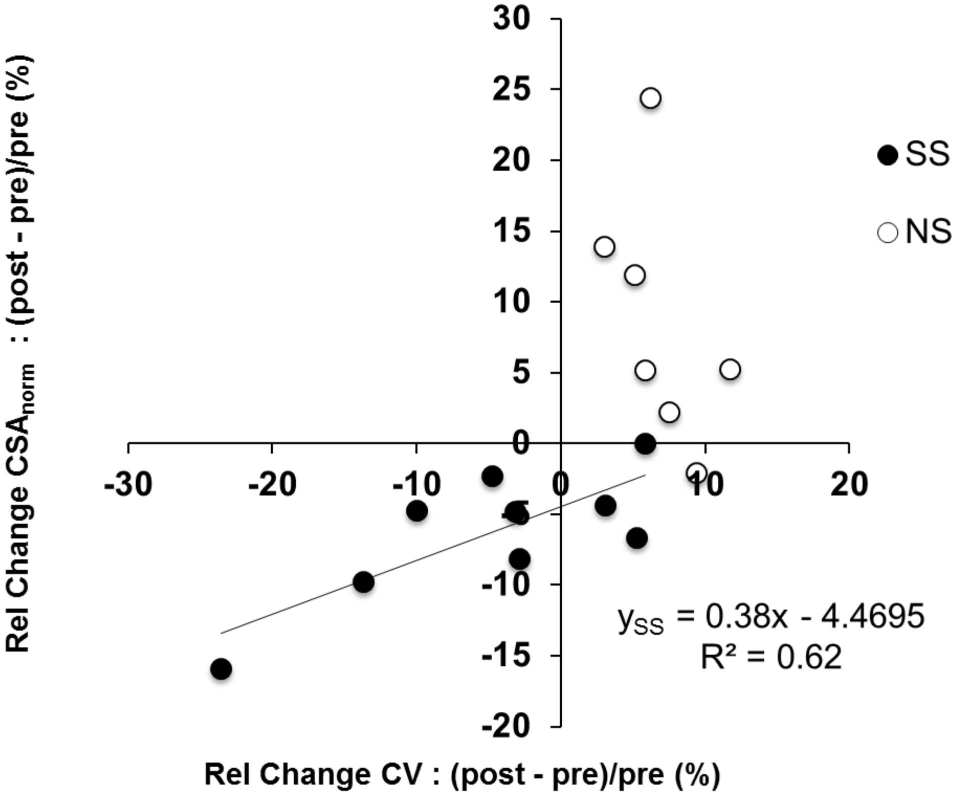

Figure 30: The association between change in CSAnorm and change in CV for the whole lung is well correlated for SS subjects (Pearson's rho = 0.78, $p<0.05$). There is clear separation between groups, underlying the differences in response to sildenafil. The positive association between CSAnorm and CV suggests that a decrease in CSA associates with a decrease in CV. This is in support of our hypothesis that decrease in central arterial dimensions, due to peripheral vasodilation, contributes to decrease in perfusion heterogeneity by redistributing blood flow to poorly perfused lung regions.

CHAPTER 7: CONCLUSION

CT is a powerful method for the noninvasive assessment of the lung disease and improvements to acquisition speed and detector technology have provided high-resolution structural and functional information of the lung. This has helped make a transition from characterizing the severity of lung disease to phenotyping and potentially predicting which types of patients will progress with disease.

CT measures have largely focused on airway and parenchymal density based measures (73, 132) but the structural alterations are likely to be a result of small-scale changes in lung, requiring more sensitive detection of regional lung function, including regional perfusion and ventilation. This body of work focuses on dual energy CT (DECT)-based perfused blood volume (PBV) as a predictive vascular phenotype in smoking-associated centri-acinar emphysema (CAE). We address our main hypothesis, that smoking-associated pulmonary perfusion heterogeneity, in the midst of lung inflammation, is a reversible process, utilizing advanced functional and structural measures of the pulmonary vascular bed and central vessels to support the notion that pulmonary perfusion heterogeneity is reversible and a direct result of peripheral (downstream) arteriolar vasodilation.

As a precursor study to using PBV imaging to phenotype lung disease, we explored DECT PBV techniques in a pig model to refine the imaging protocol, relating several DECT PBV functional and structural measures with known physiological changes in a hypoxic pig model. We developed the technique for regional PBV and CV assessment, utilizing a carefully controlled imaging protocol and a timed test-bolus. We also provided a normalization approach for the PBV analysis which strongly correlated with pulmonary artery pressure (PAP) and demonstrated that changes in CV and central arterial volume were sensitive measures to PAP increases, reflecting the downstream peripheral vascular changes occurring in the lung with hypoxia. This protocol development and analysis provided a framework to assess regional lung physiology in human studies.

DECT PBV and central vascular measures were applied to smokers with and without the presence of centri-acinar emphysema (CAE). Using the PBV imaging technique and analysis of regional PBV heterogeneity, we demonstrated that the increased heterogeneity, previously characterized by Alford et al. (3), is reversible with sildenafil by inhibiting vasoconstricted regions in the lungs of CAE-susceptible smokers, thus increasing blood flow to regions that are inflamed due to smoking but are poorly perfused. In addition to functional PBV measures, we demonstrated, through the use of sensitive CT measurements of the central arterial tree, that this vascular phenotype (and response to treatment) helps differentiates between CAE-susceptible and CAE non-susceptible smokers.

Expanding on the CT-based measures of total pulmonary vascular volume (TPVV), we demonstrated that separation of the total arterial volume (TPAV) was crucial in differentiating between smoking cohorts. We additionally showed that treatment with sildenafil, by relieving peripheral vasoconstriction, leads to upstream changes in central arteries. This has further characterized the pathologic pulmonary vascular-related changes in COPD subjects. As an alternative to TPVV, the TPAV and central cross sectional arterial measurements normalized to the associated airway segments (CSA_{norm}), developed in this study, provide new and sensitive measures of the pulmonary vascular tree that may elucidate downstream vascular dysfunction independent of PBV imaging. Most importantly, this study provides evidence that vascular-related changes from a pharmaceutical intervention reverse perfusion heterogeneity and that these pharmaceutical responses can be directly measured with sensitive CT methods. By relieving the downstream vasoconstriction with sildenafil and restoring blood flow to inflamed tissue would not only help normalize perfusion throughout the lung but may potentially correct the known physiological abnormalities in smokers with early disease by making the delivery of progenitor cells to damaged lung regions possible. These newly developed structural and functional CT-based phenotypes are crucial to the development of targeted lung therapies.

CT continues to play an important role in diagnosis of various lung diseases, such as COPD and asthma. Sensitive functional imaging methods, such as perfusion CT and DECT PBV help provide a better understanding of the pathogenesis and progression of disease stages and identify sub phenotypes of disease. These functional measures are intended to compliment structural information to help characterize the physiological changes in lung in hopes of developing targeted therapies. Imaging of ventilation and perfusion using DECT have been attempted in a single patient with lung disease. Figure 31 shows an example of a back-to-back xenon-enhanced DECT ventilation study and iodine-enhanced PBV study, showing the distribution of both patchy ventilation and perfusion (164). With such methods, radiation dose is a concern, so the pursuit of low-dose combined ventilation and perfusion imaging in patients with early disease is ideal and is possible with improvements in scanner technology, including the use of multi-spectral CT scanners and photon counting detectors, This will allow for better energy spectral separation so that imaging of multiple functional parameters can be achieved, including ventilation and perfusion.

In summary, functional CT measures of pulmonary perfused blood volume is an extension of functional dynamic perfusion imaging but with a simple-to-implement protocol with combined structural and functional information of the whole lung. Our experimental development and validation in humans helped to characterize a novel vascular phenotype in smoking-associated emphysema in terms of its regional parenchyma and central vascular response to pharmaceutical intervention.

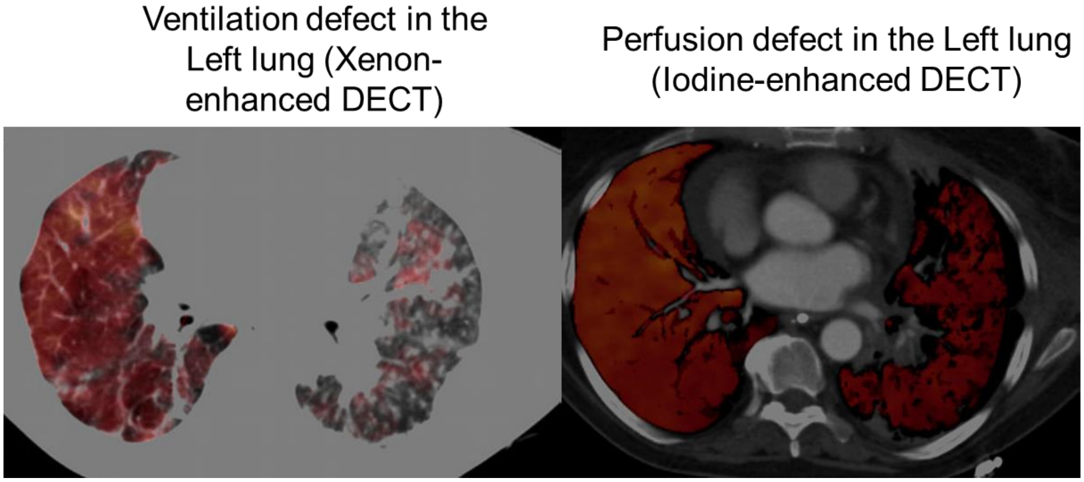

Figure 31: Successive DECT ventilation and perfusion (PBV) imaging performed in a patient with pulmonary fibrosis, showing patchy hypoventilation and patchy perfusion in the left lung. Such studies require washout of the xenon before iodine infusion. With better spectral separation of xenon and iodine, dual technique ventilation and perfusion imaging can be performed using simultaneously inhalation of xenon and injection of iodine, under the same imaging protocol.

CHAPTER 8: LESSONS LEARNED AND FUTURE DIRECTIONS

The studies described in this thesis were based on the central hypothesis that in emphysema-susceptible smokers, the lung's vascular response to lung inflammation is to regionally constrict peripheral vessels and shut off blood to areas that are well perfused, limiting resolution of inflammation and contributing to the sequela of lung destruction. The important findings from these studies are that the increased perfusion heterogeneity is a reversible process, evidenced by changes in both vascular structure and functional parameters, and not a byproduct of advanced disease. The central hypothesis is predicated on the assumption that **parenchymal inflammation is similar between emphysema-susceptible and non-susceptible smokers but it's the regional vascular response to sildenafil that is differen**t (74). In order to measure and compare regional levels of lung inflammation between smoking cohorts, to test if parenchymal inflammation is similar between groups, sensitive and quantitative imaging tools are required. In this chapter, we discuss initial experiments that were performed using single photon emission tomography (SPECT) to assess regional lung inflammation, discuss our initial findings and some important considerations to help in the design of future imaging studies of inflammation in COPD.

8.1 IMAGING LUNG INFLAMMATION WITH SPECT

Studies quantifying lung inflammation in smokers in relation to disease severity have been limited. Smoking-related inflammation is thought to be dominated by the neutrophil influx into the lung. A study by Ruperalia et al. using single photon emission tomography (SPECT) measured the neutrophil migration in the lung and found increased accumulation of 99m-Technitium (^{99m}Tc) labeled neutrophils in the lungs of COPD patients, suggesting it was sensitive to lung inflammation during active smoking (139). With our goals of relating differences in peripheral vascular function, measured by our DECT-PBV protocol, with measures of regional lung inflammation in CAE-susceptible and non-susceptible smokers, we developed an initial SPECT lung protocol, tested in an animal model of gastric acid-induced acute lung injury, to compare regions of inflammation, measured with SPECT, with DECT-based PBV changes during early inflammation.

8.2 ANIMAL STUDIES AND INITIAL FINDINGS

We used ^{99m}Tc labeled white blood cells (WBCs), a common SPECT radiotracer, to measure regional inflammation on the same day as performing DECT PBV imaging. An animal model of aspiration-induced lung injury, which is a slowly developing injury (184), was used in order to simulate regional lung inflammation and measure the uptake of the radiotracer. This type of localized lung injury was possible by introduction of a spray-tipped catheter into the airways, guided by a bronchoscope, to inject local gastric acid within the airway lumen to several regions of the lung, as shown in Figure 32. Lung inflammation and accumulation of WBCs were measured through sequential SPECT imaging performed every 30 min for 6 hours (approximately 1 half-life of the ^{99m}Tc tracer). Figure 33 shows a planar projection image from the gamma camera (a) and a SPECT image (b) after 3D reconstruction of projection images, showing accumulation of

WBC several hours later in areas where gastric acid was instilled. This coincided with the lung areas that had fluid accumulation on CT (Figure 32 bottom panel). DECT PBV was imaged between SPECT scans to compare perfusion changes in the lung with local inflammation. This is shown in Figure 34a-b at baseline and 1 hr after instilling gastric acid. We observed an increase in PBV to the dependent lung where inflammation was observed on SPECT (Figure 34c-d). In the apical lobe, which was the second inflamed region, fluid build-up in the lung reduced perfusion to this region., It took several hours for this type of lung injury to develop, so measuring accumulation using a tracer, like ^{99m}Tc, with a short half, was a challenge. We observed regional localization of the tracer at sites of inflammation within minutes after injection of the labeled WBCs but there was a loss of counts in these regions within a few hours due to filtration of WBCs in the spleen, as show in Figure 35. Other gamma emitters, such as 111-Indium and 67-Gallium, have been used to image inflammation in the lung but since these agents have a longer half-lives, same-day imaging was not possible, since labeled neutrophils would recirculate into the lung 6-24 hours after injection (88, 101).

8.3 OBJECTIVE ASSESSMENT OF INFLAMMATION AND PBV

Regional comparison of CT, PBV and SPECT images required spatial co-registration of multi-modal images. In combined SPECT/CT systems, co-registration software is used by usually require similar between CT and SPECT to avoid large mis-registration errors. In clinical SPECT/CT studies, tidal volume breathing is sufficient to register images for diagnostic interpretation (150, 157). For our studies, we were equipped with a Siemens gamma camera with SPECT reconstruction capabilities, so the

CT imaging was performed separately on our Siemens Flash. To avoid global mis-registration, from moving the animals between SPECT and CT scanners, small quantities of radiotracer were placed in plastic vials and secured on the surface of the animal to serve as fiducials. These fiducials were easily identified on SPECT and CT. We also imaged animals on CT and SPECT at the similar lung volumes. During the CT scans, animals were breath-held during the scan duration, which was a less than 20 seconds. The acquisition time for SPECT was at least 20 min, so intermittent breath holds of 30 seconds was performed using a step-and-shoot acquisition mode, with tidal volume breathing at a mean airway pressure close to the breath-held airway pressure (15 cmH_20) of CT images. The images for sequential SPECT scans were well registered to CT, as shown in Figure 35a, without the use of image warping software. The use of SPECT/CT system with respiratory gating would help reduce the motion artifacts even further (157). Sequential SPECT image were registered to measure uptake kinetics. Since background signal (i.e. mean lung counts) was high, we needed at least a 4-5 fold higher counts in inflamed lung regions to differentiate them from the background, as shown in Figure 35b. This was difficult to achieve with every animal, as the extent of lung injury varied with the same quantity of instilled gastric acid. In a few studies, it was striking how subtle PBV changes were detectable in animals, such as the increase in PBV in the dependent lung, even with mild and localized lung injury.

8.4 TECHNICAL CONSIDERATIONS

The intrinsic resolution limitations of SPECT make it difficult to compare voxel-by-voxel changes in PBV with regional WBC signal. High resolution collimators and detectors with better energy separation can improve resolution enough to better discriminate regions of heterogeneous blood flow at or near transition zones of inflamed lung (121). Positron emission tomography (PET) is another imaging modality that has been frequently used for detecting lung inflammation, using 18-fluorodeoxyglucose (18-FDG) as a common radiotracer. In models of lung inflammation, uptake of FDG PET is predominantly from neutrophil influx. This imaging can provide more quantitative information about uptake, in relation to mass or volume of tissue in the lung (31). In addition, the improved spatial resolution, compared to SPECT, allows for comparable assessment of anatomical and/or functional data from CT (5).

While 18-FDG imaging studies have only recently been performed in smokers (146, 156), it remains to be seen how diffuse inflammation, in relation to regional PBV heterogeneity, can be used to differentiate CAE-susceptible smokers. We provide some initial findings using SPECT to address the technical aspects of multi-modal comparison of DECT and SPECT and show this type of imaging and cross-correlation between functional PBV measures and measures of inflammation is possible and likely a future direction of research.

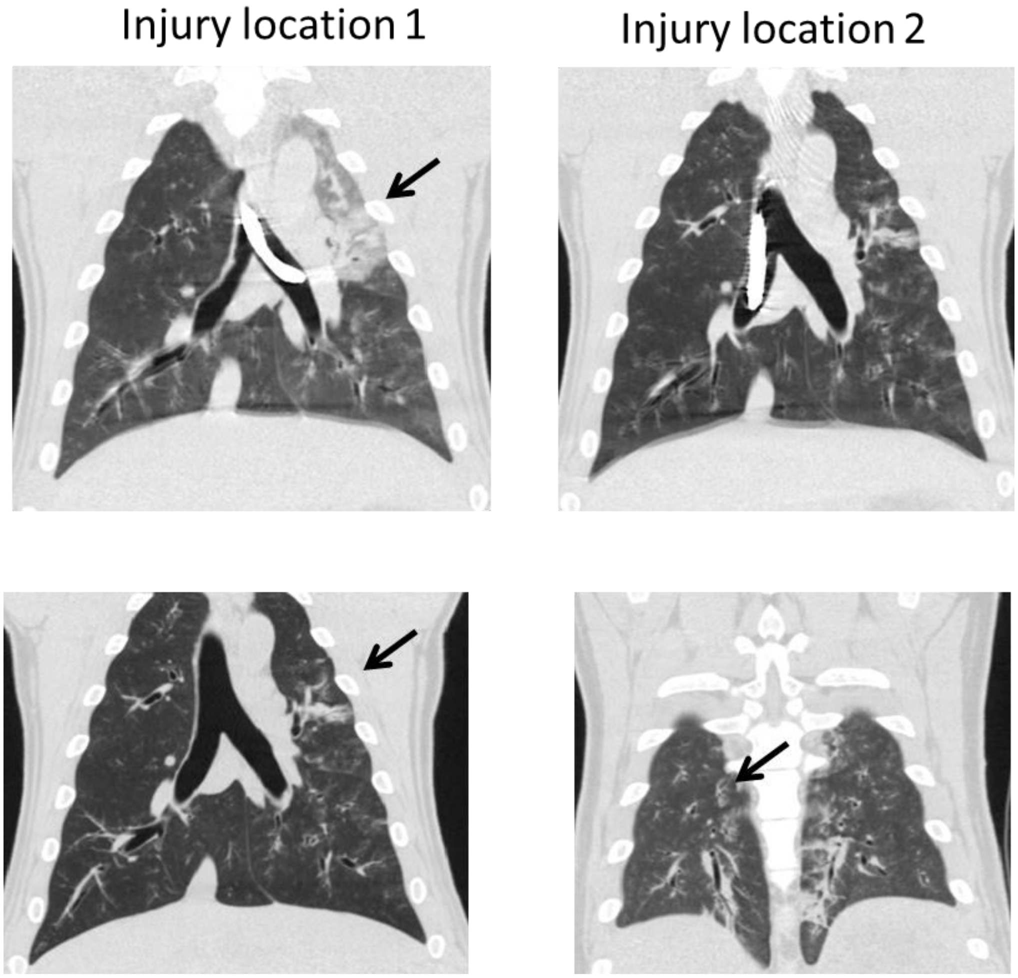

Figure 32: Aspiration-induced lung injury initiated by introduction of gastric acid into the apical (location 1) and basal (location 2) regions of the lung. The bronchoscope, shown in the top left panel, is introduced in the central airway and helps visualize the airway and guide the spray-tipped catheter, which injects gastric acid to the sites in the apical and dependent regions of the lung (arrows).

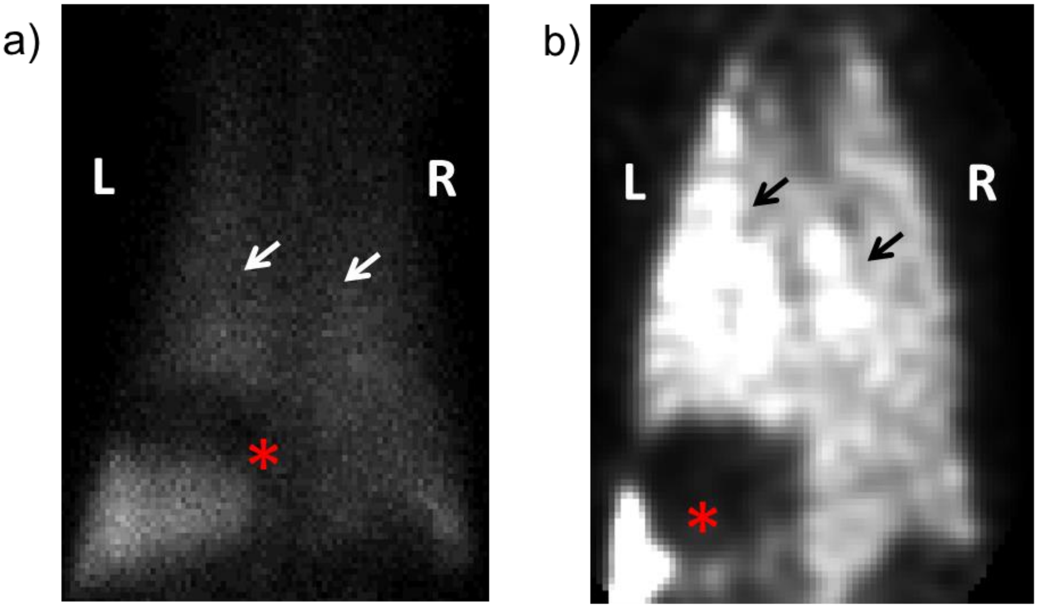

Figure 33: Anterior-posterior planar views showing accumulated WBC in the lung (arrow) and spleen (*). (b) Reconstructed SPECT images showing regionally distinct “hotspots”(arrows) of WBCs in the left and right lungs.

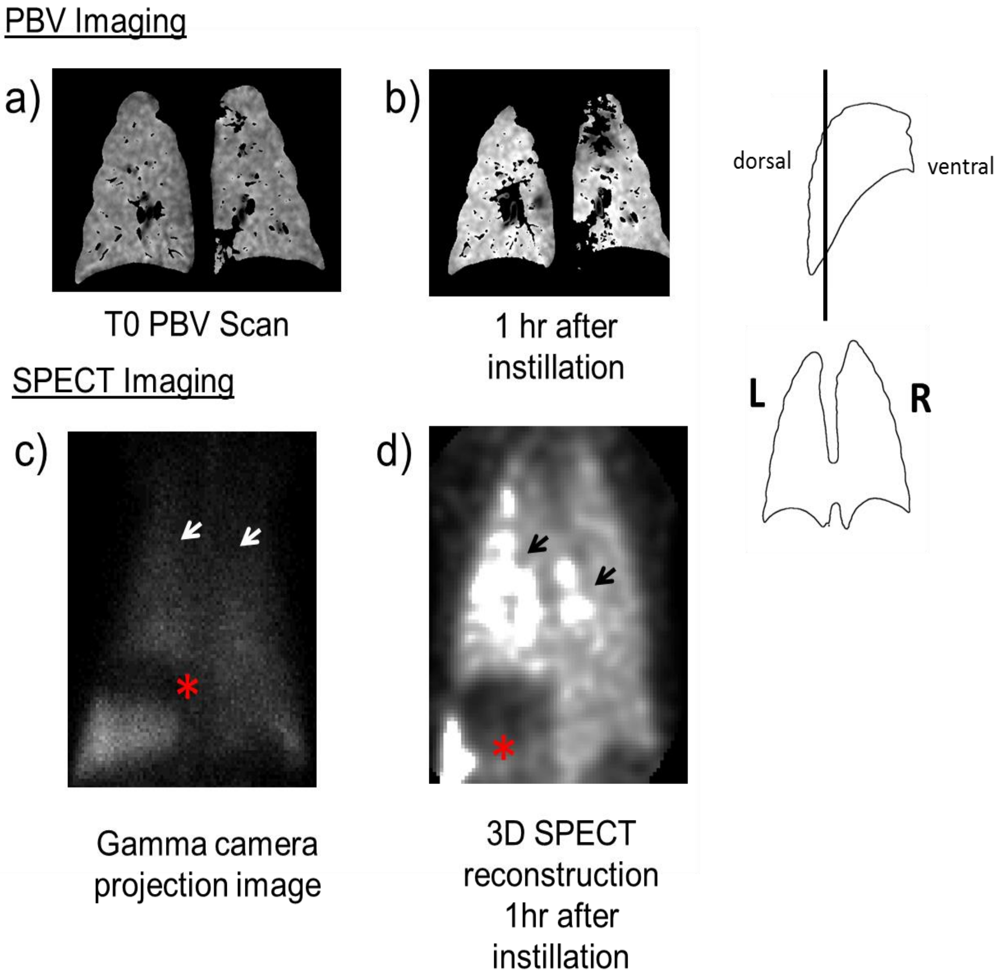
PBV Imaging

T0 PBV Scan

1 hr after instillation

SPECT Imaging

Gamma camera projection image

3D SPECT reconstruction 1hr after instillation

Figure 34: (a) PBV images at baseline (T0) and (b) several hours later (T2), demonstrating an increase in blood flow to the dependent (dorsal) region of the lung (shown in the diagram at the right) after inflammation was initiated. (c) Gamma camera and (d) SPECT images from Figure 33, showing the local “hotspots” of accumulated WBCs.

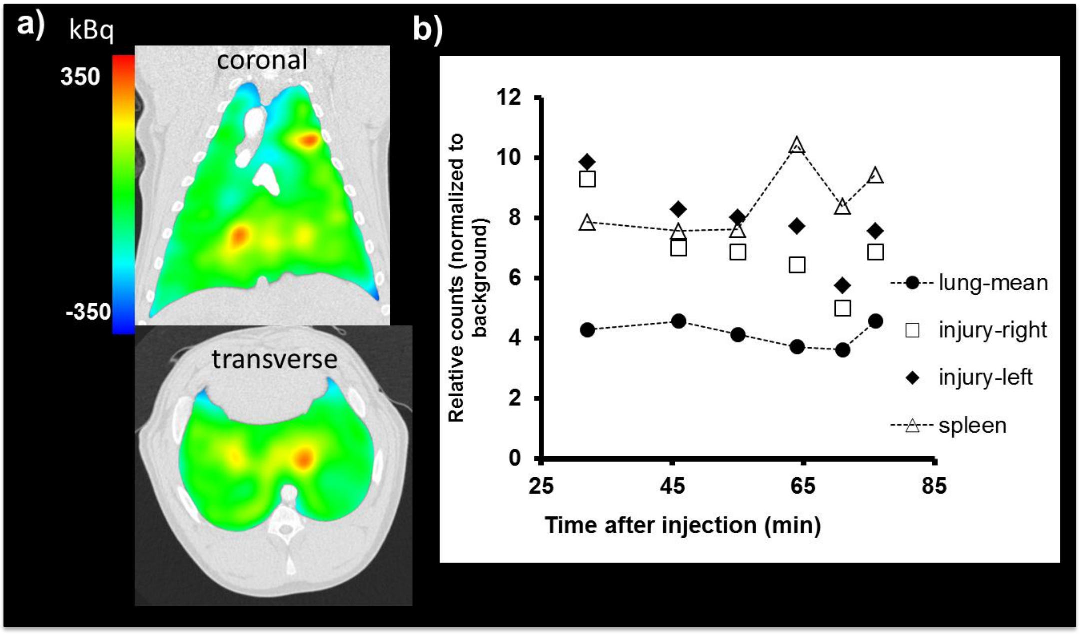

Figure 35: (a) coronal and transverse views of SPECT images co-registered to MDCT images, showing regional hot spots in the apical and basal lung where gastric acid was instilled in the airway (b) WBC kinetics, after correcting for ^{99m}Tc decay, showing gradual loss of counts in the inflamed regions and increase in counts in the spleen.

REFERENCES

1. Aaron CP, Hoffman EA, Lima JAC, Kawut SM, Prince MR, Watson K, Budoff M, Kalhan R, Barr RG. Total pulmonary vascular volume (tpvv) on ct, pulmonary perfusion on MRI and left ventricular filling in the multi-ethnic study of atherosclerosis (MESA). American Thoracic Society International Conference Abstracts: American Thoracic Society; 2014. p. A1040-A1040.

2. Ahmed T, Oliver W, Jr., Wanner A. Variability of hypoxic pulmonary vasoconstriction in sheep. Role of prostaglandins. *Am Rev Respir Dis* 1983;127:59-62.

3. Alford SK, van Beek EJ, McLennan G, Hoffman EA. Heterogeneity of pulmonary perfusion as a mechanistic image-based phenotype in emphysema susceptible smokers. *Proc Natl Acad Sci U S A* 2010;107:7485-7490.

4. Asadi AK, Cronin MV, Sa RC, Theilmann RJ, Holverda S, Hopkins SR, Buxton RB, Prisk GK. Spatial-temporal dynamics of pulmonary blood flow in the healthy human lung in response to altered fi(o2). *J Appl Physiol* 2013;114:107-118.

5. Bal H, Guerin L, Casey ME, Conti M, Eriksson L, Michel C, Fanti S, Pettinato C, Adler S, Choyke P. Improving PET spatial resolution and detectability for prostate cancer imaging. *Phys Med Biol* 2014;59:4411-4426.

6. Barbera JA, Peinado VI, Santos S, Ramirez J, Roca J, Rodriguez-Roisin R. Reduced expression of endothelial nitric oxide synthase in pulmonary arteries of smokers. *Am J Respir Crit Care Med* 2001;164:709-713.

7. Bardo DME, Brown P. Cardiac multidetector computed tomography: Basic physics of image acquisition and clinical applications. *Curr Cardiol Rev* 2008;4:231-243.

8. Barnes GT, Sones RA, Tesic MM, Morgan DR, Sanders JN. Detector for dual-energy digital radiography. *Radiology* 1985;156:537-540.

9. Barr RG. The epidemiology of vascular dysfunction relating to chronic obstructive pulmonary disease and emphysema. *Proc Am Thorac Soc* 2011;8:522-527.

10. Barr RG, Bluemke DA, Ahmed FS, Carr JJ, Enright PL, Hoffman EA, Jiang R, Kawut SM, Kronmal RA, Lima JA, Shahar E, Smith LJ, Watson KE. Percent emphysema, airflow obstruction, and impaired left ventricular filling. *N Engl J Med* 2010;362:217-227.

11. Barr RG, Mesia-Vela S, Austin JH, Basner RC, Keller BM, Reeves AP, Shimbo D, Stevenson L. Impaired flow-mediated dilation is associated with low pulmonary function and emphysema in ex-smokers: The emphysema and cancer action project (emcap) study. *Am J Respir Crit Care Med* 2007;176:1200-1207.

12. Berend N, Woolcock AJ, Marlin GE. Relationship between bronchial and arterial diameters in normal human lungs. *Thorax* 1979;34:354-358.

13. Blanco I, Gimeno E, Munoz PA, Pizarro S, Gistau C, Rodriguez-Roisin R, Roca J, Barbera JA. Hemodynamic and gas exchange effects of sildenafil in patients with chronic obstructive pulmonary disease and pulmonary hypertension. *Am J Respir Crit Care Med* 2010;181:270-278.

14. Borrill ZL, Houghton CM, Woodcock AA, Vestbo J, Singh D. Measuring bronchodilation in COPD clinical trials. *Br J Clin Pharmacol* 2005;59:379-384.

15. Brogan TV, Mellema JD, Martin LD, Krueger M, Redding GJ, Glenny RW. Spatial and temporal heterogeneity of regional pulmonary blood flow in piglets. *Pediatr Res* 2007;62:434-439.

16. Buist AS. Similarities and differences between asthma and chronic obstructive pulmonary disease: Treatment and early outcomes. *Eur Respir J Suppl* 2003;39:30s-35s.

17. Burgel PR. The role of small airways in obstructive airway diseases. *Eur Respir Rev* 2011;20:23-33.

18. Busacker A, Newell JD, Jr., Keefe T, Hoffman EA, Granroth JC, Castro M, Fain S, Wenzel S. A multivariate analysis of risk factors for the air-trapping asthmatic phenotype as measured by quantitative CT analysis. *Chest* 2009;135:48-56.

19. Busch T, Laudi S, Kaisers U. Anatomical and functional intrapulmonary shunt in acute respiratory distress syndrome. *Crit Care Med* 2008;36:2713-2714; author reply 2714-2715.

20. Calamante F, Thomas DL, Pell GS, Wiersma J, Turner R. Measuring cerebral blood flow using magnetic resonance imaging techniques. *J Cereb Blood Flow Metab* 1999;19:701-735.

21. Castro PF, Bourge RC, McGiffin DC, Benza RL, Fan P, Pinkard NB, McGoon MD. Intrapulmonary shunting in primary pulmonary hypertension: An observation in two patients treated with epoprostenol sodium. *Chest* 1998;114:334-336.

22. Chae EJ, Seo JB, Jang YM, Krauss B, Lee CW, Lee HJ, Song KS. Dual-energy CT for assessment of the severity of acute pulmonary embolism: Pulmonary perfusion defect score compared with CT angiographic obstruction score and right ventricular/left ventricular diameter ratio. *AJR Am J Roentgenol* 2010;194:604-610.

23. Chandarana H, Megibow AJ, Cohen BA, Srinivasan R, Kim D, Leidecker C, Macari M. Iodine quantification with dual-energy ct: Phantom study and preliminary experience with renal masses. *AJR Am J Roentgenol* 2011;196:W693-700.

24. Choi S, Hoffman EA, Wenzel SE, Tawhai MH, Yin Y, Castro M, Lin CL. Registration-based assessment of regional lung function via volumetric CT images of normal subjects vs. Severe asthmatics. *J Appl Physiol* 2013;115:730-742.

25. Chon D, Beck KC, Larsen RL, Shikata H, Hoffman EA. Regional pulmonary blood flow in dogs by 4d-x-ray ct. *J Appl Physiol* 2006;101:1451-1465.

26. Cohen L. Minimal paths and fast marching methods for image analysis. In: Paragios N, Chen Y, Faugeras O, editors. Handbook of mathematical models in computer vision: Springer US; 2006. p. 97-111.

27. Cornfield DN. Developmental regulation of oxygen sensing and ion channels in the pulmonary vasculature. *Adv Exp Med Biol* 2010;661:201-220.

28. Couper D, Lavange LM, Han M, Barr RG, Bleecker E, Hoffman EA, Kanner R, Kleerup E, Martinez FJ, Woodruff PG, Rennard S. Design of the subpopulations and intermediate outcomes in COPD study (SPIROMICS). *Thorax* 2013.

29. Criee CP, Sorichter S, Smith HJ, Kardos P, Merget R, Heise D, Berdel D, Kohler D, Magnussen H, Marek W, Mitfessel H, Rasche K, Rolke M, Worth H, Jorres RA. Body plethysmography--its principles and clinical use. *Respir Med* 2011;105:959-971.

30. de Freitas FM, Faraco EZ, de Azevedo DF, Zaduchliver J, Lewin I. Behavior of normal pulmonary circulation during changes of total blood volume in man. *J Clin Invest* 1965;44:366-378.

31. de Prost N, Tucci MR, Vidal Melo MF. Assessment of lung inflammation with (18)-FDG PET during acute lung injury. *AJR Am J Roentgenol* 2010;195:292-300.

32. de Torres JP, Bastarrika G, Zagaceta J, Saiz-Mendiguren R, Alcaide AB, Seijo LM, Montes U, Campo A, Zulueta JJ. Emphysema presence, severity, and distribution has little impact on the clinical presentation of a cohort of patients with mild to moderate copd. *Chest* 2011;139:36-42.

33. de Vries A, Roessl E, Kneepkens E, Thran A, Brendel B, Martens G, Proska R, Nicolay K, Grull H. Quantitative spectral K-edge imaging in preclinical photon-counting x-ray computed tomography. *Invest Radiol* 2015;50:297-304.

34. Diaz AA, Valim C, Yamashiro T, Estepar RS, Ross JC, Matsuoka S, Bartholmai B, Hatabu H, Silverman EK, Washko GR. Airway count and emphysema assessed by chest CT imaging predicts clinical outcome in smokers. *Chest* 2010;138:880-887.

35. Dighe S, Castellano E, Blake H, Jeyadevan N, Koh MU, Orten M, Swift I, Brown G. Perfusion CT to assess angiogenesis in colon cancer: Technical limitations and practical challenges. *Br J Radiol* 2012;85:e814-825.

36. Dinh-Xuan AT, Higenbottam TW, Clelland CA, Pepke-Zaba J, Cremona G, Butt AY, Large SR, Wells FC, Wallwork J. Impairment of endothelium-dependent pulmonary-artery relaxation in chronic obstructive lung disease. *N Engl J Med* 1991;324:1539-1547.

37. Doeing DC, Solway J. Airway smooth muscle in the pathophysiology and treatment of asthma. *J Appl Physiol* 2013;114:834-843.

38. Dong X, Niu T, Zhu L. Combined iterative reconstruction and image-domain decomposition for dual energy CT using total-variation regularization. *Med Phys* 2014;41:051909.

39. Dournes G, Laurent F, Coste F, Dromer C, Blanchard E, Picard F, Baldacci F, Montaudon M, Girodet PO, Marthan R, Berger P. Computed tomographic measurement of airway remodeling and emphysema in advanced chronic obstructive pulmonary disease. Correlation with pulmonary hypertension. *Am J Respir Crit Care Med* 2015;191:63-70.

40. Easley RB, Fuld MK, Fernandez-Bustamante A, Hoffman EA, Simon BA. Mechanism of hypoxemia in acute lung injury evaluated by multidetector-row ct. *Acad Radiol* 2006;13:916-921.

41. Elliott AR, Steffey EP, Jarvis KA, Marshall BE. Unilateral hypoxic pulmonary vasoconstriction in the dog, pony and miniature swine. *Respir Physiol* 1991;85:355-369.

42. Estepar RS, Kinney GL, Black-Shinn JL, Bowler RP, Kindlmann GL, Ross JC, Kikinis R, Han MK, Come CE, Diaz AA, Cho MH, Hersh CP, Schroeder JD, Reilly JJ, Lynch DA, Crapo JD, Wells JM, Dransfield MT, Hokanson JE, Washko GR. Computed tomographic measures of pulmonary vascular morphology in smokers and their clinical implications. *Am J Respir Crit Care Med* 2013;188:231-239.

43. Ferrer E, Peinado VI, Castaneda J, Prieto-Lloret J, Olea E, Gonzalez-Martin MC, Vega-Agapito MV, Diez M, Dominguez-Fandos D, Obeso A, Gonzalez C, Barbera JA. Effects of cigarette smoke and hypoxia on pulmonary circulation in the guinea pig. *Eur Respir J* 2011;38:617-627.

44. Fesler P, Pagnamenta A, Rondelet B, Kerbaul F, Naeije R. Effects of sildenafil on hypoxic pulmonary vascular function in dogs. *J Appl Physiol* 2006;101:1085-1090.

45. Fishman AP. The volume of blood in the lungs. *Circulation* 1966;33:835-838.

46. Fornaro J, Leschka S, Hibbeln D, Butler A, Anderson N, Pache G, Scheffel H, Wildermuth S, Alkadhi H, Stolzmann P. Dual- and multi-energy ct: Approach to functional imaging. *Insights Imaging* 2011;2:149-159.

47. Friedman PJ. Imaging studies in emphysema. *Proceedings of the American Thoracic Society* 2008;5:494-500.

48. Fuld MK, Grout RW, Guo J, Morgan JH, Hoffman EA. Systems for lung volume standardization during static and dynamic mdct-based quantitative assessment of pulmonary structure and function. *Acad Radiol* 2012;19:930-940.

49. Fuld MK, Halaweish A, Newell JD, Krauss B, Hoffman EA. Optimization of dual-energy xenon-ct for quantitative assessment of regional pulmonary ventilation. *Invest Radiol* 2013;48.

50. Fuld MK, Halaweish AF, Haynes SE, Divekar AA, Guo J, Hoffman EA. Pulmonary perfused blood volume with dual-energy CT as surrogate for pulmonary perfusion assessed with dynamic multidetector ct. *Radiology* 2013;267:747-756.

51. Gao Z, Grout RW, Holtze C, Hoffman EA, Saha PK. A new paradigm of interactive artery/vein separation in noncontrast pulmonary CT imaging using multiscale topomorphologic opening. *IEEE Trans Biomed Eng*; 2012. p. 3016-3027.

52. Gelb AF, Hogg JC, Muller NL, Schein MJ, Kuei J, Tashkin DP, Epstein JD, Kollin J, Green RH, Zamel N, Elliott WM, Hadjiaghai L. Contribution of emphysema and small airways in copd. *Chest* 1996;109:353-359.

53. George RT, Arbab-Zadeh A, Miller JM, Vavere AL, Bengel FM, Lardo AC, Lima JA. Computed tomography myocardial perfusion imaging with 320-row detector computed tomography accurately detects myocardial ischemia in patients with obstructive coronary artery disease. *Circ Cardiovasc Imaging* 2012;5:333-340.

54. Ghofrani HA, Pepke-Zaba J, Barbera JA, Channick R, Keogh AM, Gomez-Sanchez MA, Kneussl M, Grimminger F. Nitric oxide pathway and phosphodiesterase inhibitors in pulmonary arterial hypertension. *J Am Coll Cardiol* 2004;43:68S-72S.

55. Giaid A, Saleh D. Reduced expression of endothelial nitric oxide synthase in the lungs of patients with pulmonary hypertension. *N Engl J Med* 1995;333:214-221.

56. Gierada DS, Guniganti P, Newman BJ, Dransfield MT, Kvale PA, Lynch DA, Pilgram TK. Quantitative CT assessment of emphysema and airways in relation to lung cancer risk. *Radiology* 2011;261:950-959.

57. Glenny RW, Polissar NL, McKinney S, Robertson HT. Temporal heterogeneity of regional pulmonary perfusion is spatially clustered. *J Appl Physiol* 1995;79:986-1001.

58. Glenny RW, Robertson HT. Fractal properties of pulmonary blood flow: Characterization of spatial heterogeneity. *J Appl Physiol* 1990;69:532-545.

59. Grosse C, Grosse A. Ct findings in diseases associated with pulmonary hypertension: A current review. *Radiographics* 2010;30:1753-1777.

60. Grout RW, Alford SK, Barr RG, Hoffman EA. Total pulmonary vascular volume: A new COPD phenotype correlated with quantitative CT and PFT measures of emphysema. American Thoracic Society 2010 International Conference, May 14-19, 2010 • New Orleans: American Thoracic Society; 2010. p. A1529-A1529.

61. Guimaraes LS, Fletcher JG, Harmsen WS, Yu L, Siddiki H, Melton Z, Huprich JE, Hough D, Hartman R, McCollough CH. Appropriate patient selection at abdominal dual-energy CT using 80 kv: Relationship between patient size, image noise, and image quality. *Radiology* 2010;257:732-742.

62. Gust R, Kozlowski J, Stephenson AH, Schuster DP. Synergistic hemodynamic effects of low-dose endotoxin and acute lung injury. *Am J Respir Crit Care Med* 1998;157:1919-1926.

63. Hakim TS, Michel RP, Chang HK. Effect of lung inflation on pulmonary vascular resistance by arterial and venous occlusion. *J Appl Physiol Respir Environ Exerc Physiol* 1982;53:1110-1115.

64. Heydari B, Kwong RY, Jerosch-Herold M. Technical advances and clinical applications of quantitative myocardial blood flow imaging with cardiac mri. *Prog Cardiovasc Dis* 2015.

65. Hillier SC, Graham JA, Hanger CC, Godbey PS, Glenny RW, Wagner WW, Jr. Hypoxic vasoconstriction in pulmonary arterioles and venules. *J Appl Physiol* 1997;82:1084-1090.

66. Hlastala MP, Lamm WJ, Karp A, Polissar NL, Starr IR, Glenny RW. Spatial distribution of hypoxic pulmonary vasoconstriction in the supine pig. *J Appl Physiol* 2004;96:1589-1599.

67. Hoffman EA. Effect of body orientation on regional lung expansion: A computed tomographic approach. *J Appl Physiol* 1985;59:468-480.

68. Hoffman EA, Ahmed FS, Baumhauer H, Budoff M, Carr JJ, Kronmal R, Reddy S, Barr RG. Variation in the percent of emphysema-like lung in a healthy, nonsmoking multiethnic sample. The MESA lung study. *Ann Am Thorac Soc* 2014;11:898-907.

69. Hoffman EA, Behrenbeck T, Chevalier PA, Wood EH. Estimation of regional pleural surface expansile forces in intact dogs. *J Appl Physiol Respir Environ Exerc Physiol* 1983;55:935-948.

70. Hoffman EA, Chon D. Computed tomography studies of lung ventilation and perfusion. *Proc Am Thorac Soc* 2005;2:492-498, 506.

71. Hoffman EA, Jiang R, Baumhauer H, Brooks MA, Carr JJ, Detrano R, Reinhardt J, Rodriguez J, Stukovsky K, Wong ND, Barr RG. Reproducibility and validity of lung density measures from cardiac CT scans--the multi-ethnic study of atherosclerosis (MESA) lung study. *Acad Radiol* 2009;16:689-699.

72. Hoffman EA, Munroe ML, Tucker A, Reeves JT. Histamine h1- and h2-receptors in the cat and their roles during alveolar hypoxia. *Respir Physiol* 1977;29:255-264.

73. Hoffman EA, Reinhardt JM, Sonka M, Simon BA, Guo J, Saba O, Chon D, Samrah S, Shikata H, Tschirren J, Palagyi K, Beck KC, McLennan G. Characterization of the interstitial lung diseases via density-based and texture-based analysis of computed tomography images of lung structure and function. *Acad Radiol* 2003;10:1104-1118.

74. Hoffman EA, Simon BA, McLennan G. State of the art. A structural and functional assessment of the lung via multidetector-row computed tomography: Phenotyping chronic obstructive pulmonary disease. *Proc Am Thorac Soc* 2006;3:519-532.

75. Hoffman EA, Sinak LJ, Robb RA, Ritman EL. Noninvasive quantitative imaging of shape and volume of lungs. *J Appl Physiol Respir Environ Exerc Physiol* 1983;54:1414-1421.

76. Hopkins SR, Garg J, Bolar DS, Balouch J, Levin DL. Pulmonary blood flow heterogeneity during hypoxia and high-altitude pulmonary edema. *Am J Respir Crit Care Med* 2005;171:83-87.

77. Hrometz SL, Shields KM. Sildenafil citrate for the treatment of pulmonary hypertension. Drugs Today; 2006. p. 771-784.

78. Hyatt RE. The interrelationships of pressure, flow, and volume during various respiratory maneuvers in normal and emphysematous subjects. *Am Rev Respir Dis* 1961;83:676-683.

79. Ichinose F, Zapol WM, Sapirstein A, Ullrich R, Tager AM, Coggins K, Jones R, Bloch KD. Attenuation of hypoxic pulmonary vasoconstriction by endotoxemia requires 5-lipoxygenase in mice. *Circ Res* 2001;88:832-838.

80. Ishizawa K, Kubo H, Yamada M, Kobayashi S, Numasaki M, Ueda S, Suzuki T, Sasaki H. Bone marrow-derived cells contribute to lung regeneration after elastase-induced pulmonary emphysema. *FEBS Lett* 2004;556:249-252.

81. Ito I, Nagai S, Handa T, Muro S, Hirai T, Tsukino M, Mishima M. Matrix metalloproteinase-9 promoter polymorphism associated with upper lung dominant emphysema. *Am J Respir Crit Care Med* 2005;172:1378-1382.

82. Iyer AS, Wells JM, Vishin S, Bhatt SP, Wille KM, Dransfield MT. Ct scan-measured pulmonary artery to aorta ratio and echocardiography for detecting pulmonary hypertension in severe copd. *Chest* 2014;145:824-832.

83. Iyer KS, Grout RW, Zamba GK, Hoffman EA. Repeatability and sample size assessment associated with computed tomography-based lung density metrics. *Chronic Obstr Pulm Dis (Miami)* 2014;1:97-104.

84. Janicki JS, Weber KT, Likoff MJ, Fishman AP. The pressure-flow response of the pulmonary circulation in patients with heart failure and pulmonary vascular disease. *Circulation* 1985;72:1270-1278.

85. Jin D, Iyer K, Hoffman E, Saha P. Automated assessment of pulmonary arterial morphology in multi-row detector CT imaging using correspondence with anatomic airway branches. Lecture Notes in Computer Science: Springer International Publishing; 2014. p. 521-530.

86. Jin D, Iyer KS, Hoffman EA, Saha PK. A new approach of arc skeletonization for tree-like objects using minimum cost path. Pattern Recognition (ICPR), 2014 22nd International Conference on; 2014. p. 942-947.

87. Kalender WA, Seissler W, Klotz E, Vock P. Spiral volumetric CT with single-breath-hold technique, continuous transport, and continuous scanner rotation. *Radiology* 1990;176:181-183.

88. Kashefi A, Kuo J, Shelton DK. Molecular imaging in pulmonary diseases. *AJR Am J Roentgenol* 2011;197:295-307.

89. Kaza RK, Platt JF, Cohan RH, Caoili EM, Al-Hawary MM, Wasnik A. Dual-energy CT with single- and dual-source scanners: Current applications in evaluating the genitourinary tract. *Radiographics* 2012;32:353-369.

90. Kesten S, Rebuck AS. Is the short-term response to inhaled beta-adrenergic agonist sensitive or specific for distinguishing between asthma and copd? *Chest* 1994;105:1042-1045.

91. Kim SJ, Im JG, Kim IO, Cho ST, Cha SH, Park KS, Kim DY. Normal bronchial and pulmonary arterial diameters measured by thin section ct. *J Comput Assist Tomogr* 1995;19:365-369.

92. Kim YI, Schroeder J, Lynch D, Newell J, Make B, Friedlander A, Estepar RS, Hanania NA, Washko G, Murphy JR, Wilson C, Hokanson JE, Zach J, Butterfield K, Bowler RP, Copdgene I. Gender differences of airway dimensions in anatomically matched sites on CT in smokers. *COPD* 2011;8:285-292.

93. Komatsu S, Kamata T, Imai A, Ohara T, Miyaji K, Kobayashi Y, Kodama K. Quantitative analysis of coronary vessels with optimized intracoronary CT number. *PloS One*; 2014. p. e85312.

94. Koonce JD, Vliegenthart R, Schoepf UJ, Schmidt B, Wahlquist AE, Nietert PJ, Bastarrika G, Flohr TG, Meinel FG. Accuracy of dual-energy computed tomography for the measurement of iodine concentration using cardiac CT protocols: Validation in a phantom model. *Eur Radiol* 2014;24:512-518.

95. Kuschner WG. Sildenafil citrate therapy for pulmonary arterial hypertension. *N Engl J Med* 2006;354:1091-1093; author reply 1091-1093.

96. Lee CG, Cho S, Homer RJ, Elias JA. Genetic control of transforming growth factor-beta1-induced emphysema and fibrosis in the murine lung. *Proc Am Thorac Soc* 2006;3:476-477.

97. Lee CW, Seo JB, Lee Y, Chae EJ, Kim N, Lee HJ, Hwang HJ, Lim CH. A pilot trial on pulmonary emphysema quantification and perfusion mapping in a single-step using contrast-enhanced dual-energy computed tomography. *Invest Radiol* 2012;47:92-97.

98. Lee S, Choi YN, Kim HJ. Quantitative material decomposition using spectral computed tomography with an energy-resolved photon-counting detector. *Phys Med Biol* 2014;59:5457-5482.

99. Li H, Srinivasan SR, Berenson GS. Comparison of the measures of pulsatile arterial function between asymptomatic younger adult smokers and former smokers: The bogalusa heart study. *Am J Hypertens* 2006;19:897-901.

100. Liu X, Yu L, Primak AN, McCollough CH. Quantitative imaging of element composition and mass fraction using dual-energy ct: Three-material decomposition. *Med Phys* 2009;36:1602-1609.

101. Love C, Palestro CJ. Radionuclide imaging of inflammation and infection in the acute care setting. *Semin Nucl Med* 2013;43:102-113.

102. Magee F, Wright JL, Wiggs BR, Pare PD, Hogg JC. Pulmonary vascular structure and function in chronic obstructive pulmonary disease. *Thorax* 1988;43:183-189.

103. Mahmud A, Feely J. Effect of smoking on arterial stiffness and pulse pressure amplification. *Hypertension* 2003;41:183-187.

104. Mannino DM, Buist AS. Global burden of copd: Risk factors, prevalence, and future trends. *Lancet* 2007;370:765-773.

105. Marwan M, Pflederer T, Schepis T, Seltmann M, Ropers D, Daniel WG, Achenbach S. Coronary vessel and luminal area measurement using dual-source computed tomography in comparison with intravascular ultrasound: Effect of window settings on measurement accuracy. *J Comput Assist Tomogr*; 2011. p. 113-118.

106. Matsuoka S, Kurihara Y, Yagihashi K, Nakajima Y. Quantitative assessment of peripheral airway obstruction on paired expiratory/inspiratory thin-section computed tomography in chronic obstructive pulmonary disease with emphysema. *J Comput Assist Tomogr* 2007;31:384-389.

107. Matsuoka S, Yamashiro T, Matsushita S, Fujikawa A, Yagihashi K, Kurihara Y, Nakajima Y. Relationship between quantitative CT of pulmonary small vessels and pulmonary perfusion. *AJR Am J Roentgenol* 2014;202:719-724.

108. McAllister DA, Maclay JD, Mills NL, Mair G, Miller J, Anderson D, Newby DE, Murchison JT, Macnee W. Arterial stiffness is independently associated with emphysema severity in patients with chronic obstructive pulmonary disease. *Am J Respir Crit Care Med* 2007;176:1208-1214.

109. Meinel FG, Graef A, Thieme SF, Bamberg F, Schwarz F, Sommer WH, Helck AD, Neurohr C, Reiser MF, Johnson TR. Assessing pulmonary perfusion in emphysema: Automated quantification of perfused blood volume in dual-energy ctpa. *Invest Radiol* 2013;48:79-85.

110. Melzer TR, Cook NJ, Butler AP, Watts R, Anderson N, Tipples R, Butler PH. Spectroscopic biomedical imaging with the medipix2 detector. *Australas Phys Eng Sci Med* 2008;31:300-306.

111. Miller MR, Hankinson J, Brusasco V, Burgos F, Casaburi R, Coates A, Crapo R, Enright P, van der Grinten CP, Gustafsson P, Jensen R, Johnson DC, MacIntyre N, McKay R, Navajas D, Pedersen OF, Pellegrino R, Viegi G, Wanger J, Force AET. Standardisation of spirometry. *Eur Respir J* 2005;26:319-338.

112. Milnor WR, Jose AD, McGaff CJ. Pulmonary vascular volume, resistance, and compliance in man. *Circulation* 1960;22:130-137.

113. Minematsu N, Nakamura H, Tateno H, Nakajima T, Yamaguchi K. Genetic polymorphism in matrix metalloproteinase-9 and pulmonary emphysema. *Biochem Biophys Res Commun* 2001;289:116-119.

114. Mintun MA, Ter-Pogossian MM, Green MA, Lich LL, Schuster DP. Quantitative measurement of regional pulmonary blood flow with positron emission tomography. *J Appl Physiol* 1986;60:317-326.

115. Miura S, Ohno Y, Kimura H, Kichikawa K. Quantitative lung perfused blood volume imaging on dual-energy ct: Capability for quantitative assessment of disease severity in patients with acute pulmonary thromboembolism. *Acta Radiol* 2014.

116. Moudgil R, Michelakis ED, Archer SL. Hypoxic pulmonary vasoconstriction. *J Appl Physiol* 2005;98:390-403.

117. Moudgil R, Michelakis ED, Archer SL. The role of K+ channels in determining pulmonary vascular tone, oxygen sensing, cell proliferation, and apoptosis: Implications in hypoxic pulmonary vasoconstriction and pulmonary arterial hypertension. *Microcirculation* 2006;13:615-632.

118. Nakazawa T, Watanabe Y, Hori Y, Kiso K, Higashi M, Itoh T, Naito H. Lung perfused blood volume images with dual-energy computed tomography for chronic thromboembolic pulmonary hypertension: Correlation to scintigraphy with single-photon emission computed tomography. *J Comput Assist Tomogr* 2011;35:590-595.

119. Newell JD, Jr., Fuld MK, Allmendinger T, Sieren JP, Chan KS, Guo J, Hoffman EA. Very low-dose (0.15 mgy) chest CT protocols using the copdgene 2 test object and a third-generation dual-source CT scanner with corresponding third-generation iterative reconstruction software. *Invest Radiol* 2015;50:40-45.

120. Newell JD, Jr., Sieren J, Hoffman EA. Development of quantitative computed tomography lung protocols. *J Thorac Imaging* 2013;28:266-271.

121. Norberg P, Persson HL, Carlsson GA, Bake B, Kentson M, Sandborg M, Gustafsson A. Quantitative lung spect applied on simulated early COPD and humans with advanced copd. *EJNMMI Res* 2013;3:28.

122. Pansini V, Remy-Jardin M, Faivre JB, Schmidt B, Dejardin-Bothelo A, Perez T, Delannoy V, Duhamel A, Remy J. Assessment of lobar perfusion in smokers according to the presence and severity of emphysema: Preliminary experience with dual-energy CT angiography. *Eur Radiol* 2009;19:2834-2843.

123. Pauwels RA, Buist AS, Calverley PM, Jenkins CR, Hurd SS. Global strategy for the diagnosis, management, and prevention of chronic obstructive pulmonary disease. Nhlbi/who global initiative for chronic obstructive lung disease (GOLD) workshop summary. *Am J Respir Crit Care Med* 2001;163:1256-1276.

124. Peinado VI, Barbera JA, Abate P, Ramirez J, Roca J, Santos S, Rodriguez-Roisin R. Inflammatory reaction in pulmonary muscular arteries of patients with mild chronic obstructive pulmonary disease. *Am J Respir Crit Care Med* 1999;159:1605-1611.

125. Peinado VI, Barbera JA, Ramirez J, Gomez FP, Roca J, Jover L, Gimferrer JM, Rodriguez-Roisin R. Endothelial dysfunction in pulmonary arteries of patients with mild copd. *Am J Physiol* 1998;274:L908-913.

126. Peinado VI, Gomez FP, Barberà JA, Roman A, Angels Montero M, Ramírez J, Roca J, Rodriguez-Roisin R. Pulmonary vascular abnormalities in chronic obstructive pulmonary disease undergoing lung transplant. *J Heart Lung Transplant*; 2013. p. 1262-1269.

127. Peinado VI, Pizarro S, Barbera JA. Pulmonary vascular involvement in copd. *Chest* 2008;134:808-814.

128. Peinado VI, Ramirez J, Roca J, Rodriguez-Roisin R, Barbera JA. Identification of vascular progenitor cells in pulmonary arteries of patients with chronic obstructive pulmonary disease. *Am J Respir Cell Mol Biol* 2006;34:257-263.

129. Pizarro S, Garcia-Lucio J, Peinado VI, Tura-Ceide O, Diez M, Blanco I, Sitges M, Petriz J, Torralba Y, Marin P, Roca J, Barbera JA. Circulating progenitor cells and vascular dysfunction in chronic obstructive pulmonary disease. *PLoS One* 2014;9:e106163.

130. Primak AN, Ramirez Giraldo JC, Liu X, Yu L, McCollough CH. Improved dual-energy material discrimination for dual-source CT by means of additional spectral filtration. *Med Phys* 2009;36:1359-1369.

131. Ray NB, Durairaj L, Chen BB, McVerry BJ, Ryan AJ, Donahoe M, Waltenbaugh AK, O'Donnell CP, Henderson FC, Etscheidt CA, McCoy DM, Agassandian M, Hayes-Rowan EC, Coon TA, Butler PL, Gakhar L, Mathur SN, Sieren JC, Tyurina YY, Kagan VE, McLennan G, Mallampalli RK. Dynamic regulation of cardiolipin by the lipid pump atp8b1 determines the severity of lung injury in experimental pneumonia. *Nat Med* 2010;16:1120-1127.

132. Reilly J. Using computed tomographic scanning to advance understanding of chronic obstructive pulmonary disease. *Proc Am Thorac Soc* 2006;3:450-455.

133. Reinhardt JM, D'Souza ND, Hoffman EA. Accurate measurement of intrathoracic airways. *IEEE Trans Med Imaging* 1997;16:820-827.

134. Remy-Jardin M, Remy J, Boulenguez C, Sobaszek A, Edme JL, Furon D. Morphologic effects of cigarette smoking on airways and pulmonary parenchyma in healthy adult volunteers: Ct evaluation and correlation with pulmonary function tests. *Radiology* 1993;186:107-115.

135. Rennard SI. Treatment of stable chronic obstructive pulmonary disease. *Lancet* 2004;364:791-802.

136. Richter DC, Joubert JR, Nell H, Schuurmans MM, Irusen EM. Diagnostic value of post-bronchodilator pulmonary function testing to distinguish between stable, moderate to severe COPD and asthma. *Int J Chron Obstruct Pulmon Dis* 2008;3:693-699.

137. Roessl E, Herrmann C. Cramer-rao lower bound of basis image noise in multiple-energy x-ray imaging. *Phys Med Biol* 2009;54:1307-1318.

138. Rossi A, Merkus D, Klotz E, Mollet N, de Feyter PJ, Krestin GP. Stress myocardial perfusion: Imaging with multidetector ct. *Radiology* 2014;270:25-46.

139. Ruparelia P, Szczepura KR, Summers C, Solanki CK, Balan K, Newbold P, Bilton D, Peters AM, Chilvers ER. Quantification of neutrophil migration into the lungs of patients with chronic obstructive pulmonary disease. *Eur J Nucl Med Mol Imaging* 2011;38:911-919.

140. Saha PK. Tensor scale: A local morphometric parameter with applications to computer vision and image processing. *Comp Vision Imag Understand* 2005;99:384-413.

141. Saha PK, Gao Z, Alford SK, Sonka M, Hoffman EA. Topomorphologic separation of fused isointensity objects via multiscale opening: Separating arteries and veins in 3-D pulmonary ct. *IEEE Trans on Med Imag*: IEEE; 2010. p. 840-851.

142. Sakamoto A, Sakamoto I, Nagayama H, Koike H, Sueyoshi E, Uetani M. Quantification of lung perfusion blood volume with dual-energy ct: Assessment of the severity of acute pulmonary thromboembolism. *AJR Am J Roentgenol* 2014;203:287-291.

143. Santos S, Peinado VI, Ramirez J, Melgosa T, Roca J, Rodriguez-Roisin R, Barbera JA. Characterization of pulmonary vascular remodelling in smokers and patients with mild copd. *Eur Respir J* 2002;19:632-638.

144. Schlomka JP, Roessl E, Dorscheid R, Dill S, Martens G, Istel T, Baumer C, Herrmann C, Steadman R, Zeitler G, Livne A, Proksa R. Experimental feasibility of multi-energy photon-counting K-edge imaging in pre-clinical computed tomography. *Phys Med Biol* 2008;53:4031-4047.

145. Schroeder JD, McKenzie AS, Zach JA, Wilson CG, Curran-Everett D, Stinson DS, Newell JD, Jr., Lynch DA. Relationships between airflow obstruction and quantitative CT measurements of emphysema, air trapping, and airways in subjects with and without chronic obstructive pulmonary disease. *AJR Am J Roentgenol* 2013;201:W460-470.

146. Schroeder T, Vidal Melo MF, Musch G, Harris RS, Winkler T, Venegas JG. Pet imaging of regional 18-FDG uptake and lung function after cigarette smoke inhalation. *J Nucl Med* 2007;48:413-419.

147. Schuster DP, Marklin GF. The effect of regional lung injury or alveolar hypoxia on pulmonary blood flow and lung water measured by positron emission tomography. *Am Rev Respir Dis* 1986;133:1037-1042.

148. Seaman J, Leonard AC, Panos RJ. Health care utilization history, gold guidelines, and respiratory medication prescriptions in patients with copd. *Int J Chron Obstruct Pulmon Dis* 2010;5:89-97.

149. Seimetz M, Parajuli N, Pichl A, Veit F, Kwapiszewska G, Weisel FC, Milger K, Egemnazarov B, Turowska A, Fuchs B, Nikam S, Roth M, Sydykov A, Medebach T, Klepetko W, Jaksch P, Dumitrascu R, Garn H, Voswinckel R, Kostin S, Seeger W, Schermuly RT, Grimminger F, Ghofrani HA, Weissmann N. Inducible nos inhibition reverses tobacco-smoke-induced emphysema and pulmonary hypertension in mice. *Cell* 2011;147:293-305.

150. Seo Y, Aparici CM, Hasegawa BH. Technological development and advances in spect/ct. *Semin Nucl Med* 2008;38:177-198.

151. Silva AC, Paiva FF. Dynamic magnetic resonance imaging of cerebral blood flow using arterial spin labeling. *Methods Mol Biol* 2009;489:277-295.

152. Singhal S, Henderson R, Horsfield K, Harding K, Cumming G. Morphometry of the human pulmonary arterial tree. *Circ Res* 1973;33:190-197.

153. Sommer N, Dietrich A, Schermuly RT, Ghofrani HA, Gudermann T, Schulz R, Seeger W, Grimminger F, Weissmann N. Regulation of hypoxic pulmonary vasoconstriction: Basic mechanisms. *Eur Respir J* 2008;32:1639-1651.

154. Starr IR, Lamm WJ, Neradilek B, Polissar N, Glenny RW, Hlastala MP. Regional hypoxic pulmonary vasoconstriction in prone pigs. *J Appl Physiol* 2005;99:363-370.

155. Stickland MK, Lovering AT. Exercise-induced intrapulmonary arteriovenous shunting and pulmonary gas exchange. *Exerc Sport Sci Rev* 2006;34:99-106.

156. Subramanian DR, Jenkins L, Edgar R, Quraishi N, Stockley RA, Parr DG. Assessment of pulmonary neutrophilic inflammation in emphysema by quantitative positron emission tomography. *Am J Respir Crit Care Med* 2012;186:1125-1132.

157. Suga K, Yasuhiko K, Zaki M, Yamashita T, Seto A, Matsumoto T, Matsunaga N. Assessment of regional lung functional impairment with co-registered respiratory-gated ventilation/perfusion spet-ct images: Initial experiences. *Eur J Nucl Med Mol Imaging* 2004;31:240-249.

158. Suki B, Sato S, Parameswaran H, Szabari MV, Takahashi A, Bartolák-Suki E. Emphysema and mechanical stress-induced lung remodeling. *Physiology (Bethesda)* 2013;28:404-413.

159. Suzuki S, Furui S, Kaminaga T. Accuracy of automated CT angiography measurement of vascular diameter in phantoms: Effect of size of display field of view, density of contrast medium, and wall thickness. *AJR Am J Roentgenol*; 2005. p. 1940-1944.

160. Szilasi M, Dolinay T, Nemes Z, Strausz J. Pathology of chronic obstructive pulmonary disease. *Pathol Oncol Res* 2006;12:52-60.

161. Takahashi M, Fukuoka J, Nitta N, Takazakura R, Nagatani Y, Murakami Y, Otani H, Murata K. Imaging of pulmonary emphysema: A pictorial review. *Int J Chron Obstruct Pulmon Dis* 2008;3:193-204.

162. Takahashi N, Hartman RP, Vrtiska TJ, Kawashima A, Primak AN, Dzyubak OP, Mandrekar JN, Fletcher JG, McCollough CH. Dual-energy CT iodine-subtraction virtual unenhanced technique to detect urinary stones in an iodine-filled collecting system: A phantom study. *AJR Am J Roentgenol* 2008;190:1169-1173.

163. Tessler R, Wu S, Fiori R, Macgowan CK, Belik J. Sildenafil acutely reverses the hypoxic pulmonary vasoconstriction response of the newborn pig. *Pediatr Res* 2008;64:251-255.

164. Thieme SF, Hoegl S, Nikolaou K, Fisahn J, Irlbeck M, Maxien D, Reiser MF, Becker CR, Johnson TR. Pulmonary ventilation and perfusion imaging with dual-energy ct. *Eur Radiol* 2010;20:2882-2889.

165. Thieme SF, Johnson TR, Lee C, McWilliams J, Becker CR, Reiser MF, Nikolaou K. Dual-energy CT for the assessment of contrast material distribution in the pulmonary parenchyma. *AJR Am J Roentgenol* 2009;193:144-149.

166. Townsley MI. Structure and composition of pulmonary arteries, capillaries, and veins. *Compr Physiol* 2012;2:675-709.

167. Tschirren J, Hoffman EA, McLennan G, Sonka M. Intrathoracic airway trees: Segmentation and airway morphology analysis from low-dose CT scans. *IEEE Trans Med Imaging* 2005;24:1529-1539.

168. Velazquez M, Schuster DP. Perfusion redistribution after alveolar flooding: Vasoconstriction vs. Vascular compression. *J Appl Physiol* 1991;70:600-607.

169. Wagner PD, Laravuso RB, Uhi RR, West JB. Continuous distributions of ventilation-perfusion ratios in normal subjects breathing air and 100% FiO2. *J Clin Invest* 1974;54:54-68.

170. Wagner PD, Saltzman HA, West JB. Measurement of continuous distributions of ventilation-perfusion ratios: Theory. *J Appl Physiol* 1974;36:588-599.

171. Weissmann N, Lobo B, Pichl A, Parajuli N, Seimetz M, Puig-Pey R, Ferrer E, Peinado VI, Dominguez-Fandos D, Fysikopoulos A, Stasch JP, Ghofrani HA, Coll-Bonfill N, Frey R, Schermuly RT, Garcia-Lucio J, Blanco I, Bednorz M, Tura-Ceide O, Tadele E, Brandes RP, Grimminger J, Klepetko W, Jaksch P, Rodriguez-Roisin R, Seeger W, Grimminger F, Barbera JA. Stimulation of soluble guanylate cyclase prevents cigarette smoke-induced pulmonary hypertension and emphysema. *Am J Respir Crit Care Med* 2014;189:1359-1373.

172. Wells JM, Washko GR, Han MK, Abbas N, Nath H, Mamary AJ, Regan E, Bailey WC, Martinez FJ, Westfall E, Beaty TH, Curran-Everett D, Curtis JL, Hokanson JE, Lynch DA, Make BJ, Crapo JD, Silverman EK, Bowler RP, Dransfield MT. Pulmonary arterial enlargement and acute exacerbations of copd. *N Engl J Med* 2012;367:913-921.

173. West JB. Distribution of mechanical stress in the lung, a possible factor in localisation of pulmonary disease. *Lancet* 1971;1:839-841.

174. West JB. Respiratory physiology: The Essentials. Lippincott Williams & Wilkins; 2005.

175. West JB. Pulmonary pathophysiology: The Essentials. Wolters Kluwer Health; 2011.

176. West JB, Dollery CT, Naimark A. Distribution of blood flow in isolated lung: Relation to vascular and alveolar pressures. *J Appl Physiol* 1964;19:713-724.

177. Wolfkiel CJ, Ferguson JL, Chomka EV, Law WR, Labin IN, Tenzer ML, Booker M, Brundage BH. Measurement of myocardial blood flow by ultrafast computed tomography. *Circulation* 1987;76:1262-1273.

178. Won C, Chon D, Tajik J, Tran BQ, Robinswood GB, Beck KC, Hoffman EA. Ct-based assessment of regional pulmonary microvascular blood flow parameters. *J Appl Physiol* 2003;94:2483-2493.

179. Wood SA, Zerhouni EA, Hoford JD, Hoffman EA, Mitzner W. Measurement of three-dimensional lung tree structures by using computed tomography. *J Appl Physiol* 1995;79:1687-1697.

180. Wright JL, Churg A. Effect of long-term cigarette smoke exposure on pulmonary vascular structure and function in the guinea pig. *Exp Lung Res* 1991;17:997-1009.

181. Wright JL, Churg A. Advances in the pathology of copd. *Histopathology* 2006;49:1-9.

182. Wu X, Latson LA, Wang T, Driscoll DJ, Ensing GJ, Ritman EL. Regional pulmonary perfusion estimated by high-speed volume scanning ct. *Am J Physiol Imaging* 1988;3:73-80.

183. Xu Y, Liang G, Hu G, Yang Y, Geng J, Saha PK. Quantification of coronary arterial stenoses in cta using fuzzy distance transform. *Comput Med Imaging Graph* 2012;36:11-24.

184. Yamada H, Miyazaki H, Kikuchi T, Fujimoto J, Kudoh I. Acid instillation enhances the inflammatory response to subsequent lipopolysaccharide challenge in rats. *Am J Respir Crit Care Med* 2000;162:1366-1371.

185. Yin Y, Hoffman EA, Ding K, Reinhardt JM, Lin CL. A cubic b-spline-based hybrid registration of lung CT images for a dynamic airway geometric model with large deformation. *Phys Med Biol* 2011;56:203-218.

186. Yin Y, Hoffman EA, Lin CL. Mass preserving nonrigid registration of CT lung images using cubic b-spline. *Med Phys* 2009;36:4213-4222.

187. Yu L, Liu X, Leng S, Kofler JM, Ramirez-Giraldo JC, Qu M, Christner J, Fletcher JG, McCollough CH. Radiation dose reduction in computed tomography: Techniques and future perspective. *Imaging Med* 2009;1:65-84.

188. Zach JA, Newell JD, Jr., Schroeder J, Murphy JR, Curran-Everett D, Hoffman EA, Westgate PM, Han MK, Silverman EK, Crapo JD, Lynch DA. Quantitative computed tomography of the lungs and airways in healthy nonsmoking adults. *Invest Radiol* 2012;47:596-602.

189. Zhang J, Fletcher JG, Vrtiska TJ, Manduca A, Thompson JL, Raghavan ML, Wentz RJ, McCollough CH. Large-vessel distensibility measurement with electrocardiographically gated multidetector ct: Phantom study and initial experience. *Radiology* 2007;245:258-266.